SACLANTCEN Conference Proceedings No. 17 Part 7

SACLANTCEN
Conference Proceedings No. 17

PART 7
FIELD CALCULATIONS

SACLANT ASW
RESEARCH CENTRE

OCEANIC ACOUSTIC MODELLING

Proceedings of a Conference held at SACLANTCEN
on 8-11 September 1975

Organized by

WOLFGANG BACHMANN and ROBERT BRUCE WILLIAMS

15 OCTOBER 1975

NORTH
ATLANTIC
TREATY
ORGANIZATION

VIALE SAN BARTOLOMEO 400
I - 19026 - LA SPEZIA, ITALY

Compiled and Published by

SACLANTCEN

SACLANTCEN
CONFERENCR PROCEEDINGS NO. 17

NORTH ATLANTIC TREATY ORGANIZATION
SACLANT ASW Research Centre
Viale San Bartolomeo 400
I 19026 - La Spezia, Italy

OCEANIC ACOUSTIC MODELLING

Proceedings of a Conference held at SACLANTCEN
on 8-11 September 1975

In eight parts
Part 7: Field Calculations

Organized by
Wolfgang Bachmann and Robert Bruce Williams

15 October 1975

PAPERS PRESENTED AT CONFERENCE

Pt 1: Noise (and Introductory Matter)

1. A.W. Pryce, "Keynote address: Underwater acoustics — modelling".
2. P. Wille, "Noise sources in the ocean, Pt I".
3. M. Daintith, "Noise sources in the ocean, Pt II".
4. H. Cox, "Acoustic noise models".

Pt 2: Bubbles

5. B. Williams & L. Foster, "Gas bubbles in the sea: A review and model proposals".
6. H. Medwin, "Acoustical probing for microbubbles at sea".

Pt 3: Sea surface

7. C.R. Ward, "A spectral ocean wave model".
8. H. Schwarze, "A theoretical model for doppler spread of backscattered sound from a composite-roughness sea surface".
9. O.I. Diachok, "Effects of sea-ice ridges on sound propagation in the Arctic Ocean".
10. J. Siebert, "Low-frequency acoustic measurements in a shallow-water area with a rough sea surface".
11. P.A. Crowther, "Surface wave spectra".
12. H. Trinkaus, "Scattering and reflection of sound from the sea surface".

Pt 4: Sea bottom

13. F.M. Phelan, B. Williams & F.H. Fisher, "Highlights of bottom topography inferred from received depression and bearing angles".
14. S.R. Santaniello & F.R. Dinapoli, "Ocean-bottom reflectivity (a point of view)".
15. W.A. Kuperman & F. Ingenito, "Relative contribution of surface roughness and bottom attenuation to propagation loss in shallow water".
16. R.E. Christiensen & W.H. Geddes, "Refraction of sound in the sea floor".
17. J.A. Desanto, "Scattering from a random interface".
18. E.L. Hamilton, "Acoustic properties of the sea floor".
19. H. Bucker & H. Morris, "Reflection of sound from a layered ocean bottom".
20. B. Hurdle, K.D. Flowers & J.A. Desanto, "Acoustic scattering from rough surfaces".

Pt 5: Macro-scale phenomena

21. W. Munk, "Acoustic scintillations of acoustic waves".
22. S. Flatté, "Intensity and phase fluctuations in low-frequency acoustic transmission through internal waves".
23. T.H. Bell, Jr., J.M. Bergin, J.P. Dougan, Z.C.B. Hamilton, W.D. Morris, B.S. Okawa, E.E. Rudd & J. Witting, "Two-dimensional internal-wave spectra".
24. I.M. Blatstein, "Ocean-basin reverberation from large underwater explosions, Pt I: Source-level and propagation-loss modelling".
25. J.A. Goertner, "Ocean-basin reverberation from large underwater explosions, Pt II: Computer model for reverberation".
26. J.D. Shaffer, R.M. Fitzgerald & A.N. Guthrie, "Some effects of large-scale oceanography on acoustic propagation".
27. H.H. Essen, "Influence of internal waves on sound propagation in the SOFAR channel".
28. O.M. Johannessen, "A review of oceanic fronts".
29. R. Mellen & D.G. Browning, "Some acoustic effects of internal macrostructure".

Pt 6: Micro-scale phenomena

30. D.R. Del Balzo & W.B. Moseley, "Random temperature structure as a factor in long-range propagation".
31. J.J. McCoy, "Beam spreading and loss of spatial coherence in an inhomogeneous and fluctuating ocean".
32. R. Tait, "Internal oceanographic microstructure phenomena".
33. D. Mintzer, "Acoustic effects of internal microstructure".

Pt 7: Field calculations

34. S.N. Wolf, "Measurements of normal-mode amplitude functions in a nearly-stratified medium".
35. R.D. Graves, A. Nagl, H. Uberall, A.J. Haug & G.L. Zarur, "Range-dependent normal modes in underwater sound propagation".
36. J.A. Desanto, "Inverse wave propagation in an inhomogeneous waveguide".
37. A. Gille & D. Odero, "A solution of the wave sound equation in shallow water for real-speed profiles and solid bottom under-sediment".
38. D.J. Ramsdale, "A wave-theoretic method for estimating the effects of internal tides on acoustic wave transmission".
39. J.G. Schothorst, "Effect of ship motion on sonar detection performance".
40. C.W. Spofford & H. Garon, "Deterministic methods of sound-field computation".
41. R. Goodman, "Stochastic methods of sound-field computation".

Pt 8: Sonar models

42. B.B. Adams & G.R. Giellis, "A technique of comparative analysis of underwater-sound-transmission loss curves".
43. J.A. Desanto, "Connection between the solution of the Helmholtz and parabolic equations for sound propagation".
44. F. Dinapoli, "Computer models for underwater-sound propagation".
45. D. Wood, "Assessment techniques for computer models of sound propagation".

TABLE OF CONTENTS

Pt 7: Field Calculations

(Total number of printed pages in this document: 130)

MEASUREMENTS OF NORMAL-MODE AMPLITUDE FUNCTIONS IN A NEARLY-STRATIFIED MEDIUM*

S. N. Wolf

Naval Research Laboratory, Washington, D. C. 20375

Abstract

In normal-mode treatments of acoustic propagation in nearly-stratified media, calculations are frequently based on the perfectly-stratified medium model, in which symmetry permits separation of the wave equation. In these treatments the assumption is made that the normal-modes adapt to local conditions and that the modes are not coupled by the changing environment. This assumption is frequently referred to as the adiabatic approximation. An experiment was performed in a shallow water area near Jacksonville, Fla., in which observations were made of individual normal modes propagating over two sloping bottom tracks. Over the first track the water depth increased from 30 m at the source to 41 m at the receiver, with the maximum bottom slope (0.3°) at the receiver. Isovelocity conditions prevailed on this track. Over the second track the water depth decreased from 120 m to 42 m with the maximum slope (0.3°-0.9°) at the source positions. The vertical sound speed gradient on this track was slightly negative at the receiver and more sharply negative at the source. In both cases the constant depth model gave the vertical pressure distributions observed, in agreement with the assumption that the modes adapt to local conditions. Results from the first track are in agreement with the adiabatic approximation, however, propagation over the second track indicates the presence of mode coupling.

Introduction

In investigations of acoustic propagation in shallow water environments, extensive use has been made of the normal mode representation of the acoustic field introduced by Pekeris.[1] The original model which treated isovelocity water overlying a uniform semi-infinite sediment has been extended to treat perfectly-stratified ocean environments,[2] in which the acoustical properties are functions of depth only. A normal-mode computer program of a perfectly-stratified medium has been developed at NRL.[3] This program models the ocean environment as two finite-thickness fluid layers overlying a semi-infinite region which can be a fluid or a shear-supporting medium. The two finite layers, which are usually taken to be water and surficial sediments, may have a velocity profile which is an arbitrary function of depth. The model subbottom is uniform. Vertical pressure distributions and group velocities of individual normal modes measured in real ocean environments agree with predictions of this computer model.[4] The locations of the at-sea experiments had been chosen to provide propagation paths which closely approximated the perfectly-stratified-medium model.

Many shallow water areas of interest exhibit horizontal as well as vertical variability, so there exists the need for models of regions with range-dependent as well as depth-dependent acoustical properties. The extensions of perfectly-stratified normal mode theory to slowly varying (almost-stratified) media by Pierce[5] and Milder[6] make use of the adiabatic approximation.

This approximation is applied by assuming that the horizontal changes with range are sufficiently gradual that the wave equation separates locally. Properties of the normal-modes, such as vertical pressure distribution, are then obtained from the constant-depth model using the local environment information. In addition, if this approximation is valid, the normal-modes propagate without coupling, i.e. without the transfer of energy among modes.

An experiment measuring attenuation of normal-modes in a tank with a sloping rubber bottom was reported[7] by Eby, Williams, Ryan, and Tamarkin in 1960. The attenuation data were in agreement with a model using the adiabatic approximation in the calculation of the attenuation coefficient.

In November 1973 an experiment was performed by NRL to measure the vertical distribution of pressure in individual normal modes propagating over a sloping bottom. This paper compares the measured distributions with those predicted by the adiabatic approximation.

Summary of Theory

The geometry used in the mathematical model for the perfectly-stratified medium is shown in Fig. 1. The ocean environment is divided into three fluid layers, each of constant density. The upper two layers may have arbitrary sound speed dependence on depth. The sound speed in the subbottom is assumed constant. A point source of unit strength and angular frequency ω is located

at depth z_0. A receiver is located at depth z_1 and range r_1 from the source. The pressure at the receiver is given by

$$P\ (r,z_1,z_0) = \omega\rho_1{}^2 \left(\frac{1}{8\pi r}\right)^{\frac{1}{2}} \sum_{n=1}^{N} \frac{u_n(z_0)u_n(z_1)}{k_n^{\frac{1}{2}}}\ e^{i(k_n r-\omega t)-\delta_n r} \tag{1}$$

where δ_n is the modal attenuation coefficient and the $u_n(z)$ are solutions of the z-dependent part of the separated wave equation

$$\frac{d^2u_n}{dz^2} + \left(\frac{\omega^2}{c^2(z)} - k_n{}^2\right) u_n = 0 \tag{2}$$

subject to the appropriate boundary and normalization conditions. The dependence of the pressure amplitude of the nth mode on source and receiver depth is given by

$$P_n(z_1,z_0) \propto u_n(z_1)u_n(z_0) \tag{3}$$

where other parameters in Eq. 1, such as frequency and range are kept fixed. Verification of the proportionality (Eq. 3) in at-sea experiment has been reported by Ferris.[4]

If we apply the adiabatic approximation to the nearly-stratified medium case a similar expression is obtained:[8]

$$P_n(z_1,z_0) \propto u_n(z_1)u'_n(z_0) \tag{4}$$

Here u_n is the solution of Eq. 3 using the environment in the vicinity of the receiver and u'_n is obtained using the source's immediate environment. If the environments are significantly different, there will be a considerable change in the shape of the function u_n between source and receiver. The adiabatic approximation assumes that this change takes place very slowly and that energy is not exchanged among modes of propagation.

Experimental

The site of the experiment is shown in Fig. 2. A spar buoy supporting a string of 12 hydrophones was anchored at the location indicated by the numeral 1. The signals received by the hydrophone string were telemetered back to the source ship for recording. The source ship occupied the two stations to the west of the spar buoy and operated a 400 Hz source in a pulsed

mode at five depths at each station. A similar set of runs was made with the buoy at location 2 and the source ship occupying the three stations to the east of the buoy. The track extending west from the buoy will be referred to as the shallow propagation path, the other track, extending east from the buoy will be called the deep propagation path. The sound speed in the sediment was determined by seismic refraction techniques.[9]

Results

Bathymetry of the shallow propagation path is shown in Fig. 3. The bottom slope at the receiver (zero range) is about 0.3°. Also shown are water sound speed profiles measured at the receiver and at the two source stations. The profiles indicate essentially isovelocity conditions along the entire track. Bathymetry and sound speed profiles for the deep propagation path are shown in Fig. 4. The water depth at the receiver is the same (42 m) as for the shallow path. On the deep path the slope increases with range from the receiver to about 0.9° at the 16 km range station. In addition, a considerable change takes place in the sound speed profile. Near the receiver the profile gradient is slightly negative. At the source stations the profile gradient is more negative, becoming increasingly negative with range from the receiver.

Data obtained from pressure distribution measurements of the first mode on the shallow path are shown in Fig. 5. At zero range a typical measured variation of pressure with receiver depth, keeping source depth and range fixed, is shown as dots. The distribution predicted from the constant depth model is indicated by the line. The vertical pressure distribution in the vicinity of the sloping bottom is seen to be accurately calculated from the constant depth model. The data plotted at 9 and 18 km indicate the variation in signal strength as the source depth is varied. The receiver depth and range are held constant in each comparison. In these cases the variation of signal strength with source depth is given by the eigenfunction calculated using the constant depth model and the environment near the source. The data are consistent with the adiabatic approximation.

The dependence of the signal strength of the second mode on source and receiver depth is shown in Fig. 6. Again the constant-depth model is seen to predict the dependence of the signal strength on the source or receiver depth when the appropriate local environment is used. In signal strength vs source depth data the absolute value of the eigenfunction is plotted since phase changes implied by axis crossings could not be measured.

Variation of first mode signal strength for propagation over the deep path is shown in Fig. 7. The vertical pressure distribution at the receiver is shown at zero range. Agreement with the eigenfunction calculated from the constant depth model is still good. Variation of the signal strength with source depth shows good agreement at the 8 km station only. At the 12 and 16 km stations stations the constant depth model predicts the first mode to be "trapped" near the bottom by the negative gradient profile. In

several runs the source was placed in the upper part of the water column, where the first-mode eigenfunction is very small. If the adiabatic approximation is valid the first mode should be absent from the signal field. The first mode was observed with the relative strength indicated by the uppermost square. Agreement of the predicted and measured strength of the first mode at the 16 km station is very poor. Results for the second mode are shown in Fig. 8. Again the pressure distribution (zero range) at the receiver is predicted by the constant depth model and the receiver's immediate environment. Variation of the signal strength with source depth does not agree with predictions. Similar results shown in Fig. 9 were obtained for the third mode.

Conclusions

Measurements were made of vertical pressure distributions of individual normal modes propagating in two nearly-stratified ducts. In the first case the receiver was located over a sloping bottom. The slope (0.3°) is typical of shallow continental shelf areas. In the second case the water depth varied by a factor of 2 or 3 over the propagation path and a considerable change in sound-speed profile over the path was found. As a result there was a considerable change in the shape of the eigenfunction over the second track. In both cases the vertical pressure distribution of the modes observed was in agreement with the predictions of the constant-depth normal-mode model using the immediate environment of the receiver.

On the first path, where the change in depth was relatively small and isovelocity conditions prevailed along the entire track, the measured variation of signal strength with source depth was found to be in agreement with the predictions. Over the second path the water depth changed by a factor of two and the sound speed profile changed significantly. Here the predicted dependence of mode signal strength on source depth does not agree with the measured dependence. This disagreement may be due to the failure of the theory to calculate the excitation of the modes correctly, or it may be due to the conversion of energy from one mode to another by the environmental changes. The experimental results cannot be used to determine which of these possible causes is responsible since the signal strength of the individual modes was not measured near the source. It seems probable, however, that the excitation was calculated correctly, at least at the 8 km and 12 km stations. The bottom slope at the stations is less than at the receiver station on the first track, where local separability of the wave equation appeared to be a good approximation.

The deep propagation path exhibits a horizontal variability representative of continental shelf area waters. The indication of mode conversion along this path suggests that shallow water propagation models may need to include mode coupling effects.

References

*Research supported by the NAVSEA 06H1-4 and the Office of Naval Research

1. C. L. Pekeris, "Theory of Propagation of Explosive Sound in Shallow Water," Geol. Soc. Amer. Mem 27, 1-117 (1948).

2. See I. Tolstoy and C. S. Clay, "Ocean Acoustics: Theory and Experiment in Underwater Sound," McGraw Hill, Inc. (1966) as a general reference for normal-mode theory.

3. J. Miller and F. Ingenito, "Normal Mode FORTRAN Programs for Calculating Sound Propagation in the Ocean," NRL Memo Report 3071 (1975).

4. R. H. Ferris, "Comparison of Measured and Calculated Normal-Mode Amplitude Functions for Acoustic Waves in Shallow Water," J. Acoust. Soc. Amer. 52, 981 (1972).

5. A. D. Pierce, "Extension of the Method of Normal Modes to Sound Propagation in an Almost-Stratified Medium," J. Acoust. Soc. Amer. 37, 19 (1965).

6. D. M. Milder, "Ray and Wave Invariants for SOFAR Channel Propagation," J. Acoust. Soc. Amer. 46, 1259 (1969).

7. R. K. Eby, A. O. Williams, Jr., R. P. Ryan, and P. Tamarkin, "Study of Acoustic Propagation in a Two-Layer Model," J. Acoust. Soc. Amer. 32, 88-99 (1960).

8. A. O. Williams, Jr., and M. N. Lewis, "Approximate Normal-Mode Methods of Calculation for Sound Propagation in Shallow Water," Research Analysis Group (Brown University) Tech. Rept. 56-1 (May 1956).

9. H. S. Piper, Jr., "Analysis of Seismic Refraction Data from November-December 1973 Field Trip - Constant Depth Leg," Applied Research Laboratory (The Pennsylvania State University) Technical Memorandum TM 75-12 (1975).

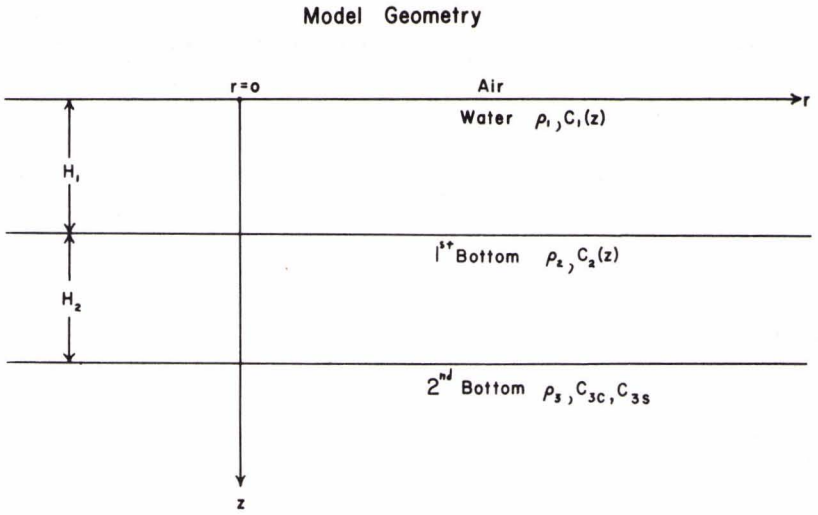

FIG. 1

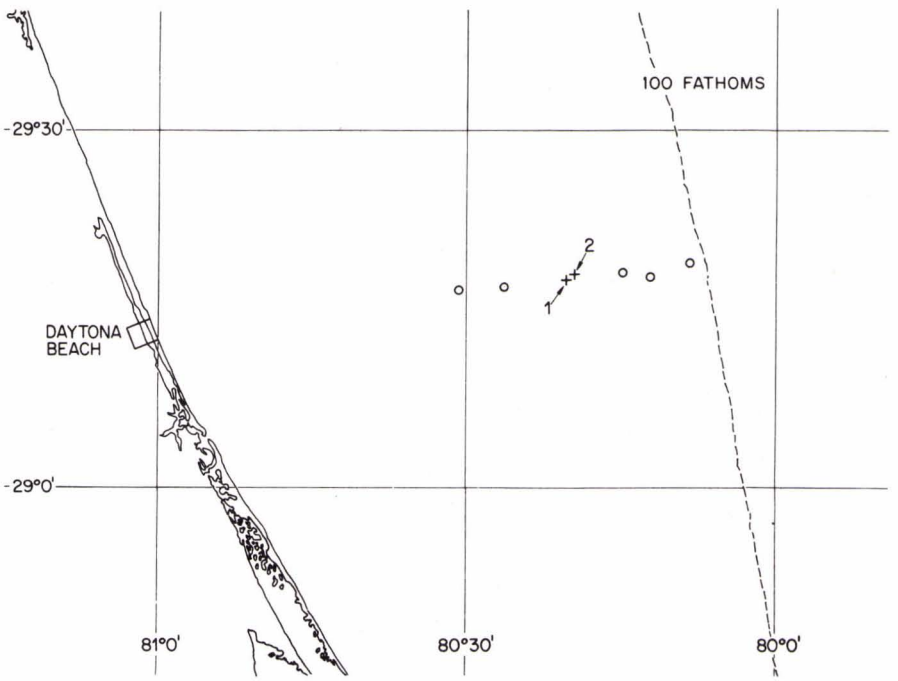

FIG. 2

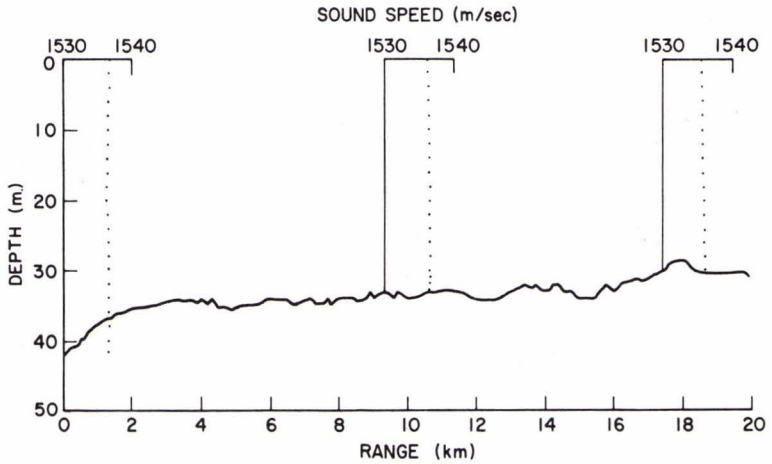

FIG. 3

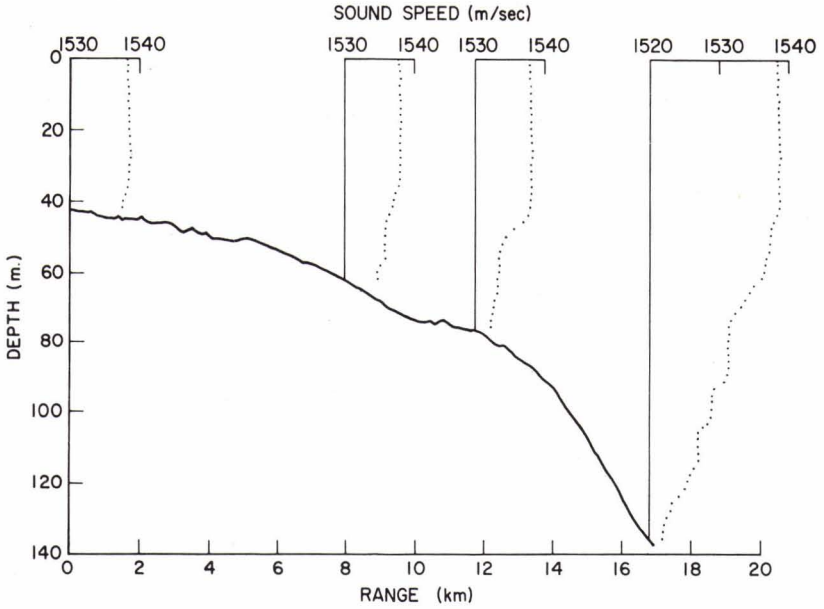

FIG. 4

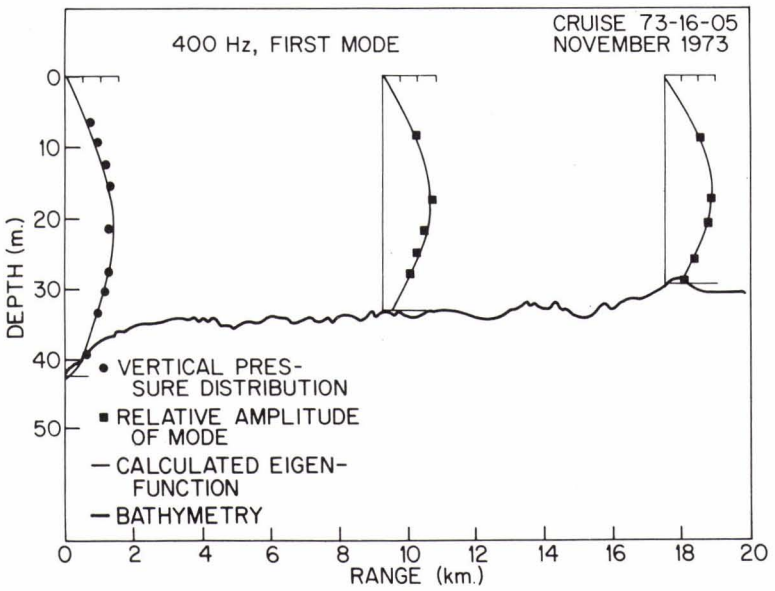

FIG. 5

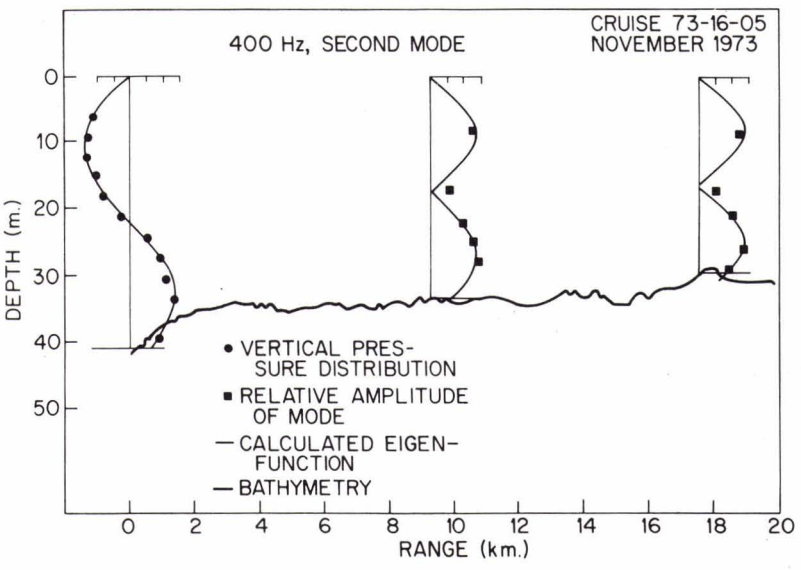

FIG. 6

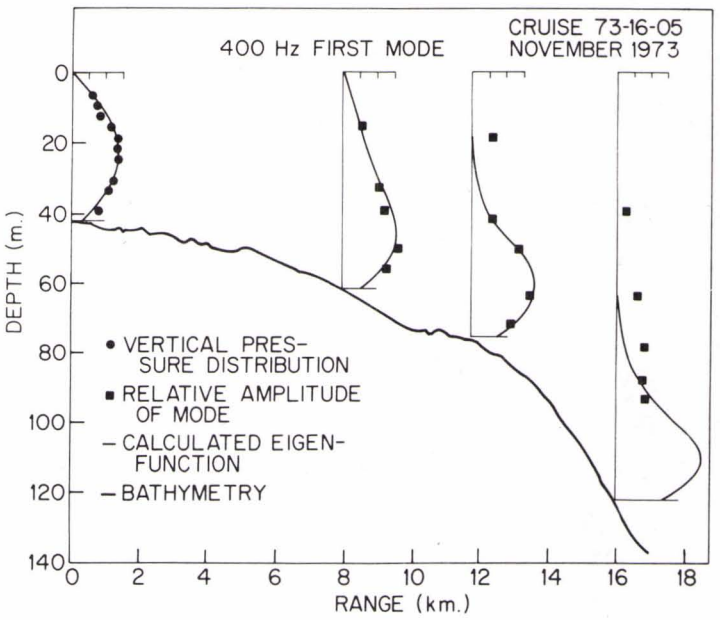

FIG. 7

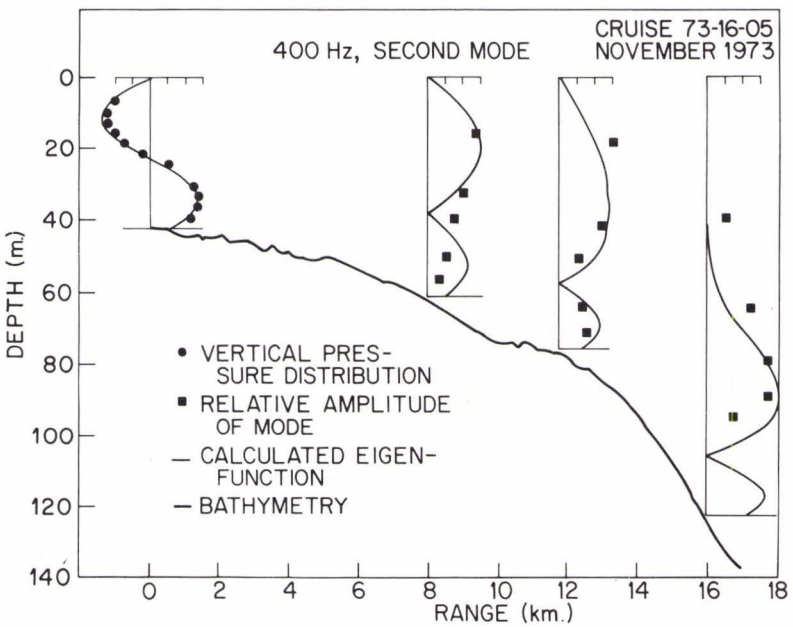

FIG. 8

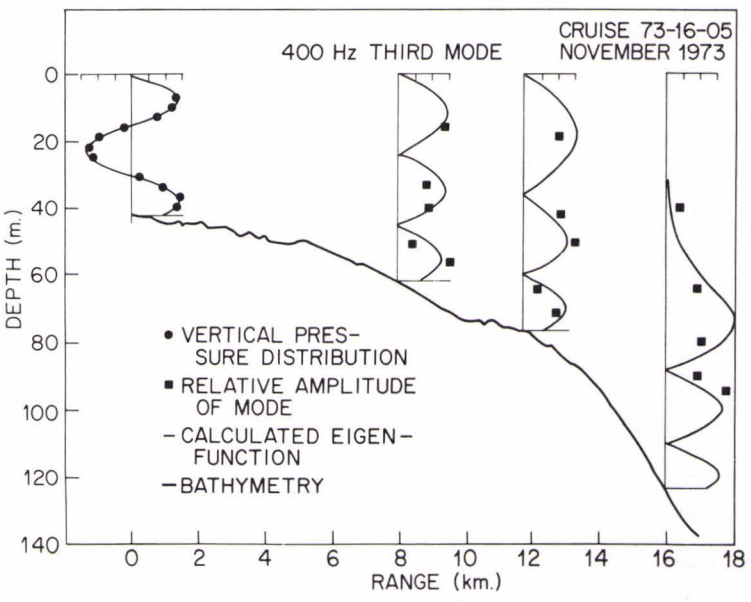

FIG. 9

RANGE DEPENDENT NORMAL MODES IN UNDERWATER SOUND PROPAGATION

by

Ronald D. Graves, Anton Nagl, and H. Uberall
Department of Physics, Catholic University
Washington, D.C.

Anton J. Haug
John Hopkins University Applied Physics Laboratory
Silver Spring, Md.

and

George L. Zarur
Versar Inc., Springfield, Virginia
U.S.A.

ABSTRACT

Normal mode theory is best suited for the case of stratified media. Range dependence of the medium properties and of its boundary may nevertheless be taken into account in the framework of an adiabatic approximation provided the changes with range are sufficiently gradual. We have extended this approach and have included possible range variations of the boundaries. To lowest order, the solution furnished by this method consists of the depth functions of a locally stratified medium; in higher order, the range functions satisfy a system of coupled equations, with the coupling terms causing an exchange of energy between modes. As an application, we have evaluated acoustic fields in an isovelocity wedge-shaped ocean (continental shelf) using the normal-mode method with adiabatic range variation, obtaining good agreement with the exact solution due to Bradley and Hudimac.

Normal mode theory of underwater sound propagation, as applied in the usual way, is useful for the case of stratified media where the wave equation separates. A range dependence of the medium properties (sound velocity profile) and of its boundaries may nevertheless be taken into account in the framework of an adiabatic approximation, provided the changes with range are sufficiently gradual. We have extended this approach, which was first indicated by Pierce[1] and by Milder[2] for the variable medium, and have included possible range variations of the boundaries. To lowest order, the solution furnished by this method contains the depth functions of a locally stratified medium, whose eigenvalues k_n at each range point enter in an equation for the range function that replaces the range function $H_o^{(1)}(k_n\rho)$ of the stratified case. To higher order (approaching the exact case), the range functions satisfy a system of coupled equations, with the coupling terms causing an exchange of energy between modes.

Starting from the wave equation corresponding to a point source in an inhomogeneous medium,

$$\nabla^2\phi(\vec{r}) + k^2(\vec{r})\,\phi(\vec{r}) = \delta(\vec{r}-\vec{r}_o) \qquad (1)$$

where $k(\vec{r}) = \omega/c(\vec{r})$, one attempts a "separation" in horizontal and vertical coordinates $\vec{r} = (\vec{\rho},z)$ of the form

$$\phi(\vec{r}) = \sum_n \psi_n(\vec{\rho})\,\mu_n(z,\vec{\rho})\ ; \qquad (2)$$

the "local depth functions" $u(z,\vec{\rho})$ satisfy the usual depth equation

$$\partial^2 u_n(z,\vec{\rho})/\partial z^2 + \left[k^2(z,\vec{\rho}) - k_n^2(\vec{\rho})\right] u_n(z,\vec{\rho}) = 0, \tag{3}$$

whose modal eigenvalues $k_n^2(\vec{\rho})$, determined from the boundary conditions at the boundaries $z = z_{\pm}(\vec{\rho})$, are now range dependent. Inserting (2) in (1) leads to a set of coupled range equations (source at $\vec{\rho} = 0$, $z = z_o$):

$$\begin{aligned}\left[\nabla_\rho^2 + k_n^2(\vec{\rho})\right]\psi_n(\vec{\rho}) &= \delta(\vec{\rho})\, u_n(z_o,0) \\ &- 2\sum_m \left[\vec{\nabla}_\rho \psi_m(\vec{\rho})\right] \cdot \int_{z_-}^{z_+} u_n(z,\vec{\rho})\, \vec{\nabla}_\rho u_m(z,\vec{\rho})\, dz \\ &- \sum_m \psi_m(\vec{\rho}) \int_{z_-}^{z_+} u_n(z,\vec{\rho})\, \nabla_\rho^2 u_m(z,\vec{\rho})\, dz .\end{aligned} \tag{4}$$

This is still an <u>exact</u> system of equations, but the lack of separability has led to the appearance of mode coupling terms, which will however be small for sufficiently gradual range dependence.

For the important special case where range variations take place in one horizontal direction only (x, say), the range function may be written as a Fourier integral,

$$\psi_n(\vec{\rho}) = \int_{-\infty}^{\infty} g_n(x,k_y)\, e^{ik_y y}\, dk_y/2\pi \tag{5}$$

Inserting in (4) and neglecting mode coupling, one finds the range equation

$$\left\{d^2/dx^2 + \left[k_n^2(x) - k_y^2\right]\right\} g_n(x,k_y) = u_n(z_o,0)\,\delta(x). \tag{6}$$

We first solved the special case of an isovelocity wedge-shaped ocean, with the origin at the shore, the source at $\vec{r}_o = (x_o, 0, z_o)$, and the ocean floor given by $z_+ \equiv h(x) = h_o(x/x_o)$, h_o being the ocean depth at the source location. We obtained the exact solution (without mode coupling)

$$\phi(\vec{r}) = (x_o/2ih_o) \sum_{n=0}^{\infty} \sin\left[(n+\tfrac{1}{2})\pi z/h\right] \sin\left[(n+\tfrac{1}{2})\pi z_o/h_o\right] \cdot \int_{-\infty}^{\infty} J_{\nu_n}(k_x x_<) H_{\nu_n}^{(1)}(k_x x_>) \exp(ik_y y)\, dk_y \tag{7}$$

where $x_{\gtrless} = \max, \min\,(x, x_o)$, and

$$\nu_n = \left\{ \tfrac{1}{4} + \left[(n+\tfrac{1}{2})\pi x_o/h_o\right]^2 \right\}^{1/2} \tag{8}$$

If $x_> \gg x_<$, a saddle-point evaluation of (7) gives

$$\phi(\vec{r}) = (x_o/h_o r)\exp(ikr) \sum_{n=0}^{\infty} \sin\left[(n+\tfrac{1}{2})\pi z/h\right] \sin\left[(n+\tfrac{1}{2})\pi z_o/h_o\right] \exp(-\tfrac{1}{2}i\pi\nu_n)\, J_{\nu_n}(kx_> x_</r), \tag{9}$$

where $r = (x_>^2 + y^2)^{\frac{1}{2}}$.

As a numerical example, we chose a free-surface, rigid-bottom wedge with $h_o/x_o = 0.2$, with the source located at $x_o = 25\lambda$, $z_o = (1/3)h_o$. The acoustic intensity $|\phi|^2$ obtained from (9) is shown in Fig. 1 in the plane $y = 0$, plotted vs. x/λ between 0 and 10. Modes cut off at positions indicated by arrows. Contour lines represent intensity variations in steps of 3 dB for three contours of highest intensity, and 6 dB otherwise. The results are compared in Fig. 2 with $|\phi|^2$ calculated from the exact solution of the same wedge problem, as found by Bradley and Hudimac[3], and likewise evaluated by the saddle point method. Small differences can be observed between the lower

right portion of the figures, and are probably attributable to mode coupling effects.

A computer program has been developed by us for solving the adiabatic range equation (Eq. (4) without coupling) for realistic sound velocity profiles with arbitrary (but gradual) variations in range, and similar variations of the ocean floor[4]; this is now being extended to the system of Eqs. (4) including the coupling. The same method is used for the depth equation (3) also, in order to apply a unified treatment to all parts of the problem.

To solve the depth equation, we divide the ocean into P horizontal layers (P $\sim$ 10 for practical purposes), and linearize the wave number $k^2(z,\vec{\rho})$ at each range point $\vec{\rho}$, so that in the p^{th} layer

$$k_p^2(z,\vec{\rho}) = \alpha_p(\vec{\rho}) + \beta_p(\vec{\rho})\left[z_{p-1}(\vec{\rho}) - z\right], \tag{10}$$

z_{p-1} being the interface between layers p-1 and p. With the new variable in the p^{th} layer

$$\zeta_{np}(z) = \left[\beta_p^2(\vec{\rho})\right]^{-1/3}\left\{\alpha_p(\vec{\rho}) + \beta_p(\vec{\rho})\left[z - z_{p-1}(\vec{\rho})\right] + k_n^2(\vec{\rho})\right\}, \tag{11}$$

the solutions of (3) are the Airy functions[5]

$$u_{np}(z,\vec{\rho}) = A_{np}(\vec{\rho})\,Ai\left(\zeta_{np}(z)\right) + B_{np}(\vec{\rho})\,Bi\left(\zeta_{np}(z)\right). \tag{12}$$

The boundary conditions at each interface, i.e. $u_{np}(z,\vec{\rho})$ and $\partial u_{np}(z,\vec{\rho})/\partial z$ to be continuous, permit to evaluate all the coefficients A_{np}, B_{np} as follows. At each interface, A_{np} and

B_{np} may be expressed by A_{np-1} and B_{np-1}. The one condition at the ocean surface z=0, namely $u_{n1}(0,\vec{\rho}) = 0$, determines A_1, while B_1 may be fixed by the overall normalization of u_n. At the ocean floor, a decaying exponential for u_{nP+1} ($B_{nP+1} \equiv 0$) matched to u_{nP} determines A_{nP+1}, while matching of the derivative furnishes the eigenvalue equation for $k_n(\vec{\rho})$.

The analogous treatment for the uncoupled range equation, in the form of e.g. Eq. (6), now linearizes the quantity $k_n^2(x) - k_y^2$, where $k_n(x)$ is obtained by solving the eigenvalue equation at the boundaries x_m of the range intervals, the subdivisions ranging from x_{-M} to x_M (with the source at $x = x_0 \equiv 0$):

$$k_n^2(x) - k_y^2 = a_m + b_m (x_{m-1} - x). \tag{13}$$

With the new variable

$$r_{nm}(x) = \left[b_m^2\right]^{-1/3} \left[b_m (x - x_{m-1}) - a_m\right], \tag{14}$$

one again has the Airy function solutions

$$g_{nm}(x) = A_{nm} Ai(r_{nm}) + B_{nm} Bi(r_{nm}). \tag{15}$$

Boundary conditions in the adiabatic case are again the continuity of $g_{nm}(x)$ and $dg_{nm}(x)/dx$ at each interface. At $x > |x_{\pm M}|$, however, one now has a radiation condition which requires outgoing waves only as $x \to \pm\infty$, while in all finite intervals in the region $x < |x_{\pm M}|$, the solutions (15) represent both in- and outgoing waves, so that in contrast to the now-fashionable

PE (parabolic equation) method[6], the possibility of backscattering towards the source is always present. Modes that have cut off by the time they reach $x = x_{\pm M}$, are matched to decaying exponentials, of course. The coefficients of the outgoing or decaying exponentials in $x > x_M$ or $x < x_{-M}$ are denoted by A_{nM+1} or $A_{n,-M-1}$, respectively .

If the coefficients of the solution (15) are normalized by

$$\alpha_{nm} = A_{nm}/A_{n,M+1}\,, \quad \beta_{nm} = B_{nm}/A_{n,M+1} \qquad (m>0),$$

$$\alpha_{nm} = A_{nm}/A_{n,-M-1}\,, \quad \beta_{nm} = B_{nm}/A_{n,-M-1} \qquad (m<0), \tag{16}$$

then the mentioned radiation condition determines $\alpha_{n,\pm M}$ and $\beta_{n,\pm M}$ completely, and by further matching at all successive boundaries of segments, all other coefficients are determined down to $\alpha_{n,\pm 1}$ and $\beta_{n,\pm 1}$. Accordingly, the only two unknowns left are the common denominators $A_{n,M+1}$ and $A_{n,-M-1}$. These cannot be determined from the normalization, but from the requirements that the solution of Eq. (6), which actually is the Green's function of the problem, (i) be continuous at $x = 0$, and (ii) have a discontinuity in slope such that the source strength in (6) is reproduced. Satisfying these condition completely solves the range-dependent problem (in the case of x-dependence only).

This approach is now being programmed by us, together with the case of cylindrical-coordinate range variation (ρ dependence only). The latter solution will be utilized for

"patching up" the solution of the PE method in regions where the latter becomes unreliable, either due to equivalent ray angles exceeding inclinations of $\sim 20^{\circ}$ (i.e. propagation up-slope, or over a seamount), or near the source. The ρ-dependent case is, however, less general than the x-dependent one, since it cannot describe e.g. sound propagating up the continental shelf at an angle, and being deflected back out to sea. Numerical results of our range-dependent normal-mode program will be published elsewhere.

References

*Supported by the Office of Naval Research, Code 486.

1. A. Pierce, J. Acoust. Soc. Am. 37, 19 (1965).

2. D.M. Milder, J. Acoust. Soc. Am. 46, 1259 (1969).

3. D. Bradley and A.A. Hudimac, Naval Ordnance Laboratory Technical Report NOLTR 70-325, November 1970.

4. For a WKB approach to this problem, cf. F. Ingenito, Proceed. Saclant Cen. Conference on Sound Propagation in Shallow Water, Sept. 1974.

5. Cf., e.g., D.C. Stickler, J. Acoust. Soc. Am. 57, 856 (1975).

6. R.H. Hardin and F.D. Tappert, Siam Review 15, 423 (1973).

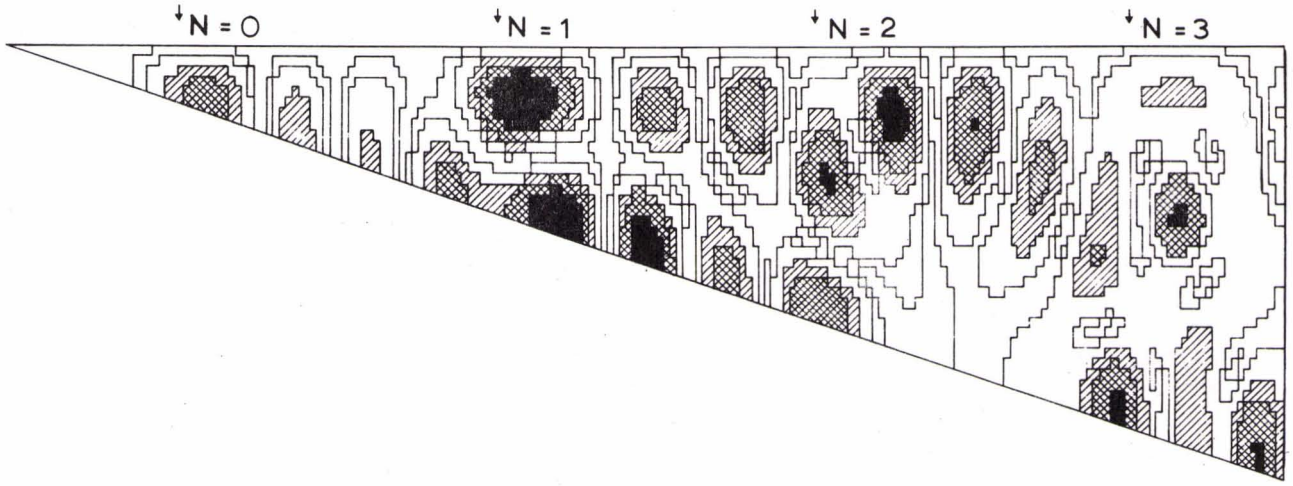

FIG. 1

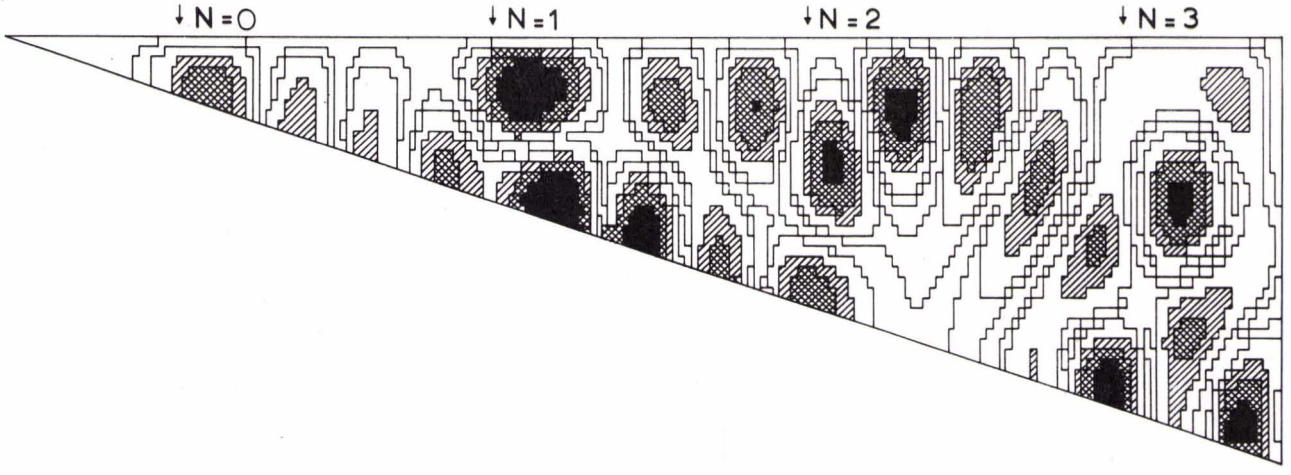

FIG. 2

INVERSE WAVE PROPAGATION IN AN INHOMOGENEOUS WAVEGUIDE

John A DeSanto, Naval Research Laboratory,
Washington, DC, and Admiralty Research Laboratory,
Teddington, England*

ABSTRACT

A solution is given for the problem of inverse propagation in an inhomogeneous rectangular two-dimensional waveguide. The sound speed is assumed to vary in depth and inverse propagation means the calculation of the field at range x_1 in terms of the field at range x_2 where $x_2 > x_1$. The method is analogous to that used by Wolf, Shewell, and Lalor for the inverse diffraction problem in a homogeneous half space. It is found that the field at x_1 can be expressed in terms of two integrals over the field at x_2. The kernel of the first integral is bounded and expresses physically the result at x_1 of the waves at x_2 reversing their direction of propagation and decay, ie they now propagate and decay in the direction of x_1. A reciprocity relation for this term is possible. The kernel of the second integral is singular and expresses the mathematical fact of the residual effect of the evanescent waves at x_1 as they reverse their direction at x_2 and now grow exponentially. Consequences of the neglect of this singular term are discussed.

INTRODUCTION

Recently, Wolf and Shewell[1] and Lalor[2] discussed the solution of the inverse diffraction problem in a homogeneous half-space. Simply, one has a field propagating into a half-space $z > 0$, and assumes the field is known on some plane $z = z_2$. The problem is then to find the field on the plane $z = z_1$ where $z_1 < z_2$. For example, one might wish to calculate the "near" field from the "far" field. The result is expressed as the inverse of one of the Rayleigh diffraction formulas. The kernel of the inversion contains two terms, one of which is singular. Methods for handling the singular term are discussed.

In this paper we briefly present a similar analysis with the problem being the calculation of the inverse field in a two-dimensional rectangular waveguide. Here, in addition, the waveguide is assumed to be inhomogeneous in the sense that the sound speed is a function of depth.

In Sec. 1 we present the basic analysis and express the field at $x_1 < x_2$ as a sum of two terms each of which is an integral over the field at x_2. The kernel of the first integral is bounded and the term describes that part of the field at x_1 due to waves at x_2 reversing their direction of propagation and decay. The kernel of the second integral is singular and the term describes exponentially growing waves at x_1 due to evanescent waves at x_2 which grow towards x_1. In Sec. 2 the reciprocity relation of the first term is derived, and in Sec. 3 a brief discussion is given of the consequences of neglect of the singular term.

1. GENERAL FORMALISM

In two dimensions the propagation of sound is governed by the Helmholtz equation

$$\phi_{xx} + \phi_{zz} + k^2\eta^2(z)\phi(x,z) = 0 \tag{1}$$

for the velocity potential field ϕ.[3] Here, $\eta(z)$, the index of refraction, is proportional to the inverse of $c(z)$, the sound speed, and $k = 2\pi/\lambda$ is the wavenumber with λ the wavelength. Since c is a function of depth the equation is said to be inhomogeneous. The general problem of sound propagation involves the solution of (1) assuming that ϕ satisfies appropriate boundary conditions. Here we first wish to solve (1) in the region $0 \leq z \leq D$ and $0 \leq x < \infty$ (see Fig. 1), where ϕ satisfies boundary conditions at $z = 0$ and D, $x = 0$, and an outgoing radiation condition as $x \to \infty$. Then we will assume that the field is known on a (far) plane $x = x_2$ and express the field on a (near) plane $x = x_1 < x_2$ in terms of the field on x_2.

The solution of (1) is separable and can be written in terms of an infinite discrete spectral representation

$$\phi(x,z) = \sum_{j=0}^{\infty} A_j\psi_j(z)\exp(ikm_jx) \tag{2}$$

where the eigenfunctions ψ_j satisfy the ordinary differential equation

$$\psi_j'' + k^2[\mu_j - q(z)]\,\psi_j = 0 \tag{3}$$

with

$$q(z) = 1 - \eta^2(z) \tag{4}$$

and

$$m_j = \begin{cases} (1 - \mu_j)^{\frac{1}{2}} & 0 < \mu_j \leq 1 \\ +\,i(\mu_j - 1)^{\frac{1}{2}} & \mu_j > 1 \end{cases} \tag{5}$$

The boundary conditions at $z = 0$ and D (which we do not specify) yield specific forms for the ψ_j and the discrete eigenvalues μ_j, which we assume for simplicity are confined to the positive real axis in the j-plane. The choice of branch in (5) is to ensure outgoing or decaying waves as $x \to \infty$. In addition we assume the ψ_j are orthonormal.

$$\int_0^D \psi_j(z)\psi_m(z)dz = \delta_{jm} = \begin{cases} 1 & j = m \\ 0 & j \neq m \end{cases} \tag{6}$$

Multiplying (2) by $\psi_i(z)$, integrating over z from 0 to D and using (6) yields

$$A_j = \exp(-ik\, m_j x) \int_0^D \phi(x,z)\psi_j(z)dz. \tag{7}$$

Now let $x = x_1$ and $z = z_1$ in (2), $x = x_2$ and $z = z_2$ in (7), and substitute the resulting (7) into (2) to get

$$\phi\,(x_1,z_1) = \sum_{j=0}^{\infty} \psi_j(z_1)\exp\,[\,ikm_j(x_1-x_2)]\int_0^D \psi_j(z_2)\phi(x_2,z_2)dz_2. \tag{8}$$

Next assume $x_1 < x_2$ and split the sum in (8) into two parts defined by

$$\sum\nolimits^{-} = \sum_{j=0}^{J} \qquad \sum\nolimits^{+} = \sum_{j=J+1}^{\infty} \tag{9}$$

where $\mu_J < 1$ and $\mu_{J+1} > 1$. To the result, add and subtract the term

$$\sum\nolimits^{+} \psi_j(z_1)\exp\{-k(\mu_j-1)^{\frac{1}{2}}(x_2-x_1)\}\int_0^D \psi_j(z_2)\phi\,(x_2,z_2)dz_2 \tag{10}$$

and rewrite the result as the sum of two terms

$$\phi(x_1,z_1) = \phi_1(x_1,z_1) + \phi_2(x_2,z_2) \tag{11}$$

where we define $(m = 1,2)$

$$\phi_m(x_1,z_1) = \int K_m(x_1,z_1;\ x_2,z_2)\phi\ (x_2,z_2)dz_2 \tag{12}$$

with

$$K_1(x_1,z_1;\ x_2,z_2) = \sum^{-} \psi_j(z_1)\psi_j(z_2)\exp[\,ikm_j(x_1-x_2)]$$

$$+ \sum^{+} \psi_j(z_1)\psi_j(z_2)\exp[\,-k(\mu_j-1)^{\frac{1}{2}}(x_2-x_1)]$$

$$= \sum_{j=0}^{\infty} \psi_j(z_1)\psi_j(z_2)\exp[\,-ikm_j^{*}(x_2-x_1)] \tag{13}$$

where the * is complex conjugation, and

$$K_2(x_1,z_1;\ x_2,z_2) = \sum^{+} \psi_j(z_1)\psi_j(z_2)\exp[\,ikm_j(x_1-x_2)]$$

$$+ \sum^{+} \psi_j(z_1)\psi_j(z_2)\exp[\,-k(\mu_j-1)^{\frac{1}{2}}(x_2-x_1)]$$

$$= \sum^{+} \psi_j(z_1)\psi_j(z_2)\sinh[\,k(\mu_j-1)^{\frac{1}{2}}(x_2-x_1)]\,. \tag{14}$$

Thus it is possible to write ϕ at (x_1,z_1) in terms of two integrals over ϕ at (x_2,z_2). The kernel of the first integral, K_1, is bounded and expresses physically the result at x_1 of the waves at x_2 reversing

their direction of propagation and decay, ie they now propagate and decay in the direction of x_1. The kernel of the second integral, K_2, is singular since the summation in (14) goes to infinity, and the problem becomes ill-posed since a small change in the "initial" condition $\phi(x_2,z_2)$ could produce a large change in $\phi(x_1,z_1)$. This is the mathematical expression of the residual effect of the evanescent waves at x_2 as they reverse their direction and grow exponentially in the direction of x_1. The neglect of this latter term means neglect of large wavenumbers, short wavelength terms and hence an inability to gather information on an obstacle or process with a characteristic length smaller than a certain amount. There is thus a lower bound on the size of obstacles which can be seen.

2. RECIPROCITY

It is possible to express the ϕ_1 term as the inverse of one of the Rayleigh diffraction formulas. This is done as follows. The incoming wave Green's function $G^-(x,z;\ x',z')$ satisfies an equation similar to (1) with a delta function source term

$$G^-_{xx} + G^-_{zz} + k^2\eta^2(z)G^- = -\delta(x-x')\delta(z-z') \tag{15}$$

as well as the boundary conditions at $z = 0$ and D which are satisfied by the eigenfunctions, and the asymptotic condition of an incoming wave. It can be written as

$$G^-(x,z;\ x',z') = \sum_{j=0}^{\infty} \psi_j(z)\psi_j(z')G^-_j(x,x') \tag{16}$$

where G^-_j satisfies the differential equation

$$\left\{ \frac{d^2}{dx^2} + k^2(1-\mu_j) \right\} G^-_j(x,x') = -\delta(x-x') \tag{17}$$

and can be written as

$$G^-_j(x,x') = (2ikm^*_j)^{-1} \exp\{-ikm^*_j|x-x'|\} \tag{18}$$

where the complex conjugate of m_j is used in the exponential to ensure that for $j > J$ the function is decaying towards x_1. From (14) it can be easily seen that

$$K_1(x_1,z_1;\ x_2,z_2) = -2\frac{\partial}{\partial x_2} G^-(x_1,z_1;\ x_2,z_2) \tag{19}$$

so that ϕ_1 by (12) can be written as the inverse of a diffraction formula.

3. SUMMARY

To use these results one must be able to neglect the singular term ϕ_2. Neglect of ϕ_2 means neglect of terms of the order of $k(\mu_{J+1}-1)^{\frac{1}{2}}$ and larger, ie high frequency terms. The term $k = \omega/c$ where c is some reference sound speed, eg the sound speed at the surface. This establishes a characteristic length $L = \lambda/2\pi(\mu_{J+1}-1)^{\frac{1}{2}}$ below which we cannot measure. The higher the frequency of sound the smaller the obstacles we can see, but high frequency sound is rapidly attenuated in the ocean anyway, so that neglect of ϕ_2 probably yields no worse results than are now available.

Footnotes

* Temporary Address

1. E. Wolf and J. R. Shewell, Phys. Lett. 25A, 417 (1967) and 26A, 104 (1967)
2. E. Lalor, J. Math. Phys. 9, 2001 (1968) and J. Opt. Soc. Am. 58, 1235 (1968). These papers also consider similar mathematical questions which arise here in greater detail.
3. The harmonic time dependence exp(-iωt) is assumed throughout.

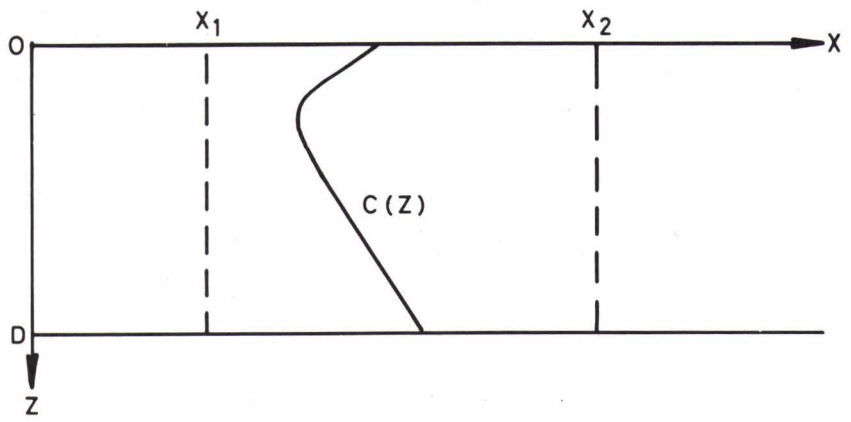

FIG. 1 INVERSE PROPAGATION IN A RECTANGULAR TWO-DIMENSIONAL WAVEGUIDE. THE SOUND SPEED C IS A FUNCTION OF DEPTH Z. THE FIELD IS ASSUMED KNOWN ON THE PLANE $X = X_2$ AND THE PROBLEM IS TO CALCULATE IT ON THE PLANE $X = X_1$

A SOLUTION OF THE WAVE SOUND EQUATION IN SHALLOW WATER FOR REAL SPEED PROFILES AND SOLID BOTTOM UNDER SEDIMENT

by

A. Gilles and D. Odero
CIT-ALCATEL Marine Dpt
Arcueil 94110, France

ABSTRACT

The wave equation has been solved by using normal mode theory. The medium is assumed to be horizontally stratified. A closed form solution has been found in the case of GANS - PEDERSEN types of density and sound-speed profiles. For real profiles of any given shape a numerical solution is employed that makes use of the VOLTERRA integral equation.

1 - INTRODUCTION

The use of normal modes theory for the calculation of shallow water sound propagation has first been developed by PEKERIS (Ref. 1, 2, 3) in 1948. His model was oversimplified as the sound speed was assumed to be constant in the water and the sea bottom was taken as an homogeneous fluid halfspace. A number of attempts have been made since to account for the variation of sound speed with depth : we can mention for instance a computer program worked out by NEWMAN and INGENITO (Ref. 4) for a two fluid model with the speed of sound varying with depth in the first fluid. This program makes use of the finite differences technique.

We develop herein a more realistic model based on a mode formulation exposed chapter 2 which is valid for horizontally stratified media (physical characteristics depending on depth only). This assumption enables the initial propagation equation to be transformed into a HELMHOLTZ type equation.

In our development the medium is taken as follows :

Sea water bounded by the atmosphere (plane surface) and infinite elastic bottom with or without an intermediate fluid layer corresponding to the sediment.

* 1, av. A. Briand ARCUEIL 94110 FRANCE

In the water and the sediment the sound speed may vary with depth in any given manner. In the elastic bottom, both compressional and shear velocities are constant .

The density may vary with depth in the sediment and it stays constant in the water and the elastic bottom (although it could vary in the former if wanted).

The sound field dealt with is that created by an omnidirectional monochromatic point source.

The formulation developed in chapter 2 will be applied in chapter 3 to analytic velocity and density profiles of the GANS-PEDERSEN type. In chapter 4, it will be applied to realistic profiles of any shape given by a discrete number of data points.

2 - FORMULATION OF THE PROBLEM.

2.1 Sound propagation equation.

Let $\Psi(\vec{r},t)$ be the velocity potential.
By definition, the acoustic pressure $p(\vec{r},t)$ and the displacement velocity $\vec{v}(\vec{r},t)$ of a fluid element are given by :

$$(1)\quad p(\vec{r},t) = \rho \frac{\partial \Psi(\vec{r},t)}{\partial t} \; ; \; \vec{v}(\vec{r},t) = - \vec{\text{grad}}\, \Psi(\vec{r},t)$$

Taking into account the equations of motion and mass conservation and the state equation relating acoustic pressure to density variation, the potential $\Psi(\vec{r},t)$ obeys the following equation (first order approximation).

$$(2)\quad \Delta \Psi - \frac{1}{C^2(z)} \frac{\partial^2 \Psi}{\partial t^2} - \frac{1}{\rho(z)} \frac{d\rho}{dz} \frac{\partial \Psi}{\partial z} = - 4\pi\delta(\vec{r} - \vec{r}_e)\, e^{j\omega t}$$

where C(z) is the speed of sound in the fluids (water or sediment) and ρ (z) the fluid density. The second member of equation (2) represents the source term :

$\vec{r}$ and $\vec{r}_e$ are the vectors joining the origin of the referential to the point of observation and to the source respectively. Owing to the symmetry of revolution, one can make use of only two cylindrical coordinates r and z.

Therefore, Ψ $(\vec{r},t)$ takes the form:

(3) Ψ $(\vec{r},t) = \Phi'(r,z)\, e^{j\omega t}$

Equation 2 can be solved by using the HANKEL Transform of $\Phi'(r,z)$.

The wanted fonction $\Phi'(r,z)$ is a solution of the equation :

$$(4) \qquad \Phi'(r,z) = \frac{-1}{J\pi} \int_{-j\infty}^{+j\infty} \Phi(z,s)\, K_0(sr)\, sds$$

where K_0 (sr) is the zero order second kind modified BESSEL function.

The $\Phi(z,s)$ function is a solution of the equation :

$$(5) \quad \frac{d^2\Phi}{dz^2} + \left[\frac{\omega^2}{C^2(z)} + S^2\right]\Phi - \frac{1}{\rho(z)}\frac{d\rho}{dz}\frac{d\Phi}{dz} = = 2\pi\delta(z - z_e)$$

where r is the horizontal range between source and observation point and z is the depth below sea level.

The s variable is a parameter that comes in when applying the HANKEL transform and that physically corresponds to the horizontal component of the wave vector.

In order to obtain the velocity potential, it is therefore necessary to first solve equation (5) and obtain the Φ (z,s) function, and then calculate integral (4).

The second order differential equation (5) obeys certain boundary conditions at the various interface levels : air-water, water-sediment, sediment-rock, which makes it a STURM-LIOUVILLE problem.

Note : The K_o function is found here instead of the usual J_o function because of the choice we made in writing $+ s^2$ in equation 5 (instead of $- s^2$). Changing s into $- js$ would lead to the forms mostly encountered in the literature. In the same way, there will be a change from real to imaginary and vice-versa when speaking of poles, integration contours, etc ....

2.2 Formulation of the boundary conditions.

Crossing (or boundary) conditions arise at each change of medium :

- Air-water interface ($z = 0$ plane) : acoustic pressure is null
- Water-sediment interface ($z = z_1$ plane) : pressure is continuous and the fluids undergo the same vertical motions on each side of the boundary
- Sediment-rock interface ($z = z_2$ plane) : the T_{zz} term of the stress tensor that acts on the elastic medium at $z = z_2+0$ must balance the pressure acting on the other side (at $z = z_2 - 0$). Furthermore, the boundary must undergo the same displacement as seen from each side. These two conditions lead to the following homogeneous condition :

$$(6)\quad \frac{1}{\rho_1(z_2)}\,\frac{1}{\Phi(z_2)}\,\frac{\partial\Phi}{\partial z}\bigg|_{z_2-0} = \frac{1}{\rho_2}\,\frac{1}{T_{zz}}\,\frac{\partial T_{zz}}{\partial z}\bigg|_{z_2+0} = K(s)$$

where the function Φ is a solution of (5) and where ρ_1 and ρ_2 are the specific masses in the sediment and the rock respectively. It can be demonstrated that the term K(s) may be expressed as a function of the compressional and shear velocities in the rock C_L and C_T, the variable s being the same as the one introduced in equation (4).
One would find :

$$(7)\quad K(s) = -\frac{j}{4\rho_2}\frac{\omega^4}{C_T^4}\frac{a}{\left[s^2+\frac{\omega^2}{2C_T^2}\right]^2 - abs^2}$$

where

$$a = \left[\frac{\omega^2}{C_L^2} + s^2\right]^{1/2} \quad ; \quad b = \left[\frac{\omega^2}{C_T^2} + s^2\right]^{1/2}$$

The fact that the acoustic field must vanish at infinite distance leads the determinations to be taken for a and b.

- Source level plane ($z = z_e$) : the source condition can be transformed into a boundary condition at the source horizontal plane as follows :
Continuity of pressure and opposite direction of the fluid motion on each side of the plane, leading :

$$(8)\quad \left.\frac{\partial\Phi}{\partial z}\right|_{z_{e-0}} - \left.\frac{\partial\Phi}{\partial z}\right|_{z_{e+0}} = -2$$

2.3 Solution of equation (5)

Let $\phi(z,s)$ be a solution of equation (5) that meets the previously exposed boundary conditions at z = 0, viz :

$$(9)\quad \phi(0,s) = 0 \; ; \; \frac{1}{\rho(0)}\frac{\partial\phi(0,s)}{\partial z} = 1$$

Let $\psi(z,s)$ be a solution of equation (5) that meets the boundary conditions at $z = z_2$, viz :

$$\psi(z,s) = \psi_1(z,s) + K(s)\,\psi_2(z,s)$$

with :

(10) $$\psi_1(z_2,s) = 1 \quad ; \quad \psi_2(z_2,s) = 0$$

$$\frac{1}{\rho(z_2)} \frac{\partial\psi_2}{\partial z}\bigg|_{z=z_2} = 1 \quad ; \quad \frac{1}{\rho(z_2)} \frac{\partial\psi_1}{\partial z}\bigg|_{z=z_2} = 0$$

If these two functions $\phi(z,s)$ and $\psi(z,s)$ are linearly independant, the solution of equation (5) that obeys the three sets of conditions : surface, bottom and source, is given by the GREEN'S function :

(11) $$\Phi(z,z_e,s) = \begin{cases} -2\,\dfrac{\psi(z_e,s)\phi(z,s)}{\rho(0)\psi(0,s)} & 0 < z < z_e < z_2 \\[2ex] -2\,\dfrac{\phi(z_e,s)\psi(0,s)}{\rho(0)\psi(0,s)} & 0 < z_e < z < z_2 \end{cases}$$

It must be emphasized that solution (11) to equation (5) is not analytically known. We have just expressed the conditions to be fulfilled by the functions that are solutions of the problem described. These conditions are necessary and sufficient for all functions ϕ and ψ that meet conditions (9) and (10) respectively to give rise to a function Φ , solution to the problem.

2.4 Solution of equation (4) - Choice of the integration contour in the complex s plane.

The Φ (z, z_e, s) function just described is a complex function that has a certain number of poles s_n (complex, imaginary or real). These poles are the zeros of Ψ (0,s).(Here the STURM-LIOUVILLE problem is not an hermitian one).

From the expression for K(s) and the determinations chosen for a and b,the integration has to be made in the Re (s) $\geqslant$ 0 plane.

The cuts at $\pm j\bar{\omega}/C_L$ and $\pm j\omega/C_T$ have been chosen so that only two of them are in the halfspace $R_e(s) > 0$ and they are parallel to the s real axis. The poles s_n of function Φ are simple and located in the fourth quadrant of the complex plane and so are their symetricals with respect to the origin, located in the second quadrant .

The chosen integration contour C is illustrated in figure 1.

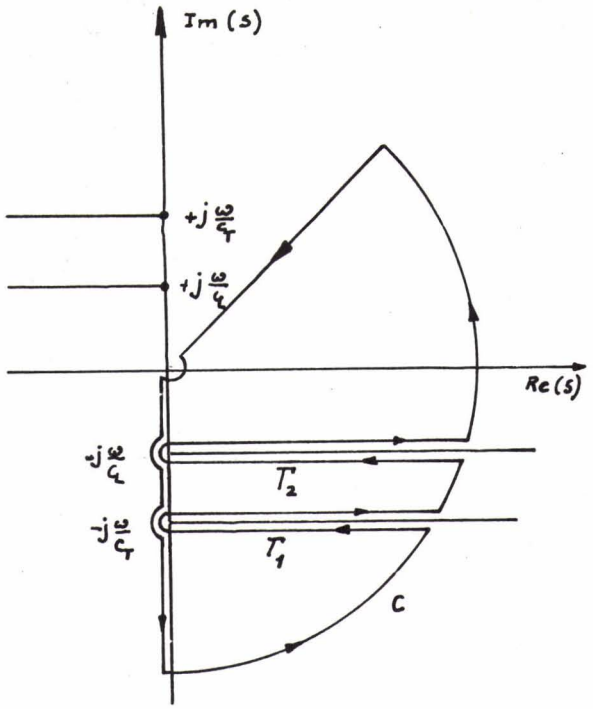

FIG. 1

Integration is made along the 1 + j straight path so that the second quadrant poles do not influence the Φ function. (This is of consideration in the case of a numerical integration of (4)).

With this integration contour, equation (4) may be written :

$$(12) \quad \phi'(r,z) = \frac{1}{j\pi} \left[\int_{\Gamma_1} + \int_{\Gamma_2} \right] - 4 \sum_n R_n K_0(s_n r)$$

where the R_n are the residues, given by :

$$(13) \quad R_n = s_n \frac{\phi(z \text{ or } z_e, s_n)\psi(z_e \text{ or } z, s_n)}{\rho(0)\partial\psi(0,s_n)/\partial s}$$

Expression (12) consists of two terms :

The first term corresponds to the branch-line integrals calculated along cuts Γ_1 and Γ_2. Physically they represent waves that propagate along the sediment-rock interface at speeds C_L and C_T with amplitudes decreasing approximately as $1/r^2$ (ref.5).

The second term is a summation of discrete values associated with the residues which correspond to the roots of the dispersion equation $\psi(0,s) = 0$. Each term of this summation constitutes a propagation mode, i.e. a wave travelling with a horizontal wave vector given by s_n. The amplitudes of these waves decrease as $1/\sqrt{r}$, so that at ranges large compared to the water depth the branch-line integrals contribution becomes negligible.

In order to verify the above mathematical development, one may use it to solve the PEKERIS model. In this two layer model, the sea water is a fluid with constant sound speed C_1 and constant density ρ_1, bounded by planes at $z = 0$ and $z = z_2$ and countaining both the source (at z_e) and the receiver (at z). The sea bottom is taken as a fluid half-space with constant velocity C_2 and constant density ρ_2, extending from $z = z_2$ to $z = \infty$.

The ϕ (z,s) and ψ (z,s) functions are then given by :

$$(14) \qquad \phi(z,s) = \rho_1 \frac{\sin\alpha_1 z}{\alpha_1}$$

$$(15) \qquad \psi(z,s) = \cos\alpha_1(z_2 - z) - \frac{\rho_1 K(s)}{\alpha_1} \sin\alpha_1(z_2 - z)$$

with :

$$\alpha_1 = \left[\frac{\omega^2}{C_1^2} + s\right]^{1/2}$$

Moreover, in this case of a fluid bottom, the expression for K(s) in (7) becomes :

$$K(s) = -j\frac{\alpha_2}{\rho_2} \qquad \text{With :} \quad \alpha_2 = \left[\frac{\omega^2}{C_2^2} + s^2\right]^{1/2}$$

In the case $z < z_e$, function Φ (z, z_e, s) transforms into :

$$(16) \qquad \Phi(z,z_e s) = \frac{\sin\alpha_1 z}{\alpha_1} \; x$$

$$\frac{\alpha_1 \cos\alpha_1(z_2 - z_e) + j\frac{\rho_1}{\rho_2}\alpha_2 \sin\alpha_1(z_2 - z_e)}{\alpha_1 \cos\alpha_1 z_2 + j\frac{\rho_1}{\rho_2}\alpha_2 \sin\alpha_1 z_2}$$

which is identical to the formula obtained by PEKERIS. Similar values for the residues R_n would also be found by applying equation (13).

3 - CLOSED FORM SOLUTIONS FOR THE GREEN'S FUNCTION

A large amount of work has been devoted, especially in the U.S.A., to study classes of C(z) function that would lead to closed form solutions for Φ (and $\partial\psi/\partial s$ that enters into the residue calculation).

In addition to C(z) = constant (PEKERIS) we can quote the GANS-PEDERSEN profile (Ref. 5 - 6), the parabolic profile (Ref. 7), the EPSTEIN profile (Ref. 8).

Among these various models we choose to program the GANS-PEDERSEN profile both as being of interest to solve a few practical cases we had to deal with, and in order to have a method for checking the program using the generalized numerical method exposed herunder. However, an improvement was brought to Pedersen's model as a density varying with depth could be introduced by the use of the exponential class of functions.

The adopted GANS-PEDERSEN modelling corresponded to the following description :

a) Sea water ($0 < z < z_1$)

Constant density $\rho = \rho_0$

Sound speed C(z) varying as :

$$C^2(z) = C_0^3/(C_0 - 2\gamma_0 z)$$

where C_0 and γ_0 are constants.

b) In the sediment ($z_1 < z < z_2$) :

Density : $\rho(z) = \rho_1 \exp(\rho'_1 (z - z_2)/\rho_1)$

where ρ_1 and ρ'_1 / ρ_1 are constants.

Sound speed : $C^2(z) = C_1^3/(C_1 - 2\gamma_1(z-z_1))$

where C_1 and γ_1 are constants.

Under these conditions, the ϕ and ψ functions that constitute Φ are given by the following expression :

(17)
$$\phi = -\frac{\pi}{3^{5/6}} \frac{C_0\rho_0}{(\gamma_0\omega^2)^{1/3}} (\zeta\zeta_0)^{1/3} \times$$

$$\left[J_{-1/3}(\zeta_0)J_{1/3}(\zeta) - J_{1/3}(\zeta_0)J_{-1/3}(\zeta) \right]$$

with :

$$\zeta = \frac{C_0^3}{3\gamma_0\omega^2} \left(\frac{\omega^2}{C^2(z)} + s^2\right)^{3/2} \quad ; \quad \zeta_0 = \frac{C_0^3}{3\gamma_0\omega^2} \left(\frac{\omega^2}{C_0^2} + s^2\right)^{3/2}$$

The ψ function may be written as :

(18) $$\psi = Y + \rho_0 k_1(s)\, X$$

with
$$X = -\frac{\pi}{3^{5/6}} \frac{C_0}{(\gamma_0\omega^2)^{1/3}} (\zeta\zeta_1)^{1/3} \times$$

$$\left[J_{-1/3}(\zeta_1)J_{1/3}(\zeta) - J_{1/3}(\zeta_1)J_{-1/3}(\zeta) \right]$$

$$Y = -\frac{\pi}{3^{1/2}} (\zeta\zeta_1^2)^{1/3} \; x$$

$$\left[J_{-1/3}(\zeta)J_{-2/3}(\zeta_1) + J_{1/3}(\zeta)J_{2/3}(\zeta_1) \right]$$

$$k_1(s) = \frac{1}{\rho_1} \exp\left[\frac{\rho'_1}{\rho_1} (z_2 - z_1) \right] x$$

$$\left\{ \frac{\rho'_1}{2\rho_1} + \frac{\left[\rho_1 K(s) - \frac{\rho'_1}{2\rho_1}\right] \frac{dX_1(\xi)}{dz} + \frac{dY_1(\xi_1)}{dz}}{\left[\rho_1 K(s) - \frac{\rho'_1}{2\rho_1}\right] X_1(\xi_1) + Y_1(\xi_1)} \right\}$$

With : $$X_1 = -\frac{\pi}{3^{1/2}} \frac{C_1}{(3\gamma_1\omega^2)^{1/3}} (\xi\xi_2)^{1/3} \; x$$

$$\left[J_{-1/3}(\xi_2)J_{1/3}(\xi) - J_{1/3}(\xi_2) J_{-1/3}(\xi) \right]$$

$$Y_1 = -\frac{\pi}{3^{1/2}} (\xi\xi_2^2)^{1/3} \; x$$

$$\left[J_{-1/3}(\xi)J_{-2/3}(\xi_2) + J_{1/3}(\xi)J_{2/3}(\xi_2) \right]$$

$$\frac{dX_1}{dz} = \frac{\pi}{3^{1/2}} (\xi^2 \xi_2)^{1/3} \quad x$$

$$\left[J_{-1/3}(\xi_2) J_{-2/3}(\xi) + J_{1/3}(\xi_2) J_{2/3}(\xi) \right]$$

$$\frac{dY_1}{dz} = \frac{\pi}{3^{1/2}} \frac{(3\gamma_1 \omega^2)^{1/3}}{C_1} (\xi_2 \xi)^{2/3} \quad x$$

$$\left[J_{-2/3}(\xi_2) J_{2/3}(\xi) - J_{2/3}(\xi_2) J_{-2/3}(\xi) \right]$$

where the $J \pm 1/3$ and $J \pm 2/3$ are fractional order first kind BESSEL functions of the complex variable ξ or ξ_2.

The variables ζ_1, ξ and ξ_2 in the above expressions are given by :

$$\zeta_1 = \frac{C_1^3}{3\gamma_1\omega^2}\left(\frac{\omega^2}{C_1^2} + s^2\right)^{3/2}$$

$$\xi = \frac{C_1^3}{3\gamma_1\omega^2}\left[\frac{\omega^2}{C(z)^2} + s^2 - \left(\frac{\rho'_1}{2\rho_1}\right)^2\right]^{2/3}$$

$$\xi_2 = \frac{C_1^3}{3\gamma_1\omega^2}\left[\frac{\omega^2}{C(z_2)^2} + s^2 - \left(\frac{\rho'_1}{2\rho_1}\right)^2\right]^{2/3}$$

The calculation of the residues corresponding to the s_n poles of $\psi(0,s)$ requires the knowledge of $\partial\psi / \partial s$. This derivative can be calculated in closed form without difficulty but this leads to a lengthy formula that will not be developed here.

4 - NUMERICAL FORM OF THE GREEN'S FUNCTION : (propagation in an under-water medium of any given characteristics).

The classes of function for $C(z)$ and $\rho(z)$ which permit to obtain closed form solutions to the wave propagation problem are too limited to account for all possible laws of variations encountered in practice. One solution is to divide the medium into layers in which sound velocity and density vary differently by a proper choice of the parameters ρ_i, ρ'_i / ρ_i, C_i, γ_i. Arrived at that degree of complexity one may as well envisage a completely numerical solution allowing any sound speed and density profile to be used. This method has been developed, programmed and will be described hereafter.

Let us rewrite equation (5) in a slightly different way by the system of two first order equations :

$$(19) \qquad \rho(z)\frac{dU}{dz} + \left(\frac{\omega^2}{C^2(z)} + s^2\right) P = 0$$

$$\rho(z)U - \frac{dP}{dz} = 0$$

It can be shown that ϕ represents the solution P(z) with the bounding conditions :

$$P(0) = 0$$
$$U(0) = 1$$

and that ψ represents the solution P(z) with the conditions :

$$P(z_2) = 1$$
$$U(z_2) = K(s)$$

Let us now divide the medium into N horizontally stratified layers, the nth one being limited between $z = z_n$ and $z = z_{n+1}$

In each layer, it is possible to define a mean sound speed C_n and a mean density ρ_n. By adding similar terms on each side of equations (19), these equations can be written as follows :

$$(20) \qquad \rho_n \frac{dU}{dz} + \left(\frac{\omega^2}{C_n^2} + s^2\right) P = \left(\frac{\omega^2}{C_n^2} - \frac{\omega^2}{C^2}\right) P + (\rho_n - \rho)\frac{dU}{dz}$$

$$\rho_n U - \frac{dP}{dz} = (\rho_n - \rho)U$$

The advantage of this form is that in each layer $(z_n - z_{n+1})$, the first member of the two equations (19) that were variable are now constant in (20). It becomes therefore possible to employ LAGRANGE's method of constants variation to solve equation (20).

This leads, after some arithmetic, to the following system :

$$(21)\quad P(z_{n+1}) = P(z_n)\cos\alpha_n(z_{n+1} - z_n) + \rho_n U(z_n)\frac{\sin\alpha_n(z_{n+1} - z_n)}{\alpha_n} + \int_{z_n}^{z_{n+1}} \left\{ \left\{ \left[\frac{\omega^2}{C_n^2} - \frac{\omega^2}{C^2(\zeta)} \right] P(\zeta) + \left[\rho_n - \rho(\zeta) \right] \frac{dU(\zeta)}{dz} \right\} \frac{\sin\alpha_n(z_{n+1} - \zeta)}{\alpha_n} - \left[\rho_n - \rho(\zeta) \right] U(\zeta)\cos\alpha_n(z_{n+1} - \zeta) \right\} d\zeta$$

$$(22)\quad \rho_n U(z_{n+1}) = - P(z_n)\alpha_n \sin\alpha_n(z_{n+1} - z_n) + \rho_n U(z_n)\cos\alpha_n(z_{n+1} - z_n) + \int_{z_n}^{z_{n+1}} \left\{ \left\{ \left[\frac{\omega^2}{C_n^2} - \frac{\omega^2}{C^2(\zeta)} \right] P(\zeta) + \left[\rho_n - \rho(\zeta) \right] \frac{dU(\zeta)}{dz} \right\} \cos\alpha_n(z_{n+1} - \zeta) + \left[\rho_n - \rho(\zeta) \right] U(\zeta)\alpha_n \sin\alpha_n(z_{n+1} - \zeta) \right\} d\zeta$$

where : $\alpha_n = \left(\frac{\omega^2}{C_n^2} + s^2 \right)^{1/2}$

The functions ϕ and ψ are now solutions of a VOLTERRA type integral equation. If $U(z_n)$ and $P(z_n)$ are known, then $U(z_{n+1})$ and $P(z_{n+1})$ can be calculated, and thus from one layer to the next until U(z) and P(z). The values of U and P being known at the boundaries from the boundary conditions, these values serve to initialize the recurrent process.

Expressions (21) and (22) cannot however be programmed on a computer as such, but if the layers' thickness is adjusted so that C(z) and $\rho(z)$ do not vary too much around C_n and ρ_n then a TAYLOR expansion under the integral signs of (21) and (22) leads to an analytical formulation of the integrals.

The following expressions are reached after some arithmetic :

$$(23)\quad P(z_{n+1}) = P(z_n)\left\{\cos\alpha_n(z_{n+1}-z_n) + \sum_0^4 a_i J_{in} - \frac{1}{\rho(z_n)}\sum_1^3 b'_i K_{in}\right\} + U(z_n)\left\{\rho_n \frac{\sin\alpha_n(z_{n+1}-z_n)}{\alpha_n} + \rho(z_n)\sum_1^3 b_i J_{in} - \sum_0^4 a'_i K_{in}\right\}$$

$$(24)\quad \rho_n U(z_{n+1}) = P(z_n)\left\{-\alpha_n \sin\alpha_n(z_{n+1}-z_n) + \sum_0^4 a_i K_{in} + \frac{\alpha_n^2}{\rho(z_n)}\sum_1^3 b'_i J_{in}\right\} + U(z_n)\left\{\rho_n\cos\alpha_n(z_{n+1}-z_n) + \rho(z_n)\sum_1^3 b_i K_{in} + \alpha_n^2 \sum_0^4 a'_i J_{in}\right\}$$

These expressions can be easily programmed as the coefficients a_i, b_i, a'_i, b'_i, J_{in} and K_{in} are analytical expressions that present no difficulty for computation. They are not presented here for the sake of simplification.

In order to calculate the residues corresponding to the poles s_n of ψ (0,s) it is necessary to get the $\partial\psi/\partial s$ values. This is done as follows :

Equating $\partial\psi / \partial s = 2sx$ leads :

$$\frac{\partial P}{\partial s^2} \equiv \frac{\partial \psi}{\partial s^2} = x \quad \text{and} \quad \frac{\partial U}{\partial s^2} = \frac{1}{\rho}\frac{d}{dz}\frac{\partial \psi}{\partial s^2} = y$$

Derivating system (19) with respect to s^2 leads :

$$\rho \frac{d}{dz}\frac{dU}{ds^2} + P + \left(\frac{\omega^2}{C^2(z)} + s^2\right)\frac{dP}{ds^2} = 0$$

$$(25)\qquad \frac{d}{dz}\left(\frac{dP}{ds^2}\right) - \rho\left(\frac{dU}{ds^2}\right) = 0$$

with this system of equations meeting the boundary conditions :

$$x\,(z_2) = 0$$

$$y\,(z_2) = \partial K / \partial s^2$$

The analogy with the equations for U and P is obvious and the same recurrent methods can be used to get $x(z_{n+1})$ and $y(z_{n+1})$ as a function of $x\,(z_n)$ and $y\,(z_n)$.

5. COMPUTER PROGRAM

From the models developed in chapters 3 and 4, different programs were written down for the calculation of propagation losses versus horizontal range at a fixed frequency.

At the present time three main programs are available, namely (from the simplest to the most elaborate) :

1) Program "PEKTO" (from the names of PEKERIS and TOLSTOY) : Constant sound speed and density in the water ; Solid bottom without sediments.

2) Program "BESSEL" (because of the formulation in terms of J $\pm$ 1/3 etc.): Sound speed and density varying as exposed in chapter 3 ; elastic bottom under the sediments.

3) Program "VOLTERRA" : Sound speed and density profiles of any given shape (as exposed in chapter 4); elastic bottom under the sediments.

The "VOLTERRA" program can obviously handle the computations corresponding to the profiles dealt with by the "BESSEL" and "PEKTO" programs but at greater cost. This was done however to check the accuracy of the "VOLTERRA"program.

These three programs have specific domains of application for which they are optimized.
Optimization was in all cases taken care of. For instance, the VOLTERRA program had to be divided into two parts : one program permitting to calculate both the branch-line integrals and the residue series of equation (12) and one program dealing only with the residues, i.e. the modes.

The reader will find hereunder a few details concerning the program structures.

In "PEKTO" and "BESSEL" the sound speed and density profiles are of course given by their analytic expressions while in VOLTERRA they are given by a set of data points. In this case the C(z) and $\rho(z)$ values for any desired z during the computation are obtained from a subroutine that makes use of the natural cubic spline interpolation method.

In "BESSEL" and "VOLTERRA" the possibility to account for an absorption coefficient in the sediment (and water if desired) was introduced by taking a complex value for the sound speed. In that case the real part of the sound speed is introduced as previously and the imaginary part is a constant depending on the frequency and the medium characteristics.

All three programs use the same technique to search for the poles and perform the numerical integration if this is the case. They only differ in the way the GREEN's function ϕ and the $\frac{\partial \psi}{\partial s}$ derivative (used in the residues calculation) are evaluated.

- Calculation of the poles location in the complex plane and of the corresponding residues.

It was mentioned in paragraph 2.4 that the poles s_n were complex and located in the fourth gradiant. They can also be imaginary and

on the half axis Im(s) < 0.

The program performs the computation of the $\phi(z\ s)$ function with s varying along Im (s) by steps Δs. At the same time it detects the minima of its denominator $\psi(o,s)$. The corresponding value of s can be regarded as the first approximate value of the imaginary part of the pole s_n. From this value the program searches for the exact location of s_n in the complex plane by the use of a NEWTON's method and then branches to the subroutine that computes the corresponding value of $\partial\psi/\partial s$, calls back to ϕ and ψ components of Φ and gives the residue as in equation (13). This procedure is carried out as long as s vary along Im(s) < 0 until a pre-established value s_{end} for which poles can no more exist.

- Numerical integration

Integral (4) is not directly computed in the program as this would present difficulties caused by too strong fluctuations of the GREEN's function along the imaginary axis. On the contrary the branch-line integrals of equation (12) are easier to calculate by an indirect method.
It can be demonstrated that these branch-line integrals may be expressed by the integral

$$(26)\quad \int_{-j\infty}^{(1+j)\infty} (\Phi - \Phi')\, K_0(sr)\, ds$$

where Φ' is given by

$$\Phi' = 2s \sum_n \frac{R_n}{s^2 - s_n^2}$$

s_n and R_n being the poles and corresponding residues.
It is possible to obtain an analytical approached value of (26) by :

$$(27) \qquad \frac{1}{2r} \sum_{p=0}^{N} \left[\frac{\Delta\Phi(s_p)}{s_p} + \frac{\Delta\Phi(s_{p+1})}{s_{p+1}} \right] \left[s_p K_1(s_p r) - s_{p+1} K_1 (s_{p+1} r) \right]$$

where K_1 is the first order modified BESSEL function and
where $\Delta\Phi = \phi - \Phi'$.

The programming of equation (27) is easy. The achieved calculation accuracy is a function of the number N of values that have been computed for Φ along the two half lines "s = 1 + j" and Im(s) < 0 of the integration contour.

In order to obtain the total sound field as given by (4), one just needs to add to the previous results (branch-lines integrals) the sum of the residues (eq.12).

6. CONCLUSION

The various programs presented above have been written down on a CDC 6600 computer. The required computation time is a function of the given source frequency F.
This is evident since the number n of poles that determine the number of modes to be added is roughly given by n = 2 FH/C where C is the mean sound velocity in the water and H the water depth.

This computation time may hence reach large values. In spite of this it was found that the use of all programs offered numerous advantages beyond the mere aspect of sound field calculation in a given situation. For example they can be used to study the influence of various sea floor parameters on the sound propagation (sediments, density and layering, compressional and shear velocities etc) and the influence of variations in the sound velocity and density profiles (by the use of the "VOLTERRA" program in particular).

The "BESSEL" program can also be employed for the study of various sound channels (ref.9).

Finally it must pointed out that the complete sound field calculation may usefully help in the study of shadow zones and caustics where the geometrical optics approximation is no more valid.

ACKNOWLEDGEMENTS

This work was sponsored by the Direction des Recherches et Moyens d'Essais of the French M.O.D.

REFERENCES

1. C.L PEKERIS "Theory of propagation of Explosive Sound in Shallow Water"
The Geological Society of America
MEMOIR 27, Propagation of Sound in the Ocean II, 1948
2. C.B OFFICER "Introduction to the theory of Sound Transmission"
Mc Graw Hill Series in Geological Sciences, 1958.
3. I. TOLSTOY, C.S CLAY "Theory and Experiment in Underwater Sound"
Mc Graw Hill Advanced Physics
Monographs Series, 1966
4. A. V NEWMAN, F. INGENITO "A Normal Mode Computer Program for Calculating Sound Propagation in Shallow Water with an Arbitrary Velocity Profile".
Naval Research Laboratory, Washington DC
Rep. 2381, 1972.
5. L.M BREKHOVSKIKH "Waves in Layered Media" Academic Press Inc, New York, 1960.
6. M. A PEDERSEN, D.F. GORDON "Normal mode theory applied to short - range propagation in an underwater acoustic surface duct"
J.A.S.A., VOL 37, n° 1, p.105-118 (1965)
7. P. HIRSCH "Acoustic field of a pulsed source in the underwater - sound channel"
J.A.S.A., VOL 38, n° 6, p.1018 - 1030 (1965)
8. H.P BUCKER, H.E MORRIS "EPSTEIN normal mode model of a surface duct"
J.A.S.A., VOL 41, n° 6, p. 1475-1478 (1967)
9. F.M LABIANCA "Normal Modes, Virtual Modes, and alternative representations in the theory of surface - duct Sound propagation"
J.A.S.A, VOL 53, n° 4, p. 1137-1147 (1973).

A WAVE THEORETIC METHOD FOR ESTIMATING THE EFFECTS OF INTERNAL TIDES UPON ACOUSTIC WAVE TRANSMISSION

D. J. Ramsdale
Naval Research Laboratory, Washington, DC 20375
U.S.A.

ABSTRACT

The effect of the first mode semidiurnal internal tide on a duct-type sound speed profile was approximated by varying the minimum velocity of the parabolic profile in a sinusoidal fashion with a period of 12.42 hours. The corresponding effect on the acoustic field was determined by using the normal mode solutions to the parabolic profile to compute the signal level and phase at a fixed receiver due to a fixed cw source. A systematic computer study was performed to determine the dependence of signal level and phase upon the source frequency, receiver range and tidal amplitudes. Numerical results showed that the acoustic phase variation over a tidal cycle was very nearly a sinusoid with 12.42 hour period and a peak-to-peak amplitude which was approximately a linearly increasing function of source frequency, receiver range and tidal amplitude. A simple analytical expression was developed which predicts these linear dependencies and closely approximates the phase variations computed numerically. The fluctuations in signal level during a tidal cycle were found to depend upon the detailed structure of the acoustic field in the immediate vicinity of the receiver. In general, however, the fluctuations in signal level increased in frequency with increasing source frequency, tidal amplitude and receiver range.

I. INTRODUCTION

Large-scale periodic motions exist in the ocean in the form of internal waves. The effect of these motions upon the passage of an acoustic wave through the ocean has received a great deal of attention in the recent literature.[1-18]

Of particular relevance to the results presented in this paper are the experimental work of Clark and Kronengold[14] and the associated theoretical analyses of Weinberg, Clark and Flanagan.[12] The experiment conducted by Clark and Kronengold involved transmitting a 406 Hz cw signal from Eleuthera, Bahamas, to hydrophones in the Eleuthera-Bermuda Propagation Range. Signals received at both Bermuda and intermediate hydrophones approximately 500 km from the source showed that the extended angle phase variation was dominated by a large semidiurnal component, suggesting that the acoustic propagation in that region was strongly influenced by a deep ocean internal tide of characteristic M2 periodicity, 12.42 hours.

The terminology "extended angle phase" means that the phase variation through more than one complete cycle is recorded as such, rather than as an angle between 0° and 360°. The distortion of the sound speed profile due to the motion of the first mode semidiurnal internal tide has been determined by Mooers.[18] For the case in which the acoustic path is perpendicular to the direction of propagation of the internal tide, Weinberg, Clark

and Flanagan varied the sound speed profile according to Mooer's prescription, using a ray-trace model to compute the associated time history of transmission loss and phase of the acoustic signal during a 12.42 hour tidal cycle. Their calculations for 406 Hz and a range of approximately 500 km showed that (1) the peak-to-peak variation in extended angle phase was linearly proportional to the amplitude of the internal tide and (2) the fluctuation in transmission loss became greater in extent and more rapid with increasing tidal amplitude.

In this paper, we report the results of a normal mode calculation using the parabolic profile in which the profile is varied to crudely approximate the effect of the first mode semidiurnal internal tide. The extended angle phase and signal level are computed as functions of source frequency, receiver range and internal tidal amplitude. Approximate analytical expressions are developed to predict the dependence of extended angle phase on these parameters and an explanation is offered for the computed fluctuations in signal level.

II. THE MODEL

The parabolic profile is one of the few for which exact closed-form solutions are available.[19-22] The acoustic pressure (p) at a range (r) and depth (z) due to a point source of angular frequency (ω) placed at the origin in range and depth z_o is given by

$$p = \frac{\omega\rho}{4} \sum_{n=o}^{\infty} \left(\frac{2}{\pi k_n r}\right)^{1/2} \exp i\left(k_n r - \pi/4 - \omega t\right) \times \exp\left[\frac{-\beta^2}{2}\left(z^2 + z_o^2\right)\right] \frac{H_n(\beta z) H_n(\beta z_o)}{2^n n! \sqrt{K\alpha/\pi}} \quad (1)$$

where ρ is the density, H_n are the hermite polynomials of order n, $K = \omega/c_o$, $\beta^2 = K\alpha$ and the eigenvalues k_n are given by

$$k_n = [K^2-(2n + 1)\ K\alpha]^{1/2} \tag{2}$$

For any set of source/receiver parameters the pressure can be written as

$$p = A \exp i(\phi-\omega t) \tag{3}$$

where the pressure amplitude A and phase ϕ are determined from the real and imaginary parts of Eq. (1) (suppressing the harmonic time dependence).

The solutions to the truncated parabolic profile, shown in Fig. 1, are very nearly those for the parabolic profile in which modes with phase velocities greater than c_1, the velocity at the edge of the duct are ignored.[22] In all our calculations the infinite sum in Eq. (1) is replaced by a finite sum in which $c_n = \omega/k_n < c_1$. This represents a more realistic model for fluctuations since it restricts the range of values of k_n to those normally encountered in the real ocean.

The distortion of the sound speed profile predicted by Mooers[18] as due to the first mode semidiurnal internal tide is shown in Figure 2. This rhythmic movement in the profile can be approximated crudely using the parabolic profile by varying the axial sound speed c_o according to

$$c_o = \bar{c}_o + \Delta c_o \sin \Omega t \tag{4}$$

where Ω is the tidal frequency and $\bar{c}_o$ is the unperturbed speed at the axis. The sound speed perturbation produced by the action of the internal wave has been shown to be very nearly proportional to the internal wave amplitude.[18] Thus, the value of Δc_o in Eq. (4) can be regarded as proportional to the internal wave amplitude.

Given the source location, frequency transmitted and receiver location, a time history of the amplitude and extended angle phase can be generated using the parabolic profile (terminated as in Figure 1) with the axial velocity c_o given in Eq. (4). In performing the computation, the extended angle phase was determined by increasing or decreasing the phase by one cycle as appropriate when the phase angle moved from quadrants one to four or vice versa; the time sampling interval was chosen sufficiently small to facilitate the phase tracking. The amplitude was represented in dB by taking 20 log A and plotted in dB as a loss in signal level.

III. NUMERICAL RESULTS

All calculations were made with both source and receiver on the axis of the parabola, the unperturbed profile specified by c_o = 1480 m/sec, c_1 = 1520 m/sec and h = 1000 m. Typical results for a source frequency of 100 Hz, receiver range of 109.5 km (8th focal zone) and a Δc = 1.0 m/sec are shown in Figure 3. These are in general similar to those computed by Weinberg, et al.,[12] in that the extended angle phase is sinusoidal with a period identical to the tidal cycle, and the fluctuations in amplitude are of higher frequency, varying over some

15 dB. Note that the amplitude of the negative part of the extended angle phase is smaller by nearly one full cycle than that of the positive half. This is due to the two 180° phase changes encountered at each deep null in signal level during the negative portion of the cycle.

A. Dependence on tidal amplitude, source frequency and receiver range.

Dependence of the extended angle phase upon Δc_o (tidal amplitude) was determined by simply holding frequency and range constant (f = 100 Hz, r = 109.5 km) and varying Δc_o. The results are summarized in Figure 4, which shows that the peak-to-peak variation in extended angle phase is a linear function of Δc_o, which is, of course, proportional to tidal amplitude. This result was also obtained by Weinberg, et al., using their ray-theory model which incorporated both the sea floor and surface and was thus considerably more complicated than the simple wave model used here.

Plots of the signal level as a function of time over a tidal cycle for these cases show that as the tidal amplitude increases, the peak-to-peak fluctuation in signal level increases while the time (τ) for the normalized autocorrelation of the signal level to drop to 0.5 decreases. The peak-to-peak fluctuation in signal level varies from 29.9 dB for Δc_o = 2.0 to 2.1 dB for Δc_o = 0.25 while the corresponding decorrelation times (τ) vary from 11.5 minutes to 55.5 minutes.

Dependence of the extended angle phase on source frequency was examined by holding the range and tidal amplitude constant

(r = 109.5 km and Δc_o = 1.0 m/sec) and varying the frequency. The results are summarized in Figure 5, which shows that the peak-to-peak variation in extended angle phase is a linear function of source frequency over the range 10 Hz to 400 Hz. Plots of signal level over the tidal cycle as a function of time showed that the peak-to-peak fluctuation increased while decorrelation time (τ) decreased with frequency, ranging from 29.9 dB and 8.25 minutes, respectively, at 400 Hz to 15.4 dB and 21 minutes, respectively, at 100 Hz, while for 10 Hz the corresponding values are 2.4 dB and a time greater than 70 minutes for 10 Hz.

Preliminary measurements have been made between a fixed source and a fixed receiver separated by some 400 nautical miles with source frequencies of 12 and 22 Hz.[23] Internal tides appeared to be modulating the phase, but the total phase change over a six-hour period was only a fraction of a cycle and the corresponding amplitude fluctuation approximately 1-2 dB. This gives credence to our theoretical results which showed that both phase and amplitude fluctuations decrease with decreasing source frequency.

The dependence of extended angle phase on receiver range was determined by keeping the source frequency and tidal amplitude constant (f = 100 Hz and Δc_o = 1.0 m/sec) and varying the receiver range. The results of such calculations carried out over ranges from 100 to 420 km are shown in Figure 6. The dependence is approximately linear but deviations are more

noticeable than in the case of frequency or tidal amplitude. These deviations are a result of phase changes due to deep fades in the signal level; thus, even though the value taken from the linear curve would be a good estimate of the peak-to-peak variation in extended angle phase at a given range, deviations can result if the amplitude structure displays deep nulls.

The complexity and variation in signal level at each of the various ranges depends on whether one is near a focal zone or between a focal zone. For example, at a range of 109.5 km (8th focal zone) the peak-to-peak fluctuation in signal level is 15.4 dB with a decorrelation time of 21 minutes, while at 117 km (between 8th and 9th focal zones) the corresponding numbers are 2.8 dB and 13.5 minutes. In general, the variations in signal level and decorrelation times are larger near focal zones than in between them. Also, in general, for both zones, focal and non-focal, the variations in signal level increase while the decorrelation times decrease as range increases.

B. Random component of axial velocity

The speed of sound near the sound channel axis is surprisingly variable.[24] To investigate the effect of a small random variability on the signal level and extended angle phase, a small amount of speed randomly selected in time from a normal distribution was added to the axial velocity in addition to that due to the internal tide. The magnitude of the random

component was determined by specifying the standard deviation of a normal distribution whose mean value was zero. The signal level, its autocorrelation function and the extended angle phase were computed over a tidal cycle for a constant range (r = 109.5 km) and constant tidal amplitude (Δc_o = 1.0 m/sec) for frequencies of 10 Hz, 100 Hz, 200 Hz and 400 Hz with the addition of a random axial velocity component determined by a standard deviation of 0.01 m/sec. These results were compared with identical calculations where the random axial component was zero. The effect of the random component upon the 10 Hz and 100 Hz results was negligible. The peak-to-peak extended angle phase at 200 Hz was 14.35 cycles with the random component as compared to 17.06 cycles without it; however, the basic sinusoid shape, although contaminated by a certain amount of "grass," was still retained. The results for the 400 Hz source are shown in Figure 7. In this case, the random component was large enough to prohibit phase tracking. Although a certain amount of "grass" was added to the signal level curves at all frequencies, the decorrelation time was substantially the same both with and without the random component.

An additional set of computations were performed with all parameters as before but with the standard deviation of the random component now set at 0.1 m/sec. The extended angle phase for the 10 Hz source was quite grassy but still basically sinusoid, and the decorrelation time was still greater than 70 minutes as in the case of no random component. However, for the 100 Hz,

200 Hz and 400 Hz cases the sinusoidal phase variation was destroyed and the signal level decorrelated in approximately one minute.

These results show that a random component in the axial velocity discriminates more against tracking phase variations due to internal tides at high acoustic frequencies than at low acoustic frequencies. This suggests that perhaps the effects of an internal tide might be masked at a high acoustic frequency while being visible at a lower acoustic frequency. The decorrelation time is not as sensitive as phase to random components in the axial velocity but eventually will be increased as the standard deviation of the random component increases.

IV. ANALYSIS

Numerical results presented in the previous section showed that the peak-to-peak value of extended angle phase is to a good approximation linearly dependent upon receiver range, source frequency and tidal amplitude. Calculations of extended angle phase as a function of range for source and receiver on the axis with a source frequency of 100 Hz showed that with the exception of deep nulls in amplitude, the phase can be represented fairly well by $\phi = kr$. The exact value one uses for k depends upon the modes which contribute most to the solution and their speeds but consider for the moment that $k = \omega/c$ where c represents some typical sound speed. The internal tide causes a variation in c with time so that the resulting phase variation

can be written as

$$\Delta\phi(r,t) = -\left(\frac{1}{c^2}\right) \omega r \, \Delta c \sin \Omega t \qquad (5)$$

which demonstrates very simply the numerically observed linear dependence on tidal amplitude (Δc), source frequency, and range. Note that it correctly predicts a phase variation which is 180 degrees out of phase with the driving function.

The prediction of accurate values of extended angle phase using Eq. (5) depends to some extent on the particular choice of c and Δc. Consider the case computed numerically in the previous section of a source/receiver on the axis, source frequency 100 Hz, Δc=1 m/sec and receiver range of 109.5 km. Taking c to be 1500 m/sec one finds a peak-to-peak value of 9.73 cycles which is in reasonable agreement with the true value of 8.65 as determined numerically. Suppose we consider applying Eq. (5) to the case computed by Weinberg, et al., where a 406 Hz source was located approximately 500 m from the surface propagating acoustic energy to a receiver some 500 km away at a depth greater than 2000 m while the medium was under the influence of a 10-m internal tide. If we take as c the sound speed at the SOFAR axis and Δc the maximum change in the axis speed produced by the internal wave, Eq. (5) predicts a peak-to-peak phase variation of 27.4 cycles, which compares perhaps fortuitiously to the value of 25 cycles computed by Weinberg, et al.[12] This suggests that perhaps a rule of thumb in using Eq. (5) is to take c equal to the speed at the SOFAR axis and Δc as the maximum change in this speed.

Now let us consider the fluctuations in signal level. In an effort to understand these fluctuations, several computations were made of the signal level as a function of range for slightly different values of c_o. The results showed that the acoustic field for two values of c_o very nearly the same was the same in form but shifted slightly in range. The amount of range shift can be approximated well by computing the change in spacing (R) between focal zones as c_o changes. Since $R = \pi/\alpha$ (source and receiver on the axis),

$$\Delta R = \frac{Rc_o\Delta c_o}{c_1^2 - c_o^2} \qquad (6)$$

Application of this expression to the case where the receiver is at the 8th focal zone (r = 109.5 km) yields a shift in range of approximately 1.3 km. Figure 8 shows the corresponding signal level as a function of range for a source frequency of 100 Hz, the dotted lines indicating the range shift corresponding to Δc_o = 1.0 m/sec centered at 109.5 km. Note that the portion of the signal within the dotted lines when sampled in a sinusoidal manner beginning at 109.5 km corresponds to the fluctuations in signal level shown in Figure 3.

A close study of the plots of transmission loss over a tidal cycle for various tidal amplitudes as computed by Weinberg, et al. (reproduced in Figure 9) leads one to the same conclusion, i.e., the effect of the internal tide is mainly to move the acoustic field back and forth in range. This can be seen in

Figure 9 by noting that a larger tidal amplitude causes the field to shift greater in range; thus, the fluctuations for a 7-m internal tide would be included as a subset of those for a 10-m internal tide. Examination of Figure 9 shows this to be the case.

According to Eq. (6), the amount of range shift depends directly upon the tidal amplitude (Δc_o) and the range (number of focal zones covered), but is independent of frequency. One conclusion reached then is that the fluctuations in signal level at any range depend upon the structure of the acoustic field nearby, since the effect of the internal tide is simply to sample the field nearby the range in question. Thus, if the acoustic field has a great deal of structure due to interference effects, the fluctuations in signal level due to the internal tide will increase in frequency and perhaps magnitude with tidal amplitude and/or range. The dependence of the signal level fluctuations on frequency is due simply to the higher frequencies having more modes contributing to the results which in turn produces a more complex interference structure in the acoustic field.

V. SUMMARY

The effect of the first mode semidiurnal internal tide upon acoustic wave propagation has been estimated using the normal mode solutions to the parabolic velocity profile. The action of the internal tide on the parabolic velocity profile was approximated by allowing the minimum velocity to vary

in a sinusoidal fashion, having a 12.42 period with the maximum variance from the unperturbed value taken to be proportional to the internal tidal amplitude. A systematic computer study was performed to determine the dependence of signal level and extended angle phase on the source frequency, receiver range and tidal amplitude. The results showed that the extended angle phase was very nearly a linear function of all three parameters. No such simple result was obtained for fluctuations in signal level, although in general the extent and frequency of these fluctuations increased with higher source frequency, greater tidal amplitude and greater receiver range.

Further computer studies using an unperturbed parabolic profile showed that as range increased, the phase was fairly well approximated by the product of wavenumber and range. This fact lead to the development of a simple formula which predicts linear dependence of extended angle phase on source frequency, receiver range and tidal amplitude. Values of extended angle phase computed using this simple expression are in reasonable agreement with those obtained numerically and also with those computed by Weinberg, et al.[12]

Fluctuations in signal were traced to the fact that the effect of the internal tide was to shift the acoustic field in range, the amount increasing linearly with range and tidal amplitude. Again, a simple analytic expression was determined which approximates this shift. The fluctuations in signal level at any range then depend upon the structure of the acoustic field nearby, but generally will increase in frequency with increasing tidal amplitude and range. The effect of source

frequency upon signal level fluctuations is mainly through the increasing complexity of the field with increasing source frequency; thus, for a constant range and tidal amplitude, signal level fluctuations decorrelate faster as frequency increases.

References

1. S. D. Chuprov, "On the Observation of a Sound Signal in the Presence of Internal Waves," Izv. Atmos. and Oceanic Phys. 2, 551-552 (1966).

2. E. J. Katz, "Effect of the propagation of internal water waves on underwater sound transmission," J. Acoust. Soc. Am. 42, 83-87 (1967).

3. J. C. Beckerle, J. L. Wagar and R. D. Worley, "Underwater Acoustic Wavefront Variations and Internal Waves," J. Acoust. Soc. Am. 44, 295-296 (1968).

4. J. C. Steinberg, J. G. Clark, H. A. DeFerrari, M. Kronengold and K. Yacoub, "Fixed System Studies of Underwater Acoustic Propagation," J. Acoust. Soc. Am. 52, 1521-1536 (1972).

5. R. N. Baer and M. J. Jacobson, "Sound Transmission in a Channel with Bilinear Sound Speed and Environmental Variations," J. Acoust. Soc. Am. 54, 80-91 (1973).

6. Weston, D. E. and H. W. Andrews, "Acoustic Fluctuations due to Shallow Water Internal Waves," J. Snd. and Vib. 31, 357-368 (1973).

7. R. N. Baer and M. J. Jacobson, "Analysis of the Effect of a Rossby Wave on Sound Speed in the Ocean," J. Acoust. Soc. Am. 55, 1178-1189 (1974).

8. H. A. DeFerrari, "Effects of Horizontally Varying Internal Wavefields on Multipath Interference for Propagation through the Deep Sound Channel," J. Acoust. Soc. Am. 56, 40-46 (1974).

9. R. H. Clarke, "Sound Propagation in a Variable Ocean," J. Sound and Vib. 34, 457-477 (1974).

10. Ibid., "Transmission of Underwater Sound through Internal Waves and Turbulence," Proceedings of the Satellite Symposium on Underwater Acoustics, 8th ICA, August, 1974.

11. R. C. Spindel, R. P. Porter and R. J. Jaffee, "Long-Range Sound Fluctuations with Drifting Hydrophones," J. Acoust. Soc. Am. 56, 440-446 (1974).

12. N. L. Weinberg, J. G. Clark and R. P. Flanagan, "Internal Tidal Influence on Deep-Ocean Acoustic-ray Propagation," J. Acoust. Soc. Am. 56, 447-458 (1974).

13. R. N. Baer and M. J. Jacobson, "Effect of a Rossby Wave on the Phase of an Underwater Acoustic Signal," J. Acoust. Soc. Am. 56, 809-816 (1974).

14. J. G. Clark and M. Kronengold, "Long-period Fluctuations of cw signals in Deep and Shallow Water," J. Acoust. Soc. Am. 56, 1071-1083 (1974).

15. R. C. Spindel, R. P. Porter and R. J. Jaffee, "Acoustic-internal Wave Interaction at Long Ranges in the Ocean," J. Acoust. Soc. Am. 56, 1426-1436 (1974).

16. V. A. Polyanskaya, "Influence of high-frequency internal waves on the sound field of a point source in the ocean," Sov. Phys. Acoust. 20, 55-59 (1974).

17. R. N. Baer and M. J. Jacobson, "SOFAR transmission fluctuations produced by a Rossby Wave," J. Acoust. Soc. Am. 57, 569-576 (1975).

18. C. N. K. Mooers, "Sound-velocity Perturbations Due to Low-frequency Motions in the Ocean," J. Acoust. Soc. Am. 57, 1067-1075 (1975).

19. H. Uberall and N. C. Nicholas, "Range Focusing in a Deep-Ocean Sound Channel with Parabolic Profile," J. Acoust. Soc. Am. 44, 1259-1261 (1968).

20. N. C. Nicholas and H. Uberall, "Normal-Mode Propagation Calculations for a Parabolic Velocity Profile," J. Acoust. Soc. Am. 48, 745-752 (1970).

21. N. C. Nicholas, "The Propagation of Sound in the Deep Ocean: A Wave Formulation," AD-754-371, pp. 131, September, 1971.

22. I. Tolstoy and C. S. Clay, Ocean Acoustics, McGraw-HIll, New York, 1966, pp. 87-93 and pp. 178-180.

23. K. D. Flowers, Naval Research Laboratory, private communication.

24. Ants T. Piip, "Fine Structure and Stability of the Sound Channel in the Ocean," J. Acoust. Soc. Am. 36, 1948-1953 (1964).

FIG. 1
TRUNCATED PARABOLIC PROFILE.

$$c(z) = c_o\left[1-\alpha^2 z^2\right]^{-\frac{1}{2}} \text{ WHERE}$$

$$\alpha = \frac{1}{h}\left[1-\left(\frac{c_o}{c_1}\right)^2\right]^{\frac{1}{2}}$$

AND $|z| < h$

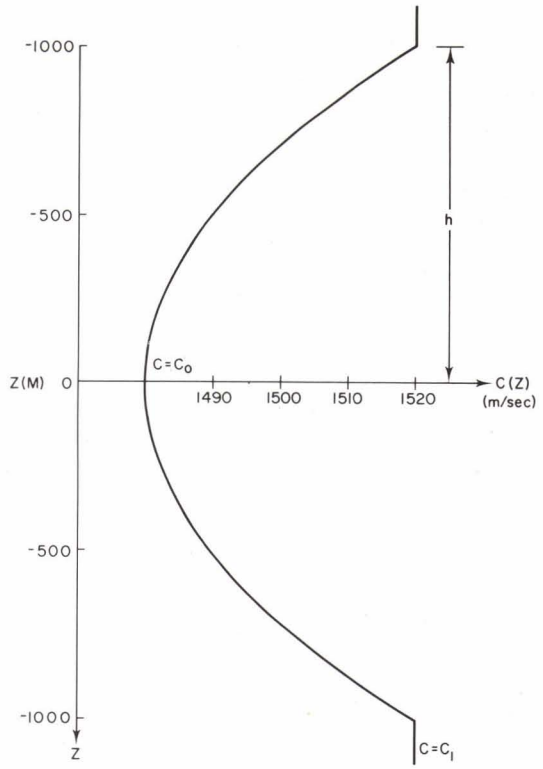

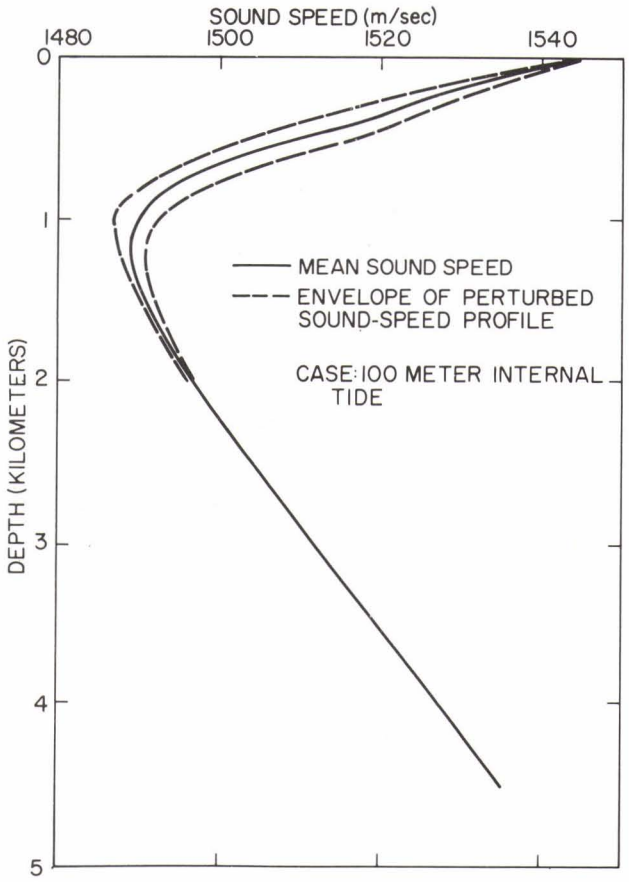

FIG. 2
MEAN SOUND SPEED AND PERTURBATION ENVELOPE
[From Mooers.[18]]

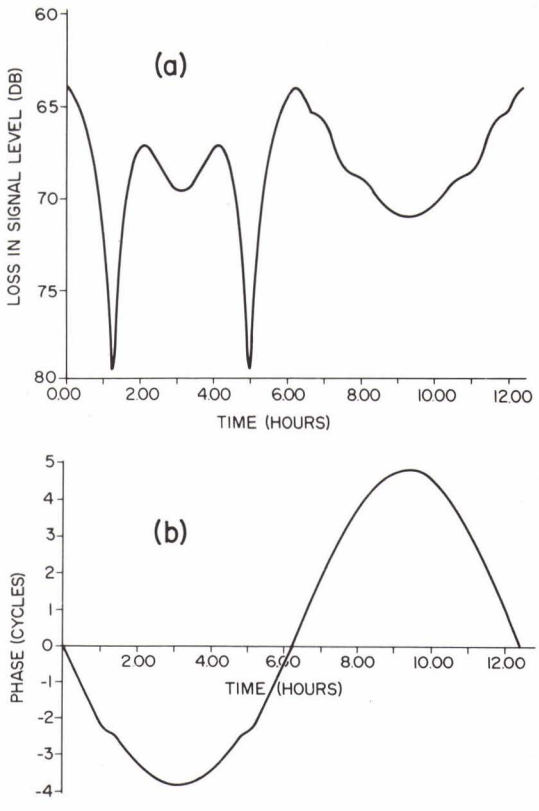

FIG. 3
ACOUSTIC TIME SERIES FOR A SOURCE FREQUENCY OF 100 Hz, A RECEIVER RANGE OF 109.5 km (8th FOCAL ZONE) AND A $\Delta c_o = 1.0$ m/sec

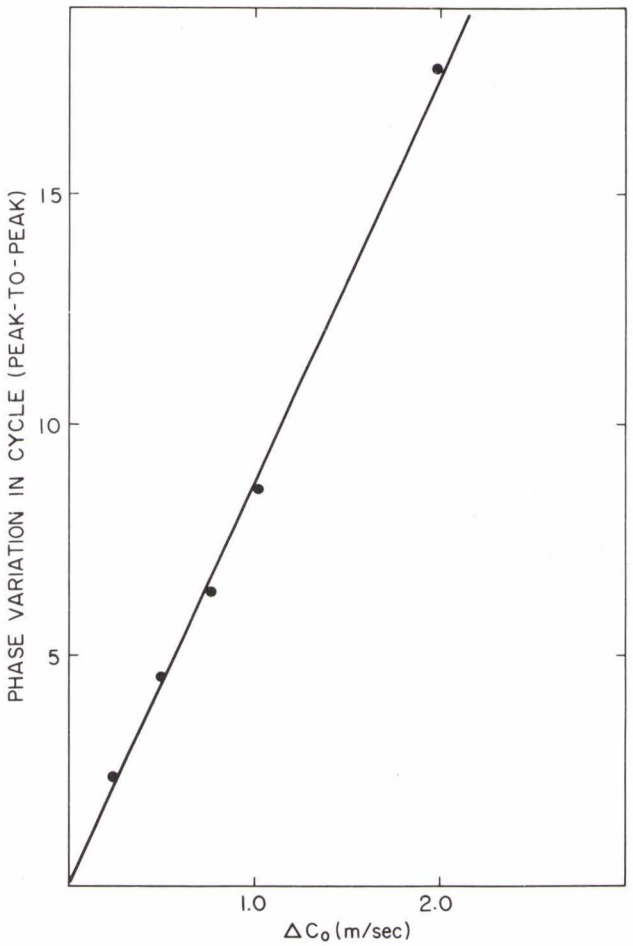

FIG. 4
PHASE VARIATIONS AS A FUNCTION OF TIDAL AMPLITUDE ($\sim \Delta c_o$) FOR A SOURCE FREQUENCY OF 100 Hz AND A RECEIVER RANGE OF 109.5 km

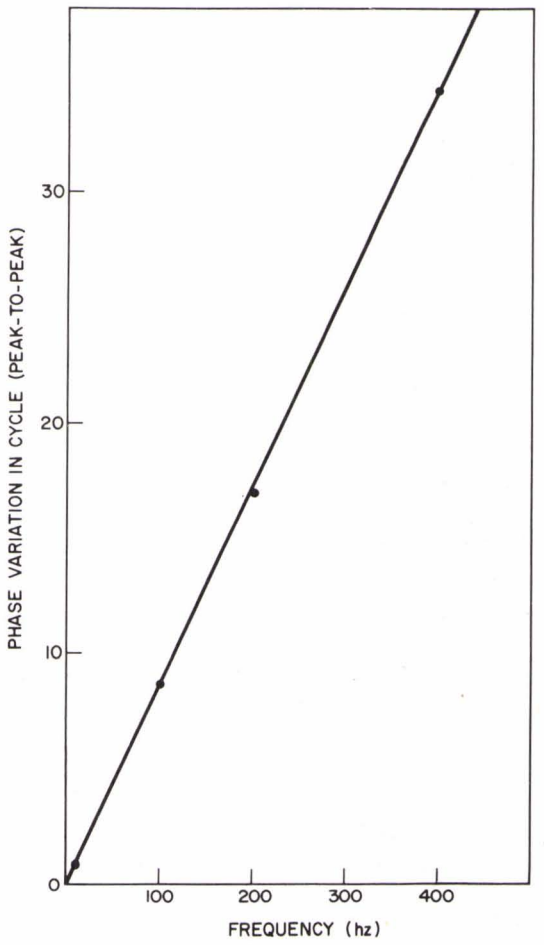

FIG. 5
PHASE VARIATIONS AS A FUNCTION OF FREQUENCY FOR A RECEIVER AT 109.5 km WITH A CONSTANT TIDAL AMPLITUDE ($\Delta c_o = 1.0$ m/sec)

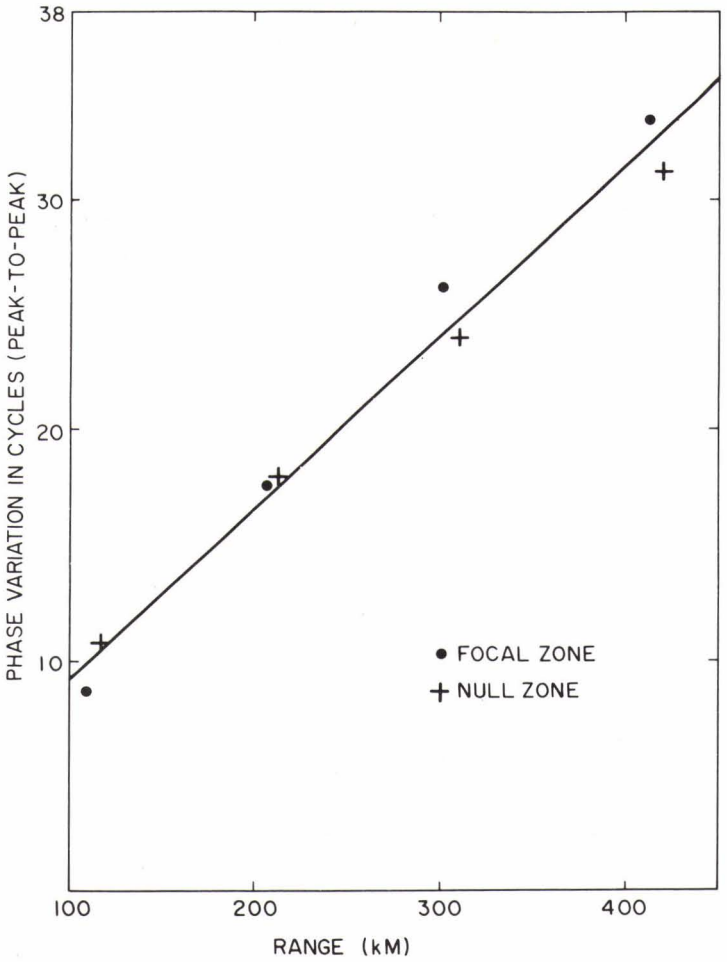

FIG. 6
PHASE VARIATIONS AS A FUNCTION OF RANGE FOR A CONSTANT SOURCE FREQUENCY (100 Hz) AND CONSTANT TIDAL AMPLITUDE ($\Delta c_o = 1.0$ m/sec)

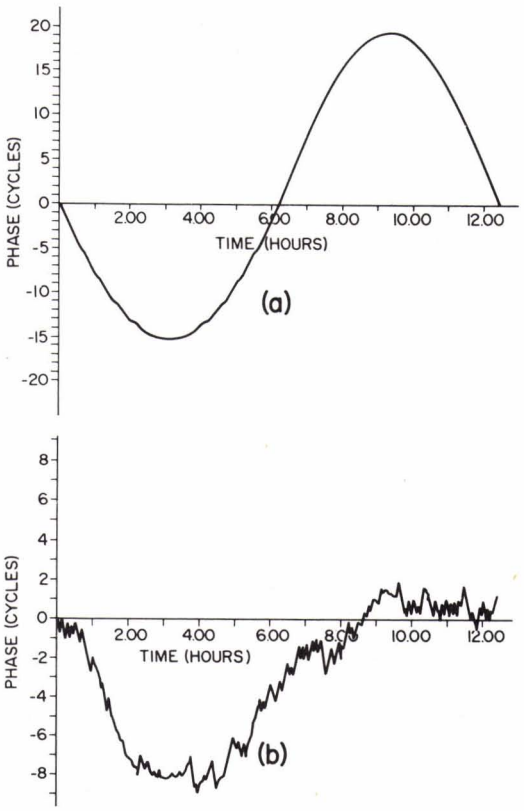

FIG. 7
EXTENDED ANGLE PHASE FOR A SOURCE FREQUENCY OF 400 Hz, RECEIVER RANGE OF 109.5 km, $\Delta c_o = 1.0$ m/sec WITH (a) NO RANDOM COMPONENT IN THE AXIAL VELOCITY AND (b) A GAUSSIAN-DISTRIBUTED RANDOM COMPONENT WITH STANDARD DEVIATION OF 1 cm/sec ADDED TO THE AXIAL VELOCITY

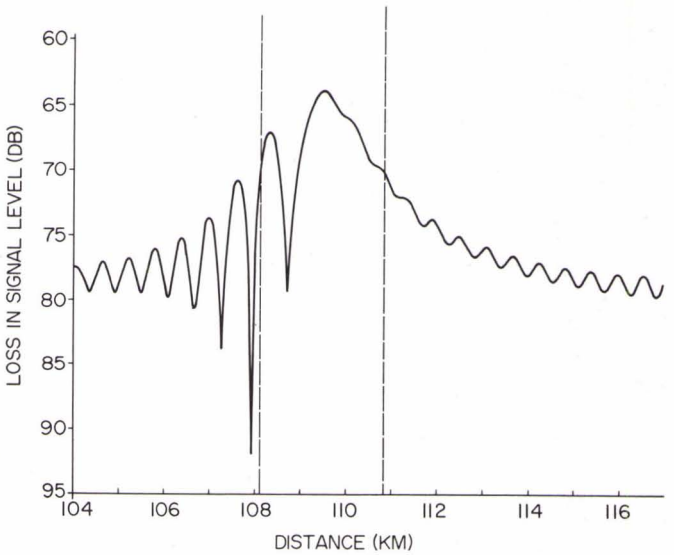

FIG. 8
SOURCE/RECEIVER ON THE AXIS, SOURCE FREQUENCY 100 Hz

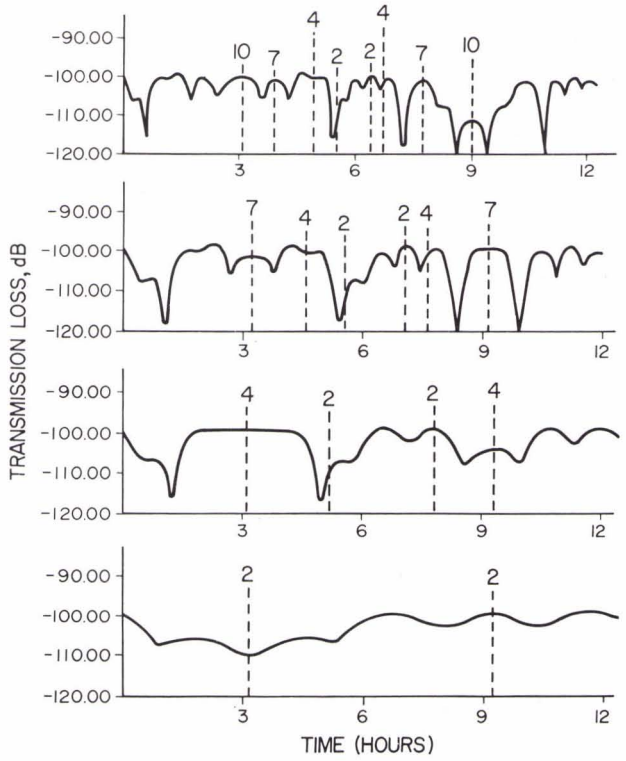

FIG. 9
TRANSMISSION LOSS OVER A TIDAL CYCLE FOR TIDAL AMPLITUDES OF 10, 7, 4 AND 2 m, TOP TO BOTTOM

EFFECT OF SHIP MOTION ON SONAR DETECTION PERFORMANCE

by

J.G. Schothorst
RVO/TNO
The Hague, The Netherlands

ABSTRACT

For an unstabilized transducer, the effect of ship motion on sonar echoes is twofold:

1. Attenuation caused by the rotational movement of the transducer in the vertical plane. The results show that the different loss figures are periodic in range. The average loss (in dB) increases about linearly with the amplitude (in degrees) of the swinging transducer.

2. Distortion caused by the irregular translational movement of the transducer in the direction of the target. In order to arrive at realistic figures for attenuation and distortion, actual ship movements are being measured. Some samples of recorded ship movement data are presented.

1.0 INTRODUCTION

In this paper a brief discussion will be given about the effect of ship motion on the detection performance of a sonar. Two effects will be dealt with: attenuation of sonar echoes due to pitch and roll of a ship with an unstabilized sonar beam, and distortion of sonar echoes due to movements of a sonar transducer in the horizontal plane.

For the case that the different types of ship motion are sinusoidal, theoretical results will be derived for the attenuation, doppler shift, frequency spread and optimum pulse length. These theoretical results will be applied to some samples of actual ship motion data.

2.0 ATTENUATION

In high seas, sonar echoes received by an unstabilized transducer will be attenuated, since the sonar beam moves with the pitch and roll of the ship.

In order to calculate this attenuation, only the movement in the vertical plane through transducer and target has to be considered. The loss in echo strength is namely due to the fact that the direction of the main beam in the vertical plane may differ from the direction in which the submarine is located. Depending on the elevation angle of the transducer at the time of transmission a considerable amount of transmitted energy may miss the target. Also energy reflected by the target may arrive at the transducer when it points in a direction differing from the target direction.

In calculation the loss in echo strength, the following assumptions were made:

a. the main beam of the transducer in the vertical plane is the same for transmission and reception and has a sin x/x - shape. (see formula for the beam shape on fig. 1, in which φ equals elevation angle and B = 3 dB beamwidth)

b. the angle of the sound ray to and from the target with the horizontal plane is close to zero

c. the movement of the transducer in the vertical plane through transducer and target can be described by a sinusoidal function of time with an amplitude A less than 1.2 B (see expression for elevation angle φ on fig.1. This sinusoidal movement of the elevation angle should be regarded as the main Fourier component of the total pitch/roll motion of the ship.

Combination of the expressions for beam shape and elevation angle results in the expression for the instantaneous attenuation f(t). The attenuation of a sonar echo however is a product of the attenuation at the time of transmission t_o and the attenuation at the time of reception $t_o + 2R/C$, in which R = range (m) and C = speed of sound in water = 1500 m/s. The resulting loss in echo strength $l(t_o,R)$ depends both on time of transmission and range. Generally the time of transmission is randomly distributed with respect to the motion of the ship, in which case the mean loss in echo strength can be obtained by averaging $l(t_o,R)$ over t_o. In addition to this mean value also the extreme values of $l(t_o,R)$ have been calculated in order to obtain a measure for the spread in loss of echo strength.

A result of these calculations is presented in fig. 2 for the case A/B = 0.8. The loss figures are plotted here as a function of R/TC, in which T = time period of periodical movement (s). A second horizontal axis with the range in km applies to a period T ≈ 10.6 seconds.

A first observation of fig. 2 shows that the result is periodical in range. The range period (equals TC/4) is of the order of 4 km. Fig. 2 shows further that depending on the time of transmission, the loss may be as low as the minimum curve or as high as the maximum curve. In order to diminish this spread it might be advantageous in certain circumstances to transmit only when the axis of the main beam is directed horizontally. The curve "HOR. TRANSMISSION" indicates for this case the loss of echo strength as a function of range.
Without such or other precautions high losses may be encountered (up to 20 dB for an amplitude of 8^o and a beamwidth of 10^o as is shown by fig.2).

In high seas, large amplitudes for pitch and roll are not uncommon. This is shown by fig. 3 and 4, which present some extreme values for pitch and roll for a frigate in sea state 6. On the basis of this information it may be concluded that in high sea conditions the detection performance of an unstabilized sonar will be severely affected by the pitch and roll of the ship.

3.0 DISTORTION

The distortion of sonar signals is caused by fluctuations in the distance between sonar and target. For the calculation of the effect of these fluctuations the following assumptions were made:

a. the angle of the sound ray to and from the target with the horizontal plane is close to zero
b. the movement of the transducer in the horizontal plane can be described by a sinusoidal function of time (see expression for X on fig. 5).

The assumed sinusoidal movement of the transducer should be regarded again as the main Fourier component of the total horizontal ship motion. Since this kind of ship motion is generally measured by means of accelerometers, the effect of it will be expressed in terms of acceleration in stead of displacement or velocity.

A measure for the distortion of sonar signals can quite easily be determined with the aid of the doppler shift, which is caused by the horizontal motion of the ship. As indicated on fig. 5 the doppler shift Δf is proportional to the instantaneous speed V in a particular direction as well as to the carrier frequency f_o. The doppler shift of a sonar echo is the sum of of this doppler shift Δf at the time of transmission t_o and at the time of reception $t_o + 2R/C$. The resulting doppler shift Δf_s is a function of several parameters, including the time of transmission t_o and the range R.
The maximum value of the doppler shift Δf_s with respect to t_o has been plotted in fig. 5 as a function of the range R. Depending on the time of transmission t_o the doppler shift may be as low as zero or as high as the plotted curve. The overall maximum of this doppler shift occurs at range intervals of TC/2 meter ($\approx$ 8 km).

A measure for the distortion of the sonar pulse can be obtained from the frequency spread during the pulse. This frequency spread has been derived from the calculated doppler shift Δf_s for the case that the pulse length $\tau \ll T$, the period of ship motion. In this case the frequency spread during the pulse can be approximated by the difference between the doppler shifts Δf_s at the end $(t_o + \tau)$ and at the start (t_o) of the pulse (see fig. 6).
The resulting expression for the frequency spread W shows again a dependance on the time of transmission t_o and the range R. The maximum value of W with respect to t_o has been plotted in fig. 6. Depending on the actual time of transmission, the frequency spread may be as low as zero or high as the plotted curve. The overall maximum value for this frequency spread occurs at range intervals of TC/2 meter ($\approx$ 8 km).

In this brief account of the effect of ship motion, attention is only paid to the "worst case" situation, for which the values for doppler shift and frequency spread are maximum. For this reason fig. 7 summarizes the expressions for the maximum values of doppler shift and frequency spread.

From the maximum doppler shift-formula an expression has been derived for the maximum error in the estimated target radial speed. As could be expected beforehand, this maximum error is equal to the maximum speed of the fluctuation in range between ship and target.

From the frequency spread-formula an expression can be derived for the optimum length of a sonar pulse. As a result of the frequency spread, the sonar pulse will be distorted and a correlation loss will occur in a coherent sonar detector. For the worst case situation of fig. 7 the frequency spread increases linearly with the pulse length τ. Because of this fact also the correlation loss will in the first instance increase with τ. For this reason, the signal to noise ratio S/N will show an optimum when it is regarded as a function of the pulse length τ. It might be expected that the optimum value of τ is of the order of the inverse of the frequency-spread. Fig. 7 shows an expression for the approximated optimum value of τ.
The actual optimum value appears to be very close. This actual value for the optimum pulse length has been obtained from a plot of computed results of S/N (see fig. 8). Beyond the optimum pulse length, the signal to noise ratio drops quite rapidly for increasing values of τ. For a

pulse length of twice the optimum one, the signal to noise ratio S/N is already 10 dB below its maximum value.

The "worst case expressions" of fig. 7 are finally applied to the ship motion data of fig. 9. In this figure typical amplitude spectra for horizontal accelerations are plotted for a destroyer in sea state 3. For this reasonable sea state condition the maximum amplitude of the acceleration is quite low (0.12 m/s^2). By consequence the error in the estimated target radial speed is not yet large.
The effect of frequency spread for this mild condition seems to be a more important factor in the case of coherent detection. Fig. 9 indicates that the maximum pulse length in this case is already limited to a value smaller than 1 second. In high sea conditions this restriction will be much more severe.
According to a rough estimate of ship motion in high sea conditions, the amplitude of acceleration in the horizontal plane may well be a factor 10-20 larger. Accordingly, the maximum error in estimated target radial speed will increase to 1.5 - 3 m/s and the maximum pulse length for f_o = 7000 Hz will be limited in this case to 0.18 - 0.25 seconds.

On the basis of the results discussed in this paper it may be concluded that in high sea conditions the motion of the ship may cause a severe degradation of the sonar detection performance. Accordingly, the effect of ship motion should be given due attention in the design and operation of a sonar system.

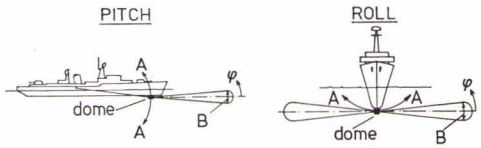

BEAM SHAPE : $\dfrac{\sin\left(2.8\,\frac{\varphi}{B}\right)}{2.8\,\frac{\varphi}{B}}$

$$\varphi = A \sin 2\pi \frac{t}{T}$$

ATTENUATION :

$$f(t) = \left[\frac{\sin\left(2.8\,\frac{A}{B}\sin 2\pi\frac{t}{T}\right)}{2.8\,\frac{A}{B}\sin 2\pi\frac{t}{T}}\right]^2$$

ATTENUATION OF SONAR ECHO

$$l(t_o, R) = f(t_o)\, f\left(t_o + \frac{2R}{C}\right)$$

$$l(R) = \frac{1}{T_o}\int_o^{T_o} l(t_o, R)\, dt_o$$

$$L = 10 \log l$$

FIG. 1

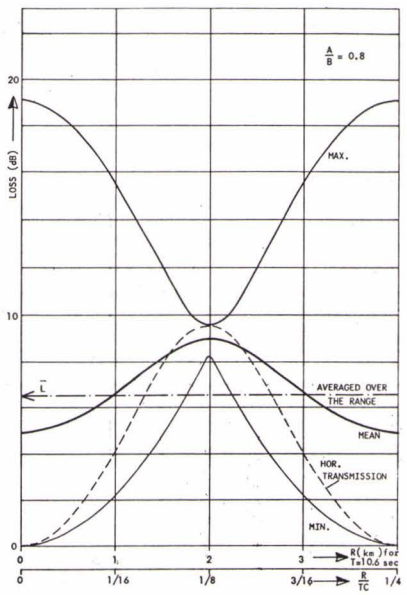

FIG. 2

EXTREME VALUES OF PITCH FOR A FRIGATE

WAVE HEIGHT 4.5 m
WIND FORCE 8 (DATA TAKEN AT SEA)
SEA STATE 6

PITCH

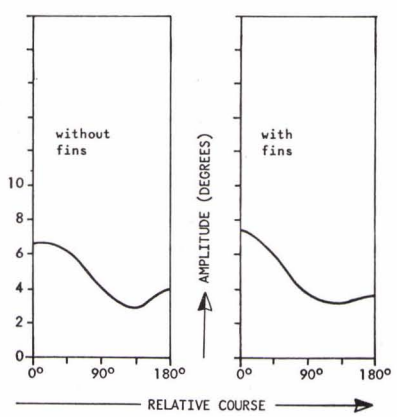

FIG. 3

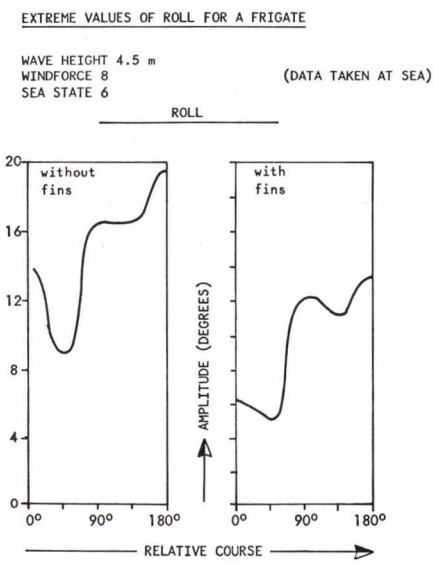

FIG. 4

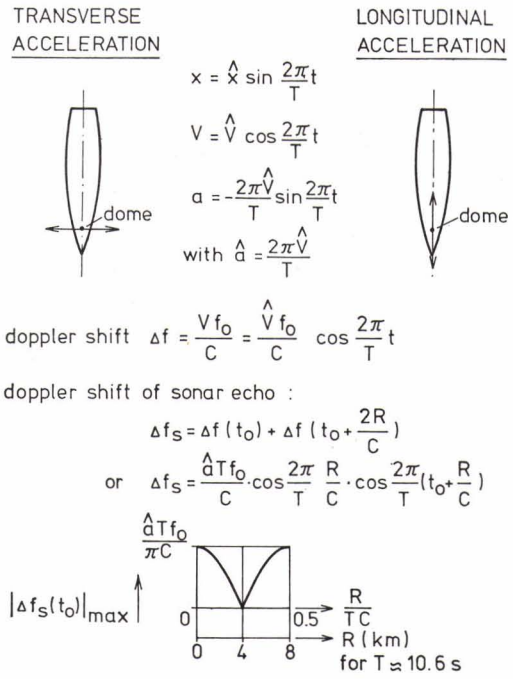

FIG. 5

FREQUENCY SPREAD DURING SONAR PULSE τ

$W = \Delta f_s(t_o + \tau) - \Delta f_s(t_o) \qquad (\tau << T)$

or $W = -\frac{2\hat{a}\tau f_o}{C} \cdot \cos \frac{2\pi}{T} \frac{R}{C} \cdot \sin \frac{2\pi}{T}(t_o + \frac{R}{C} + \frac{\tau}{2})$

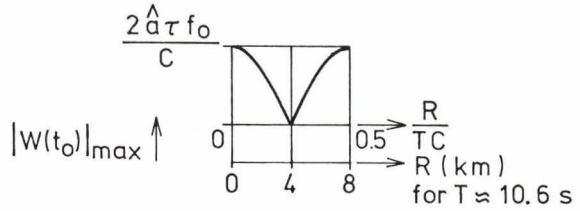

FIG. 6

"WORST CASE" SITUATION

max. doppler shift $|\Delta f_s|_{max} = \frac{\hat{a} T f_o}{\pi C}$

max. error in estimated target radial speed :

$$|\Delta V|_{max} = |\Delta f_s|_{max} \cdot \frac{C}{2 f_o} = \frac{\hat{a} T}{2\pi} \quad (=\hat{V})$$

FIG. 7

max. frequency spread $|W|_{max} = \frac{2\hat{a}\tau f_o}{C}$

approx. for τ_{opt} : $\tau \approx \frac{1}{|W|_{max}} \rightarrow \tau = 0.7\sqrt{\frac{C}{\hat{a} f_o}}$

actual optimum : $\tau_{opt} = 0.6\sqrt{\frac{C}{\hat{a} f_o}}$

COHERENT DETECTION OF TONE PULSE

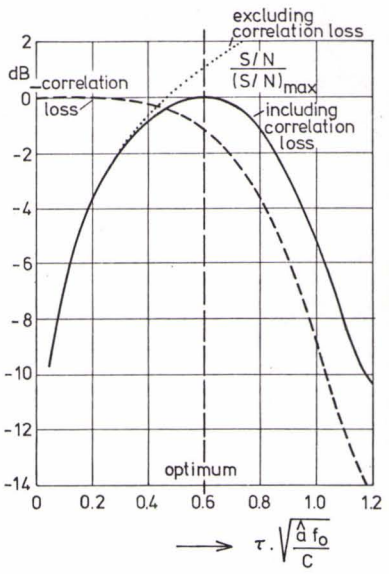

FIG. 8

TYPICAL AMPLITUDE SPECTRA FOR HORIZONTAL ACCELERATONS OF A DESTROYER

(data taken at sea) Wave height : 1 - 2 m
Wind force : 5
Sea state : 3

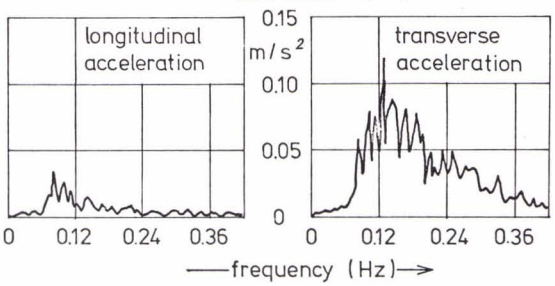

FIG. 9

maximum amplitude : $\hat{a} = 0.12$ m/s² at T = 8 s :

max. error in estimated target radial speed : 0.15 m/s
optimum pulse length at 7000 Hz : 0.8 s

REVIEW PAPERS

DETERMINISTIC METHODS OF SOUND-FIELD COMPUTATION

by

C.W. Spofford and H.M. Garon
Acoustic Environmental Support Detachment
Office of Naval Research
Arlington, Virginia 22217
U.S.A.

ABSTRACT

Models for acoustic propagation in the ocean environment have matured to a level where they are used routinely to estimate deterministic phenomena and, most recently, have been applied to the investigation of stochastic phenomena. This paper reviews the capabilities and limitations of the state-of-the-art acoustic models in the deterministic domain to assist in their fruitful applications to stochastic problems. Formulations based upon ray and wave (both normal-mode and parabolic-equation) techniques are developed from the acoustic wave equation to their most advanced forms. The applicability of these techniques to classes of stochastic phenomena is also discussed.

INTRODUCTION

The results of a series of carefully planned and executed acoustic-oceanographic measurements in the past several years have clearly demonstrated that the ocean has sufficient stability to permit the prediction of a number of acoustic phenomena by models based upon the deterministic (and in this case time-independent) acoustic wave equation. Given that the acoustic wave equation describes the significant features of propagation, the investigation of a particular phenomenon devolves to the questions of environmental inputs and solution techniques. This paper is concerned primarily with the second question: given a complete, deterministic description of the ocean environment, how does one evaluate the acoustic field?

The first portion of the discussion reviews the development of the three types of deterministic solutions currently in use: ray techniques, normal-mode approaches, and the parabolic-equation method. Solutions based upon the three techniques are compared to illustrate the accuracies of the various approximations. The environment is discussed only to the extent that it influences the formulations of a number of approaches. (For example, the continuity of the sound-speed profile is an environmental consideration which has consumed a disproportionate amount of the acoustic-modeler's attention in the ray-tracing treatments.)

Each of the techniques has certain strengths and limitations within the context of deterministic problems, but their applicability to stochastic problems introduces a number of new considerations. There has been an unfortunate tendency, paraphrasing J. B. Keller, to apply models already discredited in the deterministic domain to the solution of stochastic problems. The rush to carry the formulation of the stochastic problem as far as possible before implementation on the computer should not be so all-consuming that the underlying deterministic problem is poorly solved. The final section of this paper addresses some of the practical as well as fundamental limitations of these basic techniques when applied to study stochastic effects.

I. MATHEMATICAL DEVELOPMENT OF THE SOLUTIONS

The propagation of sound in the sea is described mathematically by solutions to the wave equation. Given a monochromatic source of angular frequency ω, at position $\underline{x}'$ in a medium with refractive index $n(\underline{x})$ $(=c_o/c(\underline{x})$, c_o a reference sound speed), then the acoustic pressure $P(\underline{x})$ is obtained from

$$\left[\nabla^2+k^2n^2(\underline{x})\right] P(\underline{x}) = -4\pi\delta(\underline{x}-\underline{x}'), \qquad (1)$$

where the wavenumber $k = \omega/c_o$.

The exact solution of this elliptic partial differential equation, even with boundary conditions at finite range and depth vice the more appropriate radiation conditions, would require an unacceptably lengthy iterative solution on a mesh of impractical size even for today's large digital computers. As an alternative, solutions have been developed which are either approximate (ray and parabolic equation) or exact for more restricted problems (normal modes).

The ray solutions correspond to a high-frequency or large k approximation which, with certain frequency-dependent extensions, may be applicable in deep-water cases for frequencies as low as 25 Hz. Normal-mode solutions, while exact in the range-independent geometry, are practical only for the lower frequencies (less than a few hundred hertz, again in deep water). The parabolic equation solution is also practical only for low frequencies, however

it does permit range variations in the environment so long as no paths of interest are propagating at steep angles (~20 degrees measured from the horizontal). The following sections describe the derivations of these solutions.

In underwater-sound applications, results are typically expressed in terms of intensity and transmission loss rather than pressure. The intensity for a time-harmonic source and locally plane waves is simply

$$I(\underline{x}) = \frac{P^*P}{\rho(\underline{x})\,c(\underline{x})}, \tag{2}$$

where ρ is the density and c the sound speed. Intensities are usually referenced to the intensity, I_o, at a unit distance of 1 yard, hence for a constant-density medium (reasonable within the water column)

$$\frac{I(\underline{x})}{I_o} = \frac{P^*P}{c(\underline{x})} \cdot \frac{c(\underline{x}')}{P_o^*P_o} \quad . \tag{3}$$

Finally, transmission loss relative to one yard is defined as

$$TL = 10\ \mathrm{Log}_{10}\left(\frac{I}{I_o}\right) \tag{4}$$

and in numerical caluclations the intensity at unit distance is taken to be 1.

A. Ray Theory

Ray acoustics traditionally begins with the "ansatz" or postulated solution that the acoustic field may be written as a discrete sum of quasi-plane waves,

$$P(\underline{x},\underline{x}') = \sum_j A_j(\underline{x},\underline{x}') e^{ik\phi_j(\underline{x},\underline{x}')} . \tag{5}$$

When this trial solution is inserted into the wave equation and only the lowest order terms in k are retained, one obtains the eikonal equation

$$\left[\nabla\phi_j(\underline{x},\underline{x}')\right]^2 = n^2(\underline{x}) \tag{6a}$$

and the transport equation

$$\nabla\cdot\left[A_j(\underline{x},\underline{x}')\nabla\phi_j(\underline{x},\underline{x}')\right] = 0. \tag{6b}$$

The eikonal equation in turn yields a set of differential equations describing the ray trajectories, while the transport equation, requiring energy to be conserved along the ray tube, provides the ray amplitudes.

For example, within media which are cylindrically symmetric about the source, the rays may be represented as propagating in a vertical plane and the intensity ratio of equation (3) may be defined as

$$\frac{I}{I_o} = \left(\frac{\cos\theta'}{x}\right)\left(\frac{1}{\sin\theta\left[\frac{\partial x}{\partial\theta'}\right]_z}\right), \qquad (7)$$

where x is the horizontal range ($x'=0$), z the depth of the field point, and the angles θ and θ' correspond to the ray angles measured with respect to the horizontal at the field point and source, respectively. The first term of equation (7) may then be interpreted as the ray-tube's azimuthal divergence and the second as its vertical divergence.

An alternative ansatz to equation (5) begins with the solution written in terms of a continuous superposition of quasi-plane waves [1],

$$P(\underline{x}) = e^{-i\pi/4}\left(\frac{k}{2\pi}\right)^{1/2}\int_{-\infty}^{+\infty} g(\underline{x},\xi)e^{ikf(\underline{x},\xi)}d\xi, \qquad (8)$$

where g and f are determined by the local geometry and the medium. Evaluated asymptotically, the integral is dominated by contributions to the integrand near the points of "stationary phase", ξ_j, which satisfy

$$\frac{\partial}{\partial\xi}f(\underline{x},\xi_j) = 0 \ . \qquad (9)$$

When these points are well-separated from each other and any singularities in $g(\underline{x},\xi)$, the formulation in equation (5) is obtained, where now

$$A_j(\underline{x}) = g(\underline{x},\xi_j) \Big/ \left(f_{\xi\xi}(\underline{x},\xi_j)\right)^{1/2} \qquad (10)$$

and

$$\phi_j(\underline{x}) = f(\underline{x},\xi_j) \ . \qquad (11)$$

These points of stationary phase then correspond to the ray paths connecting the points $\underline{x}$ and $\underline{x}'$. The phases ϕ_j correspond to the travel times along these rays plus any descrete phase shifts acquired by the rays (e.g. $-\pi$ at reflection from a pressure-release surface).

Immediately below we will consider two major areas where traditional ray theory has been found wanting, and recently improved: approaches towards the summation of the rays; and the breakdown of the ansatz, equation (5), in the vicinity of the ray envelope or caustic.

1. Multi-Path Summation

While in principle there are an infinite number of ray paths connecting the source with each observation point in a bounded medium, the total field is generally dominated by less than ten paths. The ray theoretic-solution requires the fully coherent or phased sum of these paths according to equation (5).

a. Long-Range Surface-Image Interference

Until recently, however, computations based upon ray theory assumed an incoherent or rms sum of paths - i.e., the ray intensities were summed without phase. In part, the justification for this procedure was that a range-smoothed transmission-loss curve was desired and it was hoped that the incoherent sum represented a range average. It was also postulated that uncertainties in geometry and the medium precluded sufficiently accurate phase computations to justify a coherent summation. For high frequencies (several hundred hertz) and many geometries, these were reasonable assumptions.

However at low frequencies (less than 100 Hertz) it was found that measured and incoherently computed values of transmission loss differed markedly for shallow sources. This should not be surprising since near the surface the pressure should approach zero, yet the individual ray amplitudes will remain finite. What happens, of course, is that the rays divide into pairs whose components differ only by a surface reflection (Figure 1a). In the approximation of local plane waves the phase difference can be seen (Figure 1b) to be [2]

$$k\Delta\phi = 2kz\sin\theta - \pi \quad . \tag{12}$$

This result was recently generalized by Pedersen to include refraction (Figure 1c) to [3]

$$k\Delta\phi = 2kc_o \int_{\zeta=0}^{z} \frac{\sin\theta(\zeta)}{c(\zeta)}\, d\zeta - \pi \quad . \tag{13}$$

Clearly for shallow-angle rays to sources at low frequencies, $k\Delta\phi \to -\pi$ in either expression and the up- and down-going rays destructively interfere.

The coherent combination of these pairs of paths followed by the incoherent summation of the resulting intensities represents a much better range average than the totally incoherent sum. The phase difference between the paths within a pair is predictable, preserved over significant range intervals, and easily computable from the local geometry without requiring the computation of travel time along the entire ray trajectory. This "semi-coherent" summation has been incorporated in the FACT propagation loss model [4] (along with the incoherent and fully coherent sums), and results based upon the three summations are illustrated for a typical shallow-source/shallow-receiver geometry in Figure 2.

b. Multi-Path "Fluctuations"

As a source or receiver transits the complicated multi-path interference patterns (such as the coherent curve in Figure 2) the signal level fluctuates significantly in time.

The intensity at the field point $\underline{x}$ is given by

$$I(\underline{x}) = \sum_j I_j + 2 \cdot \sum_j \sum_{m<j} (I_j \cdot I_m)^{1/2} \cos(k(\phi_j - \phi_m)), \qquad (14)$$

where I_j are the ray intensities at $\underline{x}$. Assuming that the paths near $\underline{x}$ may be represented by locally plane waves, the phase difference between paths at range $x+\Delta x$ may be obtained from that at x:

$$k(\phi_j - \phi_m) = k(\phi_j(x) - \phi_m(x)) + k\Delta x(\cos\theta_j - \cos\theta_m). \qquad (15)$$

Hence the spectrum of signal fluctuations in range (Δx) will exhibit certain periodicities governed by the cosines of the angles of the interfering paths with powers proportional to the products of their intensities. Similarly if perturbations in the medium alter the phases at $\underline{x}$ with time, the signal also fluctuates. Such temporal multipath fluctuations are significantly larger in amplitude than any individual focusing or defocusing effects produced by the medium.

2. Caustics

The second major area in which the traditional approach to ray acoustics must be augmented is the evaluation of the acoustic field in the vicinity of a caustic. As depicted in Figure 3a, a caustic corresponds to the envelope of a family of rays. On the caustic the field amplitude as predicted by equation (6a) is infinite, since the cross-section of the

ray tube converges to zero. On the shadow-zone side the classical field is zero since, in this region no rays exist. In the limit as $k \to \infty$ this is a reasonable description, however at lower frequencies, the field transits smoothly from the illuminated region (in which real rays exist) to the diffraction region where the field exponentially decays and no 'real' rays exist. In fact, as the frequency decreases the diffraction increases to the extent that large regions exist where it can no longer be ignored.

The solution to this problem has been to employ an asymptotic evaluation of the continuous representation of equation (8) involving either the method of steepest decents or the method of stationary phase, under the assumption that the integrand does not contain any singularities close to the points of stationary phase.

a. Smooth Caustics

The simplest caustic system evolves from two rays arriving at each observation point $\underline{x}$ within the illuminated region. As the caustic is approached the two stationary-phase points in equation (8) coalesce as do the two rays in the illuminated region. The field at the caustic may then be found by proper evaluation of equation (8) at this limit and involves $f_{\xi\xi\xi}$ (see Brekhovskik[5]). However, in order to use this field in the context of the traditional ray approach, it is necessary to provide a means for smoothly

connecting the field at the caustic to the diverging field in the illuminated region.

In this respect, Kravtsov[6] and Ludwig[7] independently developed a uniform asymptotic evaluation of the field valid on and near the caustic as a function of the geometrical acoustic phases ϕ_1, ϕ_2 and amplitudes A_1, A_2 of the two rays (Figure 3b) passing through each point in the illuminated region[6]:

$$P \sim \pi^{1/2} \cdot e^{ik(\phi_2+\phi_1)/2} \cdot e^{-i\pi/4} \cdot \left[u^{1/4}(A_2+A_1)\mathrm{Ai}(-u)+iu^{-1/4}(A_2-A_1)\mathrm{Ai}'(-u)\right]. \quad (16a)$$

In equation (16a), Ai and Ai′ are the Airy function and its first derivative with respect to the argument, where u is given by

$$u=\left[\frac{3}{4}\,k(\phi_2-\phi_1)\right]^{2/3} . \quad (16b)$$

In turn, Holford and Spofford[8] have used this result to obtain a non-uniform expression based upon the difference in the caustic and ray curvatures, κ, and the number of rays tangent to the caustic per unit distance along the caustic, $\frac{d\theta}{dL}$,

$$P \sim \left(\frac{\cos\theta'}{x}\right)^{1/2}\left[\left(4\pi\frac{d\theta}{dL}\right)^{1/2} e^{i(k\phi_c - \pi/4)}\right.$$

$$\left.\cdot\left(\frac{k}{2n^2|\kappa|}\right)^{1/6} \mathrm{Ai}\left(-(2n^2k^2|\kappa|)^{1/3}\Delta z\right)\right], \qquad (17)$$

where Δz in the distance measured normal to the caustic surface.

The Kravtsov-Ludwig result is "uniform" in the sense that while the coefficients of the Ai and Ai′ terms require the rays for their evaluation, they may be analytically continued from the illuminated region into the shadow zone where there are no rays. The Holford-Spofford result corresponds to the linear term in this analytic continuation and is defined for Δz both positive (illuminated region) and negative (shadow zone).

b. Cusped Caustics and Four-Ray Systems

Just as the geometrical-acoustics amplitude is invalid at smooth caustics where $f_{\xi\xi}=0$, the smooth-caustic expressions are not valid when $f_{\xi\xi\xi}=0$. In two-dimensional ray pictures the first situation occurs along caustic curves and the second occurs at points where two caustics are cotangent as shown in Figure 4a. Note that inside the cusp, C, there are three rays through each point vice the two-rays in the illuminated region of a smooth caustic. The nonuniform expression for the field near these cusped caustics was obtained by Pearcey[9] and is described in some detail in Brekhovskikh[10]. Whereas for smooth caustics the uniform field is given in

terms of two quantities κ and $\frac{d\theta}{dL}$, the cusped caustic field is governed by the single parameter β, where

$$P \sim \pi^{-1/2} e^{i(k\phi_c - \pi/4)} (nk\beta)^{1/4} \left(\frac{\cos\theta'}{x}\right)^{1/2} \cdot Pe\left\{\left[(nk)^3\beta\right]^{1/4} X', -\left[nk\beta\right]^{1/2} Y'\right\} , \qquad (18)$$

X' and Y' are cusp-centered coordinates with the Y' coordinate the axis of the cusp, and

$$\left(\frac{X'}{2}\right)^2 = \beta\left(\frac{Y'}{3}\right)^3 , \qquad (19)$$

the equation of the cusp. $Pe(x,y)$ is the Pearcey Function and is discussed in detail in Reference [1], and $k\phi_c$ is the geometrical-acoustics phase at the cusp.

Ludwig's general results have been applied to the cusped caustic yielding a result similar to Equation (18) for the uniform field near a cusped caustic in terms of the geometrical amplitudes and phases of the three rays associated with the cusp. Approaching the cusp along either smooth caustic, both smooth-caustic parameters, κ and $\frac{d\theta}{dL}$ become infinite. The rate at which they approach infinity determines β:

$$\beta = \sqrt[6]{\left(\frac{d^2L}{d\theta^2}\right)_{cusp}} . \qquad (20)$$

While β is in general quite difficult to calculate, it does simplify considerably in the case where the axis of the cusp is horizontal. As it so happens, this case becomes of extreme importance in range-independent media (i.e., $c(\underline{x})=c(z)$) since a horizontal cusp will form at the same depth as the source.

While higher order singularities are possible, the most complicated ray geometry typically encountered is when a smooth caustic is quite close to a cusp as shown in Figure 4b. In this case the two fields may no longer be treated as distinct and a basic four-ray system is generated where it is possible that even the smooth- and cusped-caustic expressions may break down. For most cases of interest, however, a phased sum of the two distinct fields has been found to be adequate.

3. False Caustics

One of the major concerns in using ray acoustics has been the functional representation for the sound-speed profile since it governs the ease with which rays may be traced and intensities computed. Pedersen[11] and others have shown that when a sound-speed profile with continuous derivatives is approximated by linear segments, there exists the possibility of introducing false or extraneous caustics. The actual problem, on the other hand, does not lie with the profile representation but instead with the traditional

approach to ray acoustics. The results of the modified ray theory [12] (MRT) developed by Murphy and Davis graphically illustrate this point.

MRT is based upon a generalized Wentzel-Kramers-Brillouin (WKB) expansion of equation (8) and, as such, includes the caustic modifications mentioned above. Murphy and Davis have shown that this procedure leads to a frequency-dependent displacement of the ordinary ray-theory ranges. Employing the simple profile depicted in figure 5 , ordinary ray theory would predict the formation of a caustic due entirely to the discontinuity in the gradients of the profile at the juncture of the two segments. The ray tangent to the caustic coincides with the minimum ($\frac{\partial x}{\partial \theta} = 0$) in range on the accompaning angle (θ)- vs. range (x) plot. The MRT angle-vs.-range plot for the same case is also shown. At a high frequency MRT still shows a caustic (in fact, two: one associated with the minimum in range, and another associated with the smooth maximum in range). However, as the frequency is decreased the angle-vs.-range curve is completely smoothed out and the caustic of ordinary ray theory disappears.

A more complicated example (figure 6) was recently provided by Weinberg [13], using three different realizations of an Epstein profile: piecewise linear, piecewise quadratic, and cubic spline. In all three forms, the

source was placed on the axis of the Epstein profile with the depth of the observation point situated somewhat shallower. The results at a frequency of 1 kHz. are also based upon a generalized WKB expansion of equation (8). Even at 1 kHz., all three representations provide essentially the same results. Thus, with a proper analysis of the caustic fields, the profile representation is not critical to the total field.

This type of insight into the frequency-dependent smoothing of the $x(\theta)$ curve lead directly to the development of the FACT model,[4] where the primary concern was not only with speed of computation, but also being able to provide meaningful asymptotic caustic values along with the effects of coherence. Representing the profile in terms of linear segments permitted a rapid trace of the rays but also introduced the possibility of false caustics as discussed above. By limiting the angle-vs.-range curve behavior for a particular ray family to two-degrees of freedom (i.e., using a quadratic fit) and also by carefully selecting the rays to be traced with respect to the profile, the problem of false caustics was reduced significantly.

In range-dependent media the profile representation takes on a different aspect, for the primary difficulty here is not in tracing rays, but in defining how the medium will vary between specified profiles.

Two methods for connecting the profiles are in common use. The first method[14] allows the sound-speed representation to be arbitrary in depth but linear, quadratic, or cubic in range at fixed depth. The second method[15] is based upon segmenting the region between the profiles into triangular sectors where two vertices of the triangle correspond to two points on one of the profiles and the third vertex corresponds to a point on the other profile. Along the connecting legs of the triangle the sound-speed varies as $c(z,x)=c_o+az+bx$. Both methods have their drawbacks. The first method is easy to automate but leads to ray-tracing difficulties since closed form expressions for the ray paths are not available. Additionally, this method can lead to totally unreasonable profiles at intermediate ranges between reasonable specified profiles. The second method is quite difficult to automate in that it usually requires an oceanographer to determine the required connections. Aside from this problem, however, the linearity of the sound speed leads to a closed form expression for a ray's path within each triangular sector enabling a relatively rapid trace.

4. Summary of Ray Acoustics

With the advances in classical ray theory described above, ray acoustics can and has been successfully extended

down to frequencies on the order of 25 Hz. The primary difficulty with these modifications lies in their complete automation. In many cases, especially for range-dependent media, the ray pathologies may be so complex as to require a hand analysis.

B. Normal Modes

Normal-mode theory in underwater acoustics is based upon the initial requirement that the sound speed vary as a function of depth only, i.e., $c(\underline{x})=c(z)$. This simplification permits the reduction of the wave equation by separation of variables, leading to a system of two linear differential equations, one for the depth dependence of the field, the other for the range dependence. The total field $P(\underline{x})$ is then given by the product of the two separable solutions integrated over the separation parameter, λ. Specifically, the result may be represented by a Bessel-Hankel transform[16],

$$P(\underline{x})=\int_{\lambda=0}^{\infty} \hat{P}(z,z',\lambda)J_o(\lambda x)\lambda d\lambda, \qquad (21)$$

where J_o is the zeroth order Bessel function, and the depth function $\hat{P}$ satisfies

$$\left[\frac{d^2}{dz^2}+(k^2n^2(z)-\lambda^2)\right]\hat{P}(z,z',\lambda)=-\frac{1}{2\pi}\delta(z-z'), \qquad (22)$$

λ is the radial wave number and may be assumed to be complex.

By modifying the integration contour an alternative to the continuous standing-wave representation of equation (21) can be derived,

$$P(\underline{x}) = \frac{1}{2}\int_{\infty e^{i\pi}}^{\infty} \hat{P}(z,z',\lambda) H_o^{(1)}(\lambda x)\, \lambda d\lambda, \qquad (23)$$

such that the zeroth-order Hankel function of the first kind, $H_o^{(1)}$, now represents an outgoing wave under the time-dependence $e^{-i\omega t}$. Equation (23) can be numerically integrated as DiNapoli has done in his Fast Field Program (FFP). In the FFP, the integral is cast into the form of a Fast Fourier Transform by employing the asymptotic form of the Hankel function. This procedure, coupled with a judicious selection of the functional form of the sound-speed profile to permit the rapid calculation of the constituents of $\hat{P}$, allows a practical evaluation of equation (23).

With respect to the normal mode expansion, the bulk of the remaining problems center about the evaluation of the depth function $\hat{P}(z,z',\lambda)$. All of these methods are subject to the boundary constraints of a pressure-release surface, Sommerfield's radiation condition, and continuity conditions at discontinuities in both the water column and bottom. Additionally, the particular form of the solution

$\hat{P}(z,z',\lambda)$ depends upon the functional description of the sound speed-profile itself.

The general normal-mode expansion may be obtained by identifying the singularities of $\hat{P}(z,z',\lambda)$ and subsequently deforming the integration contour about the singularities. Depending upon how the sound-speed profile is terminated, three classes of singularities are evident: (1) a finite number of poles along the real λ axis (assuming the medium is lossless), (2) an infinite number of complex poles, and (3) branch points which appear pairwise. For sound-speed profiles encountered in underwater acoustics, the branch-point singularities are ordinarily associated with the modeling of the ocean bottom.

In order to illustrate the physical significance of these mathematical singularities consider a sound-speed profile terminated by an isovelocity halfspace ($c(z>z_B)=c_H$) such as that illustrated in figure 7. Restricting attention to the first quadrant ($Re(\lambda)>0, Im(\lambda)>0$) of the complex λ plane, the isovelocity termination will lead to a branch point singularity at $\lambda=\lambda_H=\frac{\omega}{c_H}$ and the water column will produce a finite number of poles λ_m along the real λ axis such that $\lambda_H<\lambda_m<\lambda_{max}=\frac{\omega}{c_{min}}$. In a rather loose sense, contributions to the field from the poles along the real axis correspond to axial rays, for λ_m close to λ_{max} and

bottom-reflected rays for $\lambda_m \simeq \lambda_H$. The influence of the infinity of poles off the real-λ axis to the field depends on the choice of branch cut.

Most normal mode programs today are based upon the Pekeris-type branch cut[17] illustrated in figure 7 . The corresponding integration contour leads to a symbolic representation for equation (23) as

$$2\pi i \sum_{m=1}^{N} (\text{residues for } \lambda_m \ni : \mathrm{Im}(\lambda_m)=0) \qquad (24)$$

$$+ 2\pi i \sum_{m=N+1}^{\infty} (\text{residues for } \lambda_m \ni : \mathrm{Re}(\lambda_m), \mathrm{Im}(\lambda_m)=0)$$

$$+ \int (\text{Perkeris Branch Cut}) + \int (\text{Semi-Circle}, \ |\lambda| \sim \infty).$$

An alternative representation is obtained by employing the Ewing-Jardetsky-Press (EJP) branch cut (figure 7),

$$2\pi i \sum_{m=1}^{N} (\text{residues for } \lambda_m \ni : \mathrm{Im}(\lambda_m)=0) \qquad (25)$$

$$+ \int (\text{EJP Branch Cut}) + \int (\text{Semi-Circle}, |\lambda| \sim \infty),$$

where the integration at infinity along the semi-circle can be shown to be zero for all cases of interest. Labianca[16] has pointed out that the Pekeris cut has practical as well as theoretical problems, particularly since the residue sum

diverges for ranges less than $\sqrt{3}\cdot(z+z')$. For ranges greater than this the residue sum converges and the two representations are equivalent.

Representing the EJP branch cut in equation (25) as a finite integration on the real-λ axis and an infinite integration along the complex-λ axis, the normal mode solution can be explicitly expressed as

$$P(\underline{x}) = \sum_{m=1}^{N} C_m(\lambda_m)\hat{P}_m(z,\lambda_m)\hat{P}_m(z',\lambda_m)H_o^{(1)}(\lambda_m x) \qquad (26)$$

$$+\int_{\lambda_R=0}^{\lambda_{R_{min}}} f(\lambda_R,z,z,x)\,d\lambda_R + \int_{\lambda_c=0}^{\infty} g(\lambda_c,z,z',x)\,d\lambda_c,$$

where the so-called eigenfunctions $\hat{P}_m$ and eigenvalues λ_m satisfy the discretized form of equation (22):

$$\left[\frac{d^2}{dz} + (k^2n^2(z)-\lambda_m^2)\right]\hat{P}_m = -\frac{1}{2\pi}\delta(z-z') \qquad (27)$$

and the particular boundary conditions, and where the $C_m(\lambda_m)$ are the mode-amplitude weighting factors as determined by normalizing the eigenfunctions. Thus the normal-mode expansion consists of a classical sum of modes plus a continuum of modes which arise from the EJP branch cut. This continuous spectrum has frequently been ignored as a result of the more common usage of the Pekeris representation (equation (24)).

Considerable effort in a normal-mode solution is consumed finding the singularities of the integrand within equation (21). One such method involves guessing λ_m, integrating the differential equation (27) to one of the boundaries (usually the surface) and iterating on λ_m until the boundary condition is satisfied within prescribed tolerances. Such tolerances do not guarantee overall accuracy, and control remains a persistent problem. Also since the number of modes and the number of iterations per mode are roughly proportional to frequency, normal-mode solutions are practical only for low frequencies. However they do represent the exact control solution against which all others may be tested. These tests then allow the extension of more general techniques to the range-dependent environment with some confidence.

Some extensions of the normal-mode solutions to range-varying media (i.e., $n(\underline{x})=n(x,z)$ have been attempted. These generally fall into one of three approaches:

(i) Those which assume no cross-coupling between modes;

(ii) Those which assume at least weak coupling between modes at different range intervals;

(iii) Those which require matching a boundary condition for the total field at some x for all z.

The adiabatic approach of (i) requires that all energy propagating in mode number 'n' remain in the mode independent of range[22, 26]. The phase velocity (implicit in λ_m), then, varies with range as new sound-speed profiles are introduced. The weak-coupling approach of (ii) requires a large number of mode computations at different ranges to evaluate the weakest form of coupling between each mode and only its immediate neighbors. The third approach, (see Kanabis[18]) requires continuity of pressure across an interface at arbitrary range. The field at the interface is computed in terms of the modes just prior to the interface, and then decomposed into the new modes defined by the profile just after the interface. This procedure neglects any backscatter and requires either a large number of mode calculations, or places rather stringent requirements on the range variation.

C. Parabolic Equation

The final approach to be considered here is the parabolic-equation technique, where the solution to the elliptic wave equation, equation (1), is initially assumed to be of the form

$$P(\underline{x}) = \psi(x,z)H_o^{(1)}(kx). \qquad (28)$$

The Hankel function, $H_o^{(1)}(kx)$, represents the primary radial

dependence of the field in terms of an outward propagating cylindrical wave.

To this point the only approximation made is the assumption of cylindrical symmetry. The second approximation is that the observation point, x, is many wave lengths from the source (i.e., kx>>1). Subsequently the asymptotic form of the Hankel function may be used to obtain from equation (28)

$$\psi_{xx}+2ik\psi_x+\psi_{zz}+\psi k^2(n^2-1) = 0 \qquad (29)$$

plus terms of order ψ/kx^2. Finally, employing the approximation

$$\psi_{xx}<<2ik\psi_x \ , \qquad (30)$$

which neglects backscatter and is generally described as valid only for components of the field propagating at small angles with respect to the horizontal, the parabolic equation of Leontovich[19] and Fock[20] is derived:

$$i\psi_x+\frac{1}{2k}\psi_{zz}+\frac{k}{2}(n^2-1)\psi = 0 \qquad (31)$$

Although the parabolic approximation has been available for some time, only recently have efficient integration

schemes been applied to it, namely, the introduction by Tappert and Hardin[21] of the split-step Fast Fourier Transform numerical integration algorithm. This algorithm marches the solution away from the source on an equi-spaced depth grid. The value of ψ at a new range $x+\Delta x$ is obtained from the solution at sept x by

$$\psi(x+\Delta x,z)=e^{i\Delta x k(n^2-1)/2}\mathcal{F}^{-1}\left[e^{-i\Delta x \ell^2/2k}\mathcal{F}(\psi(x,z))\right], \quad (32)$$

where $\mathcal{F}$ is the Fourier transform, $\mathcal{F}^{-1}$ its inverse, and ℓ the transform variable. This technique is easily implemented, highly efficient, and even in the above form, sufficiently accurate for most applications.

The parabolic approximation, as expressed by the inequality in equation (30), has been shown to result in an error in the phase velocity of the normal modes in layered media[22]. The phase velocity error, in turn, can cause substantial shifts in the range of the caustic regions. Recently Brock, Buchal, and Spofford[23] have been able to reduce the magnitude of the error by using the PE technique to solve a pseudo-problem where the refractive-index profile, n(z) has been transformed into a new set of points $(\tilde{n},\tilde{z})$. This transformation takes on a particularly simple form for the majority of cases of interest, namely

$$\left.\begin{aligned}\tilde{z}&=zn^{1/2},\\ \tilde{n}&=\sqrt{2n-1}\ .\end{aligned}\right\} \quad (33)$$

Within the accuracy of the WKB approximation, the normal modes for this new environment have the same phase velocities as the equivalent wave-equation modes in the original environment, and the depth transformation preserves the relationship between observation depths and mode turning points.

It would not be an exaggeration to say that the PE has revolutionized propagation modeling by providing a wave solution with full mode coupling for the range-dependent environment. It is easy to implement, efficient, and may be used to map out the full acoustic field in both range and depth. Since both the range step and depth mesh are proportional to the acoustic wavelength, PE, like normal modes, is practical for low frequencies only. Computer codes have been implemented for deepwater studies up to 300 Hz, however, typical applications are limited to approximately 100 Hz.

II. COMPARISON OF TECHNIQUES

In this section we compare frequency-modified ray theory and the PE technique with the exact solution as given by normal-modes. Consequently the examples are limited to the range-independent environment. Additionally, the comparisons which will be made will be for a high-loss bottom concentrating on the refracted and RSR paths only.

Initially we consider a simple pressure-gradient profile for a shallow source (60 feet) at a frequency of 25 Hz and a deep receiver (7200 feet). The results of the three techniques are compared in figure 8 where, specifically, the three models are FACT[4] - a ray model with caustic corrections and surface-image interference; PE without the profile transformation described in Section I-C , and an N-layer normal-mode model developed by Stickler at Penn State Applied Research Laboratory[24]. While Stickler's model can compute contributions from the continuous spectrum, it was run for the discrete modes only. In this geometry a smooth caustic occurs at the receiver depth at approximately 30 nm intervals. The rapid oscillations seen within the caustic regions of both the normal-mode and PE results are due to the two-ray interference. The ray-theory model has intentionally averaged these oscillations, since they do not reflect a change in average level. It has, however,

included the semi-coherent combination of paths which, for this frequency and source depth increase the average transmission loss by approximately 8 dB over the value the incoherent summation would yield. This figure also illustrates the effects of excluding the continuous spectrum in the normal-mode calculations. For ranges less than 8 nm the normal-mode results are seen to depart dramatically from both the ray-theory and PE models, since the energy associated with these high-angle paths is not included in the discrete system.

The second example (figure 9) also is based upon a pressure-gradient profile but now the source is at the same depth as the receiver (7200 feet). In this geometry a horizontal cusp is developed (as illustrated in figure 4a) at 22 nm and repeats with a 22 nm period. A smooth caustic is also present at this depth at 35 nm corresponding to the surface reflection of one of the smooth caustics associated with the first cusp. In this case the smooth- and cusped-caustics are well-separated and the ray-theory results are seen to agree with the results of the other two models.

The final case considered is based upon a typical deep-water sound-speed profile (figure 10) where the source and receiver are situated such that two ray families propagate: a totally refracted (RR) family and a refracted-surface

reflected (RSR) family. Figure 11 initially compares the ray solution with that of normal modes (again at 25 Hz). The agreement is generally excellent even though the ray model does make a clearcut distinction between the RR and RSR caustic regions while the mode model does not. The apparent constructive interference between the RR and RSR caustics is not accounted for in the ray model since these families of rays are combined incoherently. Figures 12 and 13 compare the PE technique with the normal-mode solution for exactly the same case. In figure 12 PE was run without the profile transformation discussed previously, resulting in a displacement of the PE convergence zone relative to the normal-mode result. With the profile transformation PE, figure 13, now accurately matches not only the convergence-zone ranges but much of the CW multipath fine structure.

In the context of range-independent environments it is seen that the three basic techniques have largely converged. Wave-length dependent corrections to ray theory have been developed which permit its extension to much lower frequencies. Many of the limitations of the parabolic equation are now more clearly understood and the most limiting aspects of the small-angle approximation have been overcome. This apparent convergence is not intended to imply that each technique is equally applicable to any problem. In the next section we shall consider the applicability of these techniques to the study of certain classes of oceanographic phenomena.

III. APPLICATIONS TO THE STUDY OF OCEANOGRAPHIC FEATURES

Many of the acoustically interesting oceanographic features correspond to a medium which varies not only as a function of range and depth but also azimuth and time. In the deterministic techniques discussed above the environment is frozen in time and generally treated as azimuthally symmetric. The effect of transverse gradients and out-of-plane reflection can be important in some cases, however a number of significant oceanographic features can be analyzed without including these effects and without any loss of generality.

Normal-mode techniques are by far the most limited since they cannot accommodate rapid variations in range. Instead, they can be used within the context of perturbation theory to study the acoustic effects of small inhomgeneities superimposed on a basically range-independent profile. Perturbation theory has also been applied successfully by Labianca and Harper[25] to assess the influence of surface roughness on low-frequency propagation. Only the largest scale oceanographic features such as the gradual migration of the sound-channel axis towards the surface in the North Pacific can be legitimately analyzed within the adiabatic approximation[26]. Macro-scale features such as fronts and eddies are too abrupt for the adiabatic technique[27] while probably too gradual for the abrupt transition approaches of Kanabis, et al.

Ray theory, in principle, is the most powerful since it can accomodate rapid variations with refraction through large angles. In studying small perturbations, enough rays must be considered to adequately illuminate all features of interest, and, if necessary, detailed caustic calculations may be required to assess the true influence of these features on the acoustic phase and amplitude. For larger scale oceanographic features ray techniques are most useful for illustrating quatitative effects and are especially illuminating when used in conjunction with field-mapping computations such as PE.

PE is by far the most versatile technique, though of course, limited to low frequencies and shallow angles. Fortunately the propagation paths of interest in analyzing oceanographic features are sufficiently shallow to be accurately treated, and the features themselves are not expected to produce sufficient backscatter to violate the parabolic approximation[28].

In studying bottom-reflectivity questions, normal modes are most appropriate since they can accomodate both discontinuities (which PE using the split-step FFT cannot), and partial reflections (which ray theory typically does not). Additionally normal mode programs[29] have been extended to include shear waves in the bottom.

IV. SUMMARY

Concurrent advances in the application of normal-mode and ray theory to ocean acoustics, coupled with the introduction and refinement of the parabolic-equation technique, have brought what were previously considered divergent and non-intersecting approaches into agreement over a substantial common ground of applications. The demonstrated success of these techniques in the study of deterministic phenomena portends their fruitful application in the stochastic domain. While each approach has its unique strengths and weaknesses, their combined power should be sufficient to attack a large number of previously impenetrable questions.

REFERENCES

1. R. L. Holford, Continuation of LRAPP (CONFIDENTIAL), Reference 7, "Modifications to Ray Theory Near Cusped Caustics" (Unclassified), February (1972), Bell Laboratories on Contract N00014-69-C-0088, p. 5.

2. F. E. DeAngelis and C. W. Spofford, "Surface Image Interference Effects in Long-Range Active Sonar Systems" (U), 20 February (1970), Bell Laboratories on Contract N00014-69-C-0074 (SECRET).

3. M. A. Pedersen, D. F. Gordon, and D. White, "Surface Decoupling Effects," unpublished tech. memo to Long Range Acoustic Propagation Project (LRAPP).

4. C. W. Spofford, "The FACT Model", Vol. 1, Maury Center Report 109, November (1974).

5. L. M. Brekhovskikh, Waves in Layered Media, Academia Press, New York, (1960), p. 484.

6. Yu. A. Kravtsov, "One Modification of the Geometrical Optics Method," Soviet Radiophysics, Vol. 7, (1964), pp. 104-117.

7. D. Ludwig, "Uniform Asymptotic Expansions at a Caustic," Commun. Pure Appl. Math, Vol. 19 (1966), pp. 215-250.

8. C. W. Spofford and R. L. Holford, "Calculation of the Field near a Smooth Caustic by means of Uniform and Nonuniform Asymptotic Approximations Derived from Ray Theory", (to be published).

9. T. Pearcey, "The Structure of an Electromagnetic Field in the Neighborhood of a Cusp of a Caustic", Philos. Mag., Vol. 37 (1946), pp. 311-317.

10. L. M. Brekhovskikh, pp. 492-296.

11. M. A. Pedersen, "Acoustic Intensity Anomalies Introduced by Constant Velocity Gradients," Journal of the Acoustical Society of America (JASA), Vol. 33 (1961), pp. 465-474.

12. E. L. Murphy and J. A. Davis, "Modified Ray Theory for Bounded Media," JASA, Vol. 56, (1974), pp. 1747-1760.

13. H. Weinberg, "Application of Ray Theory To Acoustic Propagation In Horizontally Stratified Oceans," JASA, Vol. 58 (1975), pp. 97-109.

14. See, for example:
J. J. Cornyn, "Grass: A Digital-Computer Ray-Tracing and Transmission-Loss-Prediction System," Naval Research Laboratory Report 7621, Vol. 1, Washington, D. C., December (1973).

15. C. W. Spofford, "The Future of Long-Range Acoustic Transmission-Loss Prediction," Paper presented at the 28th U.S. Navy Symposium on Underwater Acoustics, Washington, D.C., November (1970).

16. A particularly in-depth discussion of the different representations may be found in:
F. M. Labianca, "Normal Modes, Virtual Modes, and Alternative Representations in the Theory of Surface-duct Sound Propagation," JASA, Vol. 53 (1973), pp. 1137-1147.

17. Both the Pekeris and EJP branch cuts are lucidly discussed in:
D. C. Stickler, "Normal Modes In Ocean Acoustics", Penn. State Univ. Applied Research Laboratory Tech. Memo TM 75-24, State College, Pa., February (1975).

18. W. G. Kanabis, "A Shallow Water Acoustic Model For Ocean Stratified in Range and Depth", Naval Underwater Systems Center (NUSC) Tech. Report 4887-I, New London, Conn., March (1975).

19. M. A. Leontovich and V. A. Fock, J. Phys. of the USSR, Vol. 10 (1946), p. 13.

20. V. A. Fock, J. Phys. of the USSR, Vol. 10 (1946), p. 399.

21. F. D. Tappert and R. H. Hardin, SIAM Review, Vol. 15 (1973), p. 423 (abstract).

22. S. T. McDaniel, "Propagation of Normal Modes in the Parabolic Approximation," JASA, Vol. 57 No. 2, (1975), pp. 307-311.

23. H. Brock, R. Buchal, and C. W. Spoford, "Modifying the Sound-Speed Profile to Improve the Accuracy of the Parabolic Equation Technique," (to be published).

24. D. C. Stickler, "A Normal Mode Program with both Discrete and Branch Line Contributions," JASA, Vol. 57 (1975), pp. 856-861.

25. E. Y. Harper and F. M. Labianca, "Perturbation Theory for Scattering of Sound from a Point Source By a Rough Surface In the Presence of Refraction," JASA, Vol. 57 No. 5, (1975), pp. 1044-1051.

26. R. Graves, A. Nagl, and H. Uberall, "Underwater Sound Propagation Described by Range-dependent Normal Modes," JASA, Vol. 57 Suppl. No. 1, (1975), p. 564. (abstract).

27. D. M. Milder, "Ray and Wave Invariants for SOFAR Channel Propagation," JASA, Vol. 46 No. 5 (Part 2), (1969), pp. 1259-1263.

28. H. P. Bucker, "Sound Propagation Calculations Using Bottom Reflection Functions," Physics of Sound In Marine Sediments edited by L. Hampton, Plenum Press, New York, pp. 223-239, (1974).

29. H. W. Kutschale, "The Integral Solution of the Sound Field in a Multilayered Liquid-Solid Half Space with Numerical Computations for Low-Frequency Propagation in the Artic Ocean," Lamont-Doherty Geological Observ. Tech. Report CU1-70.

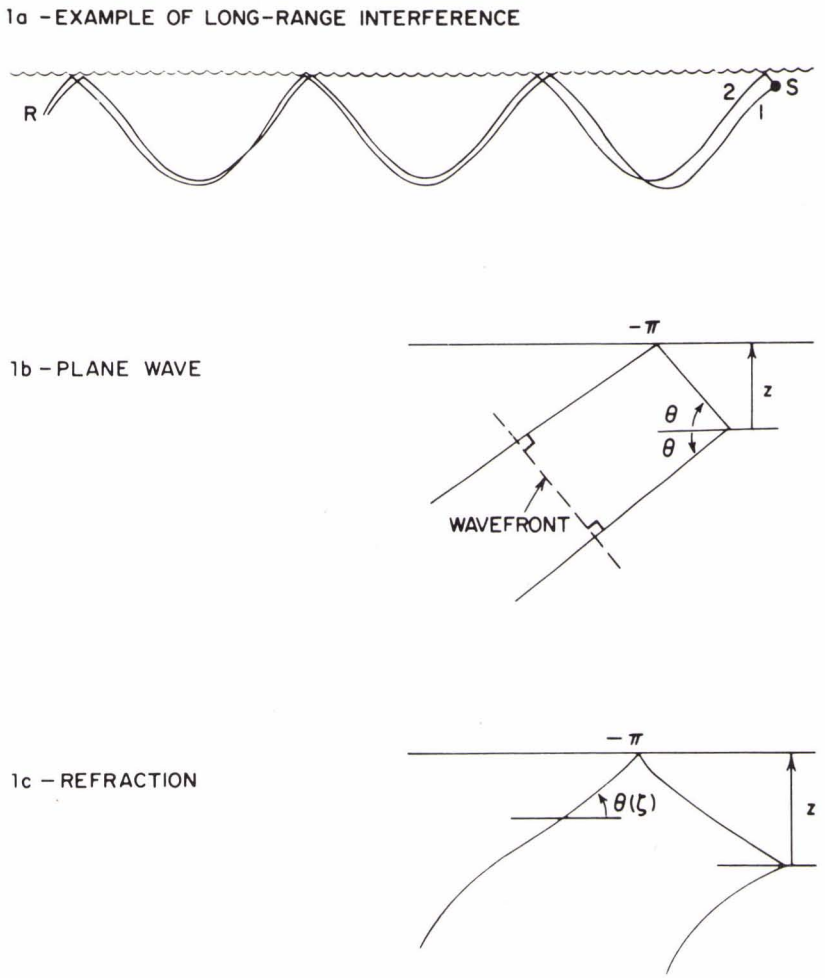

FIG. 1 SURFACE IMAGE INTERFERENCE

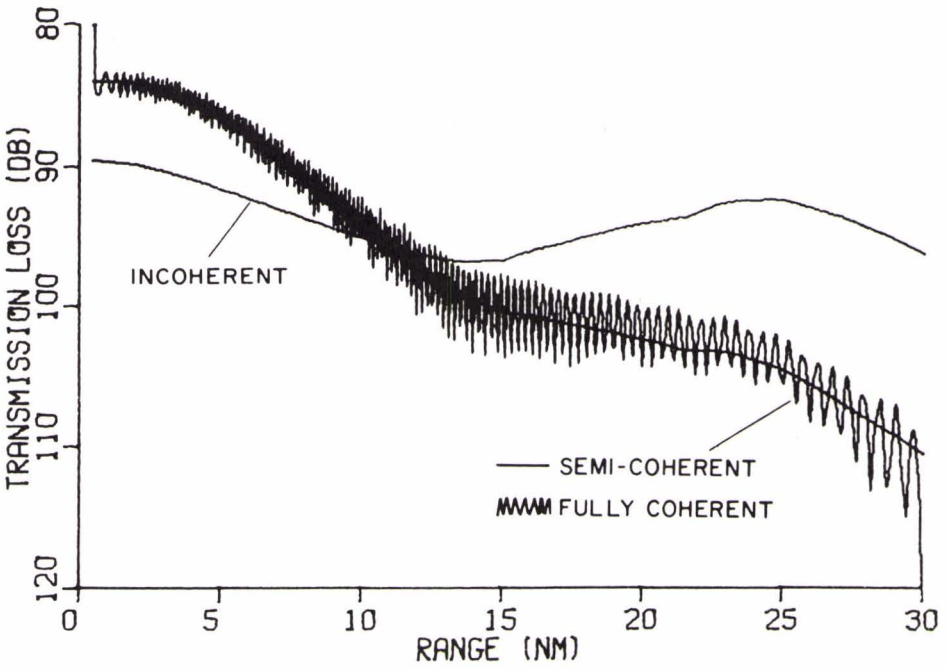

FIG. 2 FACT COMPARISON OF INCOHERENT, SEMI-COHERENT, AND FULLY COHERENT SUMMATIONS

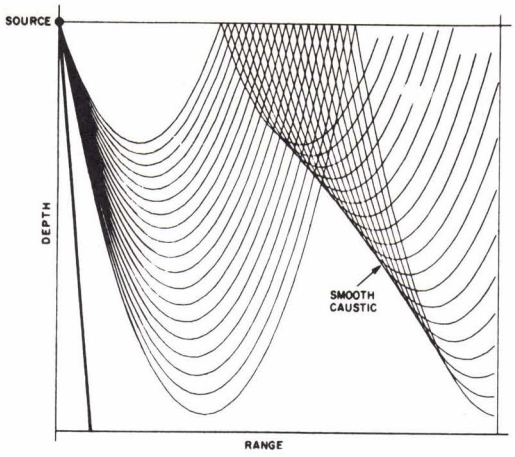

FIG. 3a
DEVELOPMENT OF A SMOOTH CAUSTIC

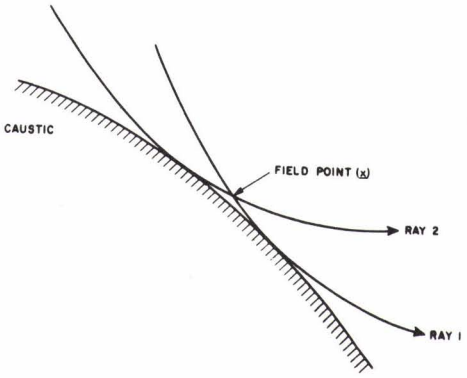

FIG. 3b
RAYS DEFINING FIELD NEAR A CAUSTIC

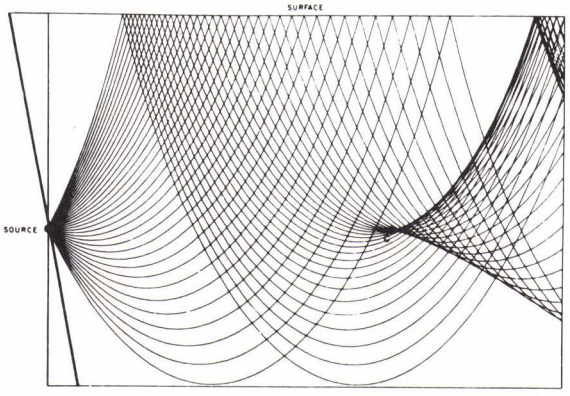

FIG. 4a
DEVELOPMENT OF A CUSPED CAUSTIC

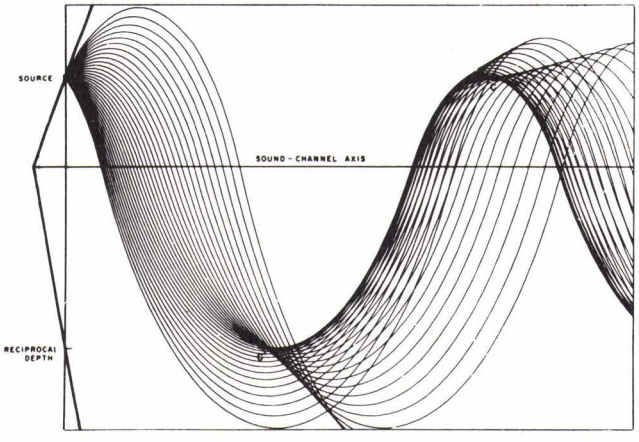

FIG. 4b
DEVELOPMENT OF A FOUR-RAY SYSTEM
(SMOOTH PLUS CUSPED CAUSTIC)

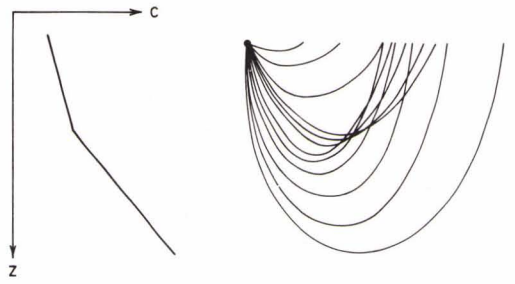

FIG. 5
GENERATION OF A FALSE CAUSTIC

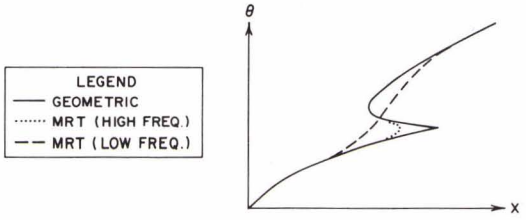

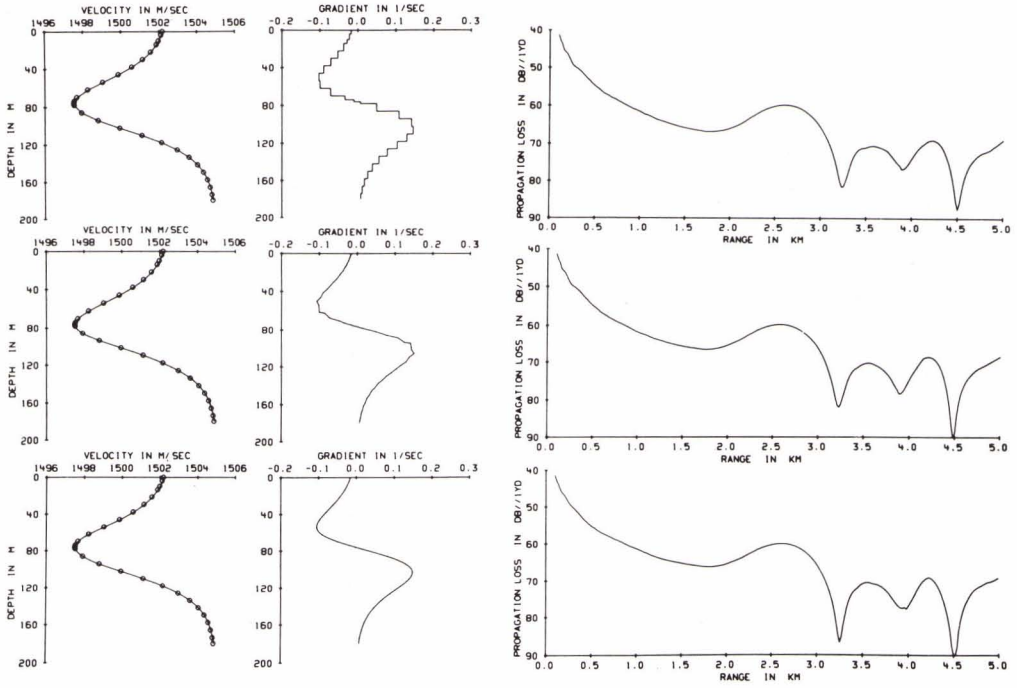

FIG. 6 THREE REPRESENTATIONS FOR AN EPSTEIN PROFILE (AFTER WEINBERG)

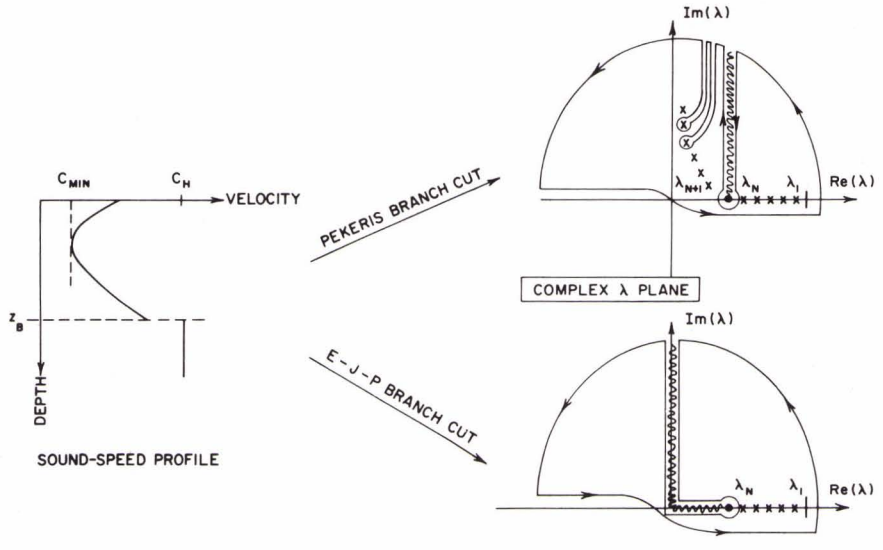

FIG. 7
TWO INTEGRATION CONTOURS DEFINING THE NORMAL MODE EXPANSION

STOCHASTIC METHODS OF SOUND-FIELD COMPUTATION

by

R.R. GOODMAN
U.S. Naval Research Laboratory
Washington, D.C.
U.S.A.

The paper, which was not received in time for publication, covered the following aspects:

I. Physical origin of the acoustic fluctuation terms
   A. The development of the dynamic oceanographic equations
      1. Internal waves, spectral characteristics
      2. Turbulence, spectral characteristics
      3. Oceanographic observations
   B. The development of the fluctuation terms in the acoustic equations

II. A Review of the general Theoretical Developments
   A. Geometric Limits
   B. Wave Theoretical Limits

III. Experimental results and their theoretical interpretation
   A. Short range, high frequency
   B. Long range, low frequency

IV. A Brief Review of Some Electromagnetic Applications

V. The design of future experiments
   A. Spatial and temporal correlations
   B. The requirement for environmental measurements in support of acoustic experiments
      1. The types of measurements
      2. Spatial and temporal frequencies of them

DISCUSSION

DISCUSSION ON SESSION 7

Reported by F.B. Jensen

FLATTE

What criterion do you have for choosing between the various propagation models?

GARON

At the AESD we have a rule as to when we apply the wave methods as opposed to the ray methods. This rule is usually a break point, actually in the amount of money it is going to cost to make the runs, but it also depends on what we are trying to get out of the runs. Within a normal deep-water environment, I would say that the best use of the parabolic equation and the normal mode techniques is at frequencies less than 250 to 300 Hz. At that point it starts to become really costly and time-consuming to make the runs.

FLATTE

You said that there are no approximations in normal mode theory, but isn't there a question to how many normal modes you actually have to use?

GARON

In a lossless environment there are discrete sets of normal modes and also a finite number of modes. Where the infinite number of modes comes into play is in the evaluation of the continuous spectrum.

FLATTE

What is the consequence of neglecting the continuous spectrum?

GARON

Both Hank Kutschale at Lamont and Dave Stickler have shown that the continuous spectrum can contribute significantly out to ranges of several water depths. I tried to bring out this point earlier, that if you haven't got any discrete modes or if the discrete modes are interfering destructively with each other, the only thing left is the continuous spectrum, and then you have to calculate it.

FLATTE

In a practical sense, what limitation does that put on the applicability of normal mode theory?

GARON

I really can't say that it will actually put a limitation on you in terms of using the modes.

FLATTE

In case someone wants to compare the parabolic equation method with the normal mode technique, it is nice to know which method is most accurate. You say that normal mode theory is exact and that parabolic equation theory is very close. In fact, normal mode theory also has some uncertainty in it.

GARON

That's right. You might also become very concerned when you know that the bottom-bounce paths themselves are going to predominate the propagation problem.

WILLIAMS

I would like to make a comment on variability. One thing that the oceanographers have brought out during this conference is how the variability is distributed in space and in time. One thing is clear. The oceanic variability cannot be described by a simple Gaussian distribution function. This is well-grounded in fully developed turbulence, and it is well-grounded in all the microstructure measurements ever made.

WITTING

Concerning the distribution of sound amplitudes around the mean for some experimental data: we have normally found a distribution that was Gaussian at high frequencies, but highly non-Gaussian in all other cases.

BRISCOE

Also for internal-wave problems the observed variability is highly non-gaussian.

WILLIAMS

At the microstructure conference in Grenoble almost everybody was showing very non-gaussian statistics for the microstructure, both in vertical and horizontal directions.

BACHMANN

I would like to change the subject a bit and ask the following questions: How would a future stochastic sound-propagation model look? How would the structure be? Would we first have to make a deterministic calculation and then add some stochastic extentions based on this deterministic field, or would it be an approach as indicated by GOODMAN, going back to the wave equation and starting everything from that point?

GOODMAN

I think there will be an entire spectrum of models, depending very much on the role data banks will play in the future. If one is going out making environmental measurements, very complete ones with fairly good sampling over long ranges, I don't think you need to develop this very general model. On the other hand, in those cases where I might have to predict propagation completely on the basis of data banks, or if I wanted to make predictions for much longer times than I can make environmental measurements, then I would probably learn very quickly to go to a more universal model. So I think there will be an entire spectrum of models. It will be a function of range, the sampling that I have in the experiments, and the kind of questions I am asking of the model.

FLATTE

I have a comment on the solution to the wave equation in range-independent situations, which in general is talked about in terms of normal modes. I'm not sure what the applicability of this new method is, but I want to put it before you. Suppose we are dealing with an arbitrary but range-independent sound-speed profile. The field can then be calculated by means of normal modes or by the parabolic equation method, except that the parabolic equation method has a disadvantage in this case, since you have to step along in range, while the normal mode solution gives you the answer for the entire field immediately. If you want the answer at various range points, you still have to add up the modes for every range point, but that goes fast. However, the parabolic equation, which enables you to step from range position to range position where we know the amplitude of the wave function over depth, uses the fast Fourier transform technique to create the movement of the wave function from step to step. The FFT technique basically enables you to reduce the number of calculations involved in evaluating a double integral, from n^2 to $n \cdot \lg n$. This is in fact the power of the FFT technique. If we apply the parabolic equation method to a case with a range-independent sound-speed profile, it turns out that we can reduce the n steps in range by the same technique. The FFT is used in the range variable, and we can then reduce the n steps to lg n steps — a dramatic reduction in most cases. This fact came to my attention because a group of physicists at the University of California in Santa Cruz were trying to solve the Schrödinger equation from quantum mechanics:

$$\frac{h^2}{8\pi^2 m} \nabla^2 \psi - \frac{h}{2\pi i} \frac{\partial \psi}{\partial t} - V(x, y, z)\, \psi = 0 \quad ,$$

which is dependent on time in the same way as the parabolic wave equation:

$$\frac{\partial^2 \psi}{\partial z^2} + 2ik_o \frac{\partial \psi}{\partial r} + k_o^2 (n^2 - 1)\, \psi = 0$$

is dependent on range. However they found this trick for reducing n steps in time down to lg n steps without realizint that they have the same possibility in the other dimensions. So we learn from each other.

DINAPOLI

Also the fast-field program uses the FFT technique in the range variable. Here the field is calculated in a discrete number of range points equal to the number of FFT points.

BACHMANN

I would like to change subject again. I think that one way to create a stochastic sound propagation model could be by introducing something like the Garrett-Munk model into one of the existing computer models, and then seek answers so such questions as: what is the variance, what is the spectral type of fluctuation you should expect at any point in space, what is the angular distribution, etc. My feeling is that the oceanographers already have a large portion of the necessary input, but that the acousticians are not ready to digest it yet.

GOODMAN

I guess I don't believe that. The fact that the acoustic field is expanded in a scattered field and a direct field, and one performs statistics on the scattered field, lead directly to the same set of statistics on the oceanographic properties. Mintzer made the right comment: Make sure that you use the right mathematical scattering model to go with the statistics that you see.

BACHMANN

It's just that such a model does not exist at the moment. We have only deterministic models. That's the state of art.

INITIAL DISTRIBUTION

	Copies
MINISTRIES OF DEFENCE	
MOD Belgium	1
DND Canada	10
CHOD Denmark	8
MOD France	8
MOD Germany	15
MOD Greece	11
MOD Italy	10
MOD Netherlands	12
CHOD Norway	10
MOD Portugal	5
MOD Turkey	5
MOD U.K.	16
SECDEF U.S.	60
NATO AUTHORITIES	
Defence Planning Committee	3
NAMILCOM	2
SACLANT	10
SACLANTREPEUR	1
CINCWESTLANT/COMOCEANLANT	1
COMIBERLANT	1
CINCEASTLANT	1
COMSUBACLANT	1
COMCANLANT	1
COMMAIREASTLANT	1
COMNORLANT	1
SACEUR	2
CINCNORTH	1
CINCSOUTH	1
COMNAVSOUTH	1
COMSTRIKFORSOUTH	1
COMEDCENT	1
COMSUBMED	1
COMMARAIRMED	1
CINCHAN	1

	Copies
SCNR FOR SACLANTCEN	
SCNR Belgium	1
SCNR Canada	1
SCNR Denmark	1
SCNR Germany	1
SCNR Greece	1
SCNR Italy	1
SCNR Netherlands	1
SCNR Norway	1
SCNR Portugal	1
SCNR Turkey	1
SCNR U.K.	1
SCNR U.S.	2
NATIONAL LIAISON OFFICERS	
NLO Denmark	1
NLO Italy	1
NLO U.K.	1
NLO U.S.	1
NLR TO SACLANT	
NLR Belgium	1
NLR Canada	1
NLR Germany	1
NLR Greece	1
NLR Italy	1
NLR Norway	1
NLR Portugal	1
NLR Turkey	1
ESRO/ELDO Doc. Service	1
ATTENDEES	110